Institut
Institut für Physik und Astronomie
Arbeitsgruppe
Lehrstuhl Nichtlineare Dynamik

Nonlinear dynamics in complex networks and modeling human dynamics

Dissertation
zur Erlangung des akademischen Grades
"doctor rerum naturalium"
(Dr. rer. nat.)
in der Wissenschaftsdisziplin " Physik "

eingereicht an der
Mathematisch-Naturwissenschaftlichen Fakultät
der Universität Potsdam

von
Ye Wu

Potsdam, 08.06.2010

Published online at the
Institutional Repository of the University of Potsdam:
URL http://opus.kobv.de/ubp/volltexte/2010/4735/
URN urn:nbn:de:kobv:517-opus-4735
http://nbn-resolving.org/urn:nbn:de:kobv:517-opus-47358

Nonlinear dynamics in complex networks and modeling human dynamics

Ye Wu

Institute of Physics and Astrophysics, University Potsdam

Abstract

The availability of large data sets has allowed researchers to uncover complex properties in complex systems, such as complex networks and human dynamics. A vast number of systems, from the Internet to the brain, power grids, ecosystems, can be represented as large complex networks. Dynamics on and of complex networks has attracted more and more researchers' interest.

In this thesis, first, I introduced a simple but effective dynamical optimization coupling scheme which can realize complete synchronization in networks with undelayed and delayed couplings and enhance the small-world and scale-free networks' synchronizability.

Second, I showed that the robustness of scale-free networks with community structure was enhanced due to the existence of communities in the networks and some of the response patterns were found to coincide with topological communities. My results provide insights into the relationship between network topology and the functional organization in complex networks from another viewpoint.

Third, as an important kind of nodes of complex networks, human detailed correspondence dynamics was studied by both data and the model. A new and general type of human correspondence pattern was found and an interacting priority-queues model was introduced to explain it. The model can also embrace a range of realistic social interacting systems such as email and letter communication. My findings provide insight into various human activities both at the individual and network level.

Fourth, I present clearly new evidence that human comment behavior in on-line social systems, a different type of interacting human dynamics, is non-Poissonian and a model based on the personal attraction was introduced to explain it. These results are helpful for discovering regular patterns of human behavior in on-line society and the evolution of the public opinion on the virtual as well as real society.

Finally, there are conclusion and outlook of human dynamics and complex networks.

Nonlinear dynamics in complex networks and modeling human dynamics

Ye Wu

Institute of Physics and Astrophysics, University Potsdam

Zusammenfassung

Durch große Datenmengen können die Forscher die Eigenschaften komplexer Systeme untersuchen, z.B. komplexe Netzwerk und die Dynamik des menschlichen Verhaltens. Eine große Anzahl an Systemen werden als große und komplexe Netzwerke dargestellt, z.B. das Internet, Stromnetze, Wirtschaftssysteme. Immer mehr Forscher haben großes Interesse an der Dynamik des komplexen Netzwerks.

Diese Arbeit besteht aus den folgenden drei Teilen. Der erste Teil ist ein einfacher dynamischer Optimierungs-Kopplungs-Mechanismus, aber sehr wirksam. Durch den Mechanismus kann synchronisation in komplexen Netzwerken mit und ohne Zeitverzögerung realisiert, und die Fähigkeit der Synchronisation von small-world und scale-free Netze verbessert werden.

Im zweiten Teil geht um die Verstärkung der Robustheit der scale-free Netze im Zusammenhang mit der Gemeinden-Struktur. Einige Reaktionsmuster und topologische Gemeinden sind einheitlich. Die Ergebnisse zeigen einen neuen Aspekt der Beziehung zwischen den Funktionen und der Netzwerk-Topologie von komplexen Netzwerken.

Im dritten Teil welche eine wichtige Rolle in komplexen Netzwerken spielt, wird die Verhaltens-Dynamik der menschliche Mitteilung durch Daten- und Modellanalysierung erforscht, dann entsteht ein neues Mitteilungsmodell. Mit Hilfe von einem Interaktion priority-Queue Model kann das neue Modell erklärt werden. Mit Hilfe des Models können viele praktische Interaktions-Systeme erklärt werden, z.B. E-Mail und Briefe (oder Post). Mit Hilfe meiner Untersuchung kann man menschliches Verhalten auf der Individuums- und Netzwerkebene neu kennenlernen.

Im vierter Teil kann ich nachweisen, dass menschliches Kommentar-Verhalten in on-line Sozialsystemen, eine andere Art der Interaktionsdynamik von Mensch non-Poisson ist und dieses am Modell erklären. Mit Hilfe der non-Poisson Prozesse kann man das persönliche Anziehungskraft-Modell besser verstehen. Die Ergebnisse sind hilfreich zum Kennenlernen des Musters des menschlichen Verhaltens in on-line Gesellschaften und der Entwicklung von öffentlicher Meinung nicht nur in der virtuellen Gesellschaft sondern auch in der Realgesellschaft.

Am Ende geht es um eine Prognose von menschlicher Dynamik und komplexen Netzwerken.

Chapter 1 Introduction 2
1.1 Basic concept of complex networks 2
1.1.1 Introduction of complex networks 2
1.1.2 History of complex networks 2
1.1.3 Some statistical characterizations of complex networks 3
1.1.4 Nonlinear dynamics in complex networks 4
1.2 Basic concept of human dynamics 5
1.2.1 Introduction of human dynamics 5
1.2.2 Basic property of human dynamics 5
1.2.3 Bursts and heavy tails in human dynamics 6
1.2.4 The origin of bursts and heavy tails in human dynamics 7
1.3 Outline 12
Chapter 2 Synchronization in small world networks 14
2.1 Introduction 14
2.2 Synchronization in small world network 15
2.3 Synchronizability of small world networks 20
2.4. Conclusion 24
Chapter 3 Response of scale-free networks with community structure to external stimuli 25
3.1 Introduction 25
3.2 The model of the network 26
3.3 The dynamic model 27
3.4 Numerical simulations and analysis 28
3.5 Response of cat brain networks to stimuli 31
3.6 Conclusion 34
Chapter 4 Modelling the human communication dynamics 35
4.1 Introduction 35
4.2 Empirical result 36
4.2.1 Data description 36
4.2.2 Bimodal distribution 37
4.3 Our model 40
4.3.1 Model description 40
4.3.2 Estimating important parameters from data 42
4.4 Fitting the model to the data 46
4.5 Analysis of the model 46
4.5.1 The effect of the parameters 46
4.5.2 From bimodal to truncated power-law distribution 49
4.6 Discussion 50
4.6.1 Extension to other human activity 50
4.6.2 Extension of our analysis and modelling 51
4.7 Conclusion 52
Chapter 5 Human comment dynamics in on-line social systems 53
5.1 Introduction 53
5.2 Data description 54
5.3 Statistic results 55
5.4 Model and simulation 57
5.5 Conclusion 59
Chapter 6 Conclusion and outlook 61
References 64
Acknowledgement 70
Appendix A Enhanced synchronizability in scale-free networks
Appendix B Matrix measure criterion for synchronization in coupled map networks
Appendix C Synchronization in small world networks
Appendix D Response of scale-free networks with community structure to external stimuli

Chapter 1 Introduction

1.1 Basic concept of complex networks

1.1.1 Introduction of complex networks

It is a true saying that the 21st century is the world of networks [R. Albert, 2002, S. Boccaletti, 2006]. Networks arise in our daily life by various ways. The first task we did when we open our eyes and get up in the morning was to turn on the light. There was complex power grid network [R. V. Solé, 2008] under the light. We used the traffic network to go to office, meanwhile public traffic networks [J. Sienkiewicz, 2005, P. Sen, 2003, R. Guimera, 2004], including bus, train, ship, and plane help us to travel all over the world. After we arrive at the office, we read the news, send E-mails to friends by the internet networks [S. Maslov, 2004, G. Yan, 2006]. When some individuals meet together, there is a friendship networks [A. Arenas,2008, K. Klemm, 2003], etc. In general, complex networks are a set of nodes and edges. All kinds of individuals such as human, load, bus, power station, web side, etc are the nodes of complex networks and the relationships between any pairs of nodes are the edges.

The complex network is changeable, even if the nodes maintain the same. The change is according to the reaction of edges. For example, we consider students as the nodes, and the edges are created when two students send emails to each other, the behavior is defined as *Email Network.* If they make phone calls, the action will be *Phone Network***.** Not only human can build an invisible network, but also all kind of substance, such as: food chain networks [T. Gross, 2006, 2008, 2009], finance institute networks, computer networks, brain networks. Obviously, the edge actions will be crucial factor in defining a complex network.

Complex networks theory is growing up gradually with the development of the simulation function of computer. Without the help of computers, it is hardly to figure out the statistic properties and the model mechanism of complex networks. Under the assistance from the computer power and the data access technology, researchers can study the statistic properties of complex networks composed from millions of nodes. That will be a great help to propose more and more models to explain the origin of networks, Furthermore, relationships between the function and topology of the networks are studied extensively.

1.1.2 History of complex networks

There are three landmarks on the origin and history of complex networks. The first one is the Euler graph [H. Ren, 2009]. There was a very famous mathematics problem which was called “Konigsberg seven-bridge problem”. Euler who is an intelligent guy, solved the problem very artifice. He demonstrated that it is an impossible task by considering the islands as nodes and

the bridges as edges. His considering the individual as nodes and the relationship between individuals as edges was the origin of networks theory.

The second one is the Erdös-Rényi graph (ER random graph) [H. Ren, 2009]. Two mathematicians Erdös and Rényi presented a random graph model which enhanced the development of graph theory in 1960. Researchers consider the ER random graph as the best model to describe networks in the following years. The ER model still has many applications nowadays. However, with the development of computer power in the 20th century, people can understand the network in more details. More and more evidences have shown that realistic complex networks were neither random nor regular. The ER model can not describe some important topologies and statistic properties of networks. At the end of the 20th century, the third landmark appeared. There are two excellent works leading to the development of complex networks. One is "Collective behavior of small-world networks" which was published in "Nature" by Watts and Strogatz in 1998[D. J. Watts, 1998]. The other one is "Emergence of scaling in random networks" which was published in "Science" by Barabási and Albert in 1999[A. L. Barabási, 1999]. The two works announce the small-world effect and the scale-free effect of complex networks and introduce a model to explain it. Of course, more and more other interesting properties of complex networks have been found and different models have been proposed up until now.

However, there is no agreement about the clear definition of complex network. In general, complex network is any system that admits an abstract mathematical representation as a graph, whose nodes identify the elements of the system and the set of links represent the presence of a relation or interaction among those elements. Complex networks are helpful to understand an important problem "why complex systems are complex", which is the basic elements of many complex systems.

1.1.3 Some statistical characterizations of complex networks

Our intention is to select those notions and notations which will be used throughout the rest of this book.

1) Graphs

An undirected graph G is defined by a pair of sets $G = (V, E)$, where V is a non-empty countable set of nodes and E is a set of edges. From a mathematical point of view, it is convenient to define a network by means of the adjacency matrix $A = \{A_{ij}\}$ $(N \times N)$ which is defined:

$$A_{ij} = \begin{cases} 1, & if \quad (i,j) \in E \\ 0, & if \quad (i,j) \notin E \end{cases} .$$

The adjacency matrix is symmetric for undirected networks and not symmetric for directed networks.

2) Degree and degree distribution

The degree k_i of a vertex i is defined as the number of edges in the graph incident on the vertex i. The degree distribution $P(k)$ of undirected networks is defined as the probability that any randomly chosen vertex has degree k. For scale free networks, the degree distribution is power-law. $P(k) \propto k^{-\gamma}$.

3) Weighted networks [S. H. Yook, 2001, A. Barrat, 2004**]**

In a number of real-world networks, not all links in a network have the same capacity. In other words, many networks are intrinsically weighted, their edges having different strengths. For example, in the friendship network, some individuals are acquaintances, but some individuals maybe meet each other only few times. In bus networks, the number of buses between two stops is different. In other words, the edges between two any stops have different weighted. The weighted on the edges can be note as: $W_{i,j}$.

4) Community structure

In the context of networks, community structure is defined as collections of nodes within which the connections are dense, while between the communities the connections are sparse. Community structures are supposed to play an important role in many real networks. For example, communities in a citation network might represent related papers on a single topic [S. Render, 1998]; communities on the web might represent pages on related topics [G. W. Flake, 2002]; communities in a biochemical network or neuronal system might correspond to special functional units [P. Holme, 2003, O. Sporns, 2004a].

1.1.4 Nonlinear dynamics in complex networks

In the past decade, the dynamics of complex networks has been extensively investigated, with special emphasis on the interplay between the complexity in the overall topology and the dynamics process in the complex networks [A. Barrat, 2008]. Such as: phase transitions on complex networks, resilience and robustness of networks, synchronization phenomena in networks, walking and searching on networks, epidemic spreading in population networks, social networks and collective behavior, traffic on complex networks. One of our aims of this thesis is to study the synchronization in complex networks and the response of scale-free networks with community structure to external stimuli.

1.2 Basic concept of human dynamics

Human which is a kind of nodes of complex networks, participate various kinds of activities everyday. How to understand these dynamics of human behavior is a very interesting problem. Human dynamics in complex networks will open a new insight on the flow modeling and prediction. Here we give a short introduction about human dynamics.

1.2.1 Introduction of human dynamics

Human participate various kinds of activities everyday. He/She gets up in the morning and then goes to work. He/She may send emails to his friend in the middle of day, go shopping in the afternoon, and make a phone with his best friend in the evening. How to understand regular pattern of these human activities which is called human dynamics always attracts sociology, psychology, economic and physics interest. It seems very hard to find a scaling in human activities due to complexly and diversity of human behavior and it is difficult to describe it by mathematical and physical models. But patterns of deliberate human activity and behavior are of utmost importance in areas as diverse as information spread, resource allocation and emergency, especially in phone line availability and bandwidth allocation in the case of Internet or Web use.

Research about human dynamics has a long history. It was modeled firstly in the probability theory and has reemerged at the beginning of the 20th century when the phone was devised due to the phone system required a quantitative understanding of the call patterns of individuals.

1.2.2 Basic property of human dynamics

Human behavior is so complexity that it is hard to quantitative understanding. So far, researchers mainly pay attention to the inter-event time distribution $P(\tau)$ and the waiting time distribution $P(\tau_W)$ of human dynamics only.

1) Inter-event time:

The time interval between two consecutive events was denoted by the inter-event time τ . For example, an individual sends two consecutive Emails, two consecutive visits on a web by the same user, two consecutive transactions by the broker. The inter-event time distribution $P(\tau)$ is the most important character to study a human dynamics. For example, different kinds of distribution need different design for the phone system.

2) Waiting time:

In some systems, for example, E-mail communication, surface mail correspondences, on-line chat, waiting time τ_W , denotes the time interval between the time one individual send a

message, and the time the other one reply it. Waiting time is an important variable to study a human dynamics too.

We expect that more and more features of human dynamics will be introduced to understand the regularity patterns of human activities in the future.

1.2.3 Bursts and heavy tails in human dynamics

In the early stage of study, researchers assumed that human activity is a homogeneous Poisson process. Such processes are very popular to model a large class of phenomena, including some aspects of human activity, such as traffic flow patterns or accident frequencies. Especially, they are at the heart of the celebrated Erlang formula [Erlang, 1909]. The most important statistical properties of Poisson processes are that their inter-event time follows an exponential distribution [F. A. Haight, 1967]. However, an increasing number of recent measurements indicate that the inter-event time of some human activities are better approximated by a heavy tailed or power-law distribution. Here we list some typical evidences bellow [A. Vázquez, 2006].

1) E-mail communications

Barabasi [A. L. Barabási, 2005] studied a dataset which contains the email exchange between 3,188 individuals in a university for three months. He showed that both the inter-event time distribution and the waiting time distribution are power-law with an exponent approximated to 1.

2) Surface mail communications

Three famous scientists' (Einstein, Darwin and Freud) surface mail communications records were analyzed by Vazquez and his co-workers [J. G. Oliveira, 2006, A. Vázquez, 2006]. They showed that the distributions of response times follow a power-law from with an exponent approximated to 1.5 which is different from E-mail activity.

3) Financial activities

Vazquez analyzed a dataset that contains all buy/sell transactions initiated by a stock broker at a Central European bank between June 1999 and May 2003[A. Vázquez, 2006]. There were in total 54,374 transactions during the 3 years. Although the inter-event time distribution for stock transactions is obviously differ from a power-law function which is different from the communication activity. They display clearly heavy-tailed distribution which is different from an exponential form. This result was confirmed by a recent empirical analysis on a double-auction market [E. K. Scalas, 2006].

4) Library loans

48,409 checks out records of books or periodicals by 2,247 individuals at a University during three years were studied by Vazquez [A. Vázquez, 2006]. The inter-event time between two consecutive books or periodicals checked out by the same patron follows power-law distribution with exponent from 0.5 to 1.5, with the average around 1.0.

5) Web browsing

The dataset of web browsing contains the visiting records of 25,000 unique visitors to the site www.origi.hu between 8th, Nov. to 8th, Dec, 2002. Dezsõ shown [Z. A. Dezsõ, 2006] that the inter-event time distribution of a single user is power-law with exponent 1.0.

There are other evidences that the timing of human activities follows non-Poisson statistics, such as surface mail communication of Chinese scientist, on-line moving watching, and on-line chat. We expect that more and more non-Poisson regularly of human dynamics will be found in the future.

1.2.4 The origin of bursts and heavy tails in human dynamics

Until now, there are mainly three kinds of models proposed to explain the non-Poisson activities which would be listed bellow.

1) Queue-based model

Most of the time a person needs to face many tasks in his/her daily life, such as shopping, sending emails, making telephone call, reading news, going to a theater, playing basketball and so on. Indeed, person only can do one work at a moment. In the modeling of human behaviors, these activities on human life can be considered as tasks on a queue and person do the task as a server process. Accordingly, Barabasi [A. L. Barabási, 2005] proposed a model based on queuing theory which is call queue-based-model.

The underlying mechanism of the queue-based-model is that person always needs to do more than one task at a moment and he prefers to finish important task first. The model was separated into two parts:

1) Priority queue. An individual has a priority list with L tasks, ie. a person needs to do L tasks at a moment. Each task is assigned a priority parameter $x_i (i = 1,2,\cdots L)$ which means that some task is more important than others and needs to do first. In the model, x_i is chosen from a uniform distribution $x_i \in [0,1]$. At each time step, a task from the list was chosen to execute and removed from the list at the same time. A new task was added in the list after the old one was executed.

2) Selection protocol. At each time step, it assumes that the individual executes the task with the highest priority with probability p, and with probability 1-p executes a randomly task. If $p \to 1$, it means a person prefers to do the most important task first, but not always.

Simulation results are shown in Fig 1.1. For $p \to 0$, the waiting time distribution $P(\tau)$ decays exponentially as a Poisson process, for $p \to 1$, it follows a power-law distribution with exponent 1, which agrees well with the empirical data of Email communication. These results imply that higher p could be an important mechanism leading to the non-Poisson statistics of human dynamics.

Numerical simulations indicate that the tail of $P(\tau)$ is independent of the length of the priority list. It means a burst, heavy-tailed inter-event dynamics will emerge even when individuals balance at least two tasks. In order to simulate different individual behaviors, the queue-based-model can be extended by considering a stochastic version of the model in which the probability to choose a task with priority x for execution in a unit of time is $\prod(x) \approx x^{\gamma}$ where x is chosen from the $\rho(x)$ distribution. From the analysis in Ref [A. L. Barabási, 2005], the waiting time distribution $P(\tau) \approx \frac{\rho(\tau^{-1/\gamma})}{\tau^{1+1/\gamma}}$. In the $\gamma \to \infty$ limit, which converges to $p \to 1$ in the model, both predicts $P(\tau) \approx \tau^{-1}$.

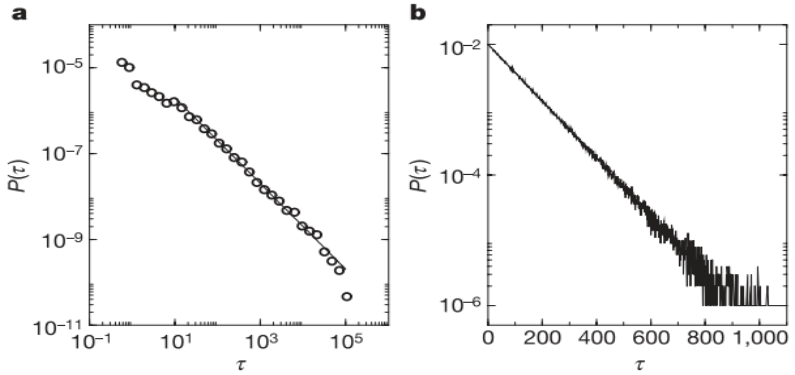

Fig. 1.1 The waiting time distribution predicted by the investigated queuing model. The priority were chosen from a uniform distribution $x_i \in [0,1]$, and the parameter $L = 100$, it was monitored over 10^6 time steps. (a), Log-Log plot of the tail of probability $P(\tau)$ that a task spends τ time on the list obtained for $p = 0.99999$, corresponding to the deterministic limit of the model. The continuous line of log-log plot has slope -1, in agreement with the numerical results and the analytical predictions. The data were log-binned, to reduce the uneven statistical fluctuations common in heavy-tail distributions, a procedure that does not alter the slope of the tail. (b), Linear-log plot of the $P(\tau)$ distribution for $p = 0.00001$, corresponding to the random choice limit of the model. The fact that the curve follows a straight line on a linear-log plot indicates that $P(\tau)$ decays exponentially. It is an exact copy from Ref. [A. L. Barabási, 2005], and its copyright belongs to the Nature Publishing Group.

After the queue-based-model was proposed by Barabasi, many researchers pay attention to it and its extension. A. Vázquez [A. Vázquez,, 2005] and C.Anteneodo [C. Anteneodo, 2009] used different methods to give exact result for the queue-based-model independent. A.

Vázquez [A. Vázquez,, 2006] etc. discussed two queuing models that capture two kinds of human activity. The first model assumes that there are no limitations on the numbers of tasks an individual can handle at any time, resulting that the waiting time follows a heavy tailed distribution with exponent $\alpha = 3/2$, which corresponds to human surface mail based communication. The other model imposed limitations on the queue length, predicting a heavy tail waiting time distribution with exponent $\alpha = 1$ which corresponds to human Email, web browsing and library visitation dynamics. A.Gabrielli [A. Gabrielli, 2007] and his co-worker studied the invasion and critical transient in the queue-based-model of human dynamics. G. Grinstein and R.Linsker [G. Grinstein, 2006] study the structure and robustness of universality classes for queuing. They derivied analytic results for priority-basic models with continuous-valued priorities.

J. G. Oliveira and A. Vazquez [J. G. Oliveira, 2009] considered the impact of interaction on human dynamics. They introduced a minimal queuing model of human dynamics that already takes into account human-human interactions. They showed that the exponent of the power-law distributed inter-event times were changed by the interactions. Byungjoon M and his co-workers [M. Byungjoon, 2009] considered a scalable interaction protocol to the queue-based-model and then examined the effects of the network topology on the human dynamics. They found power-law tails in all cased considered, yet with model-dependent power-law exponents.

2) Non-homogeneous Poisson model.

R. D Malmgren and his co-workers [R. D Malmgren, 2008] introduced a totally different model from the queue-based-model to explain heavy tails in E-mail communication. They considered that human behavior is primary driven by external factors such as circadian and weekly cycles. Heavy tails are results of distinct characteristic time scales. They also demonstrated that the distribution of inter-event times in E-mail correspondence patterns display systematic deviations from the truncated power-law null model. They relate the rate of the non-homogeneous Poisson process to the daily and weekly distribution of activity interval initiation: $\rho(t) = N_w p_d(t) p_w(t) = \rho(t+W)$, where the period W is one week and N_w is the average number of activity intervals per week. $p_d(t)$ and $p_w(t)$ are the probabilities of starting an active interval at a particular time of day and week respectively. The result was shown in Fig. 1.2 which fit well with the data.

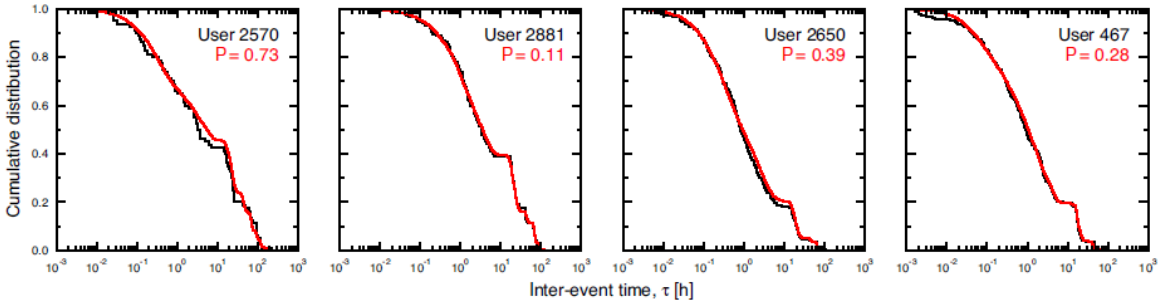

Fig. 1.2 Comparison of the predictions of the cascading non-homogeneous Poisson process (red line) with the empirical cumulative distribution of inter-event times(black line) for four users. It is an exact copy from Ref [R. D Malmgren, 2008]. and its copyright belongs to PNAS.

Furthermore, similar with the Non-homogeneous Poisson model, R.D Malmgren and his co-workers [R. D. Malmgen, 2009] introduce another cascading Poisson process to explain the heavy tails in human letter correspondence activity. They consider two additional ingredients for modeling letter correspondence. First, circadian and weekly cycles of activity may influence when individuals communicate as Non-homogeneous Poisson model. All time are divided into some segments. Then the non-homogeneous Poisson process $\rho(t)$ is approximated by a homogeneous Poisson process with constant rate ρ_i during time segment i. Second, there is a probability ξ_i that individuals will write another letter when they finish writing a letter. This process repeats itself at which point the individual's behavior is again governed by a homogeneous Poisson process with rate ρ_i .

3) Interest-driven model

Han, Zhou and Wang [X. P. Han, 2008] proposed a very interesting model to explain the real-world human activities. The underlying mechanism is from our life habit. For example, you had eaten a kind of food (for example, hamburger) with very good taste at time t. You will eat the hamburger with high probability in the following time until you feel you have eaten too much hamburger. Then the good feeling of hamburger disappears, and you will not like eating hamburger anymore.

To mimic these habits, two simple assumptions were exacted in the modeling of the interest-driven model. Firstly, each activity will update the current interest and the more interest, the more frequency of activities. Secondly, the interest will be depressed when the inter-event time τ is too small; otherwise, the interest will increase. A casual action will be occurrence when the time gap τ is too long. The formula describes of the model is listed as follows:

The time is discrete and labeled by $t = 0,1,2,\cdots,$. $r(t)$ denotes the occurrence probability of an event at time step t.

If the (i+1)th event occurred at time step t, the value of r is updated as $r(t+1) = a(t)r(t)$. And

$$\begin{cases} a(t) = a_0, & if \quad \tau_i \le T_1 \\ a(t) = a_0^{-1}, & if \quad \tau_1 \ge T_2 \\ a(t) = a(t-1), & if \quad T_1 < \tau_1 < T_2 \end{cases}$$

The result was shown in Fig. 1.3 Some simple activities, such as watching TV, browsing web, playing on-line game can be indicated by the interest-driven model.

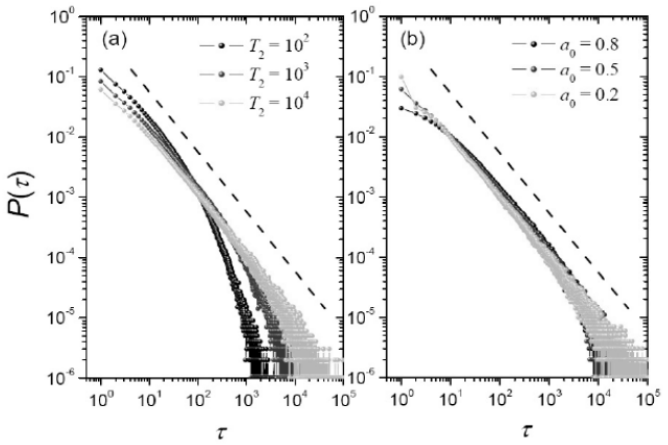

Fig. 1.3 The inter-event time distributions in log-log plots. (a) Given $a_0 = 0.5$, $P(\tau)$ for different T_2 , where the black, dark gray and bright gray curves denote the cases of $T_2 = 10^2, 10^3$,and 10^4 , respectively. (b) Given $T_2 = 10^4$, $P(\tau)$ for different a_0 , where the black, dark gray and bright gray curves denote the cases of $a_0 = 0.8, 0.5 \; and \; 0.2$, respectively. The black dash line in both (a) and (b) has slope -1. All the data points are obtained by averaging over 100 independent runs, and each includes 10^4 events. It is a black-white copy from the Ref. [Han, 2008].

Thought the three kinds of model can explain the power-law distribution of inter-event time in some kinds of human dynamics, they have a common limitation. They did not consider the interaction between individual's own behavior and his partners' behavior. Obviously, individual's communication activities, such as Email and letter communication are influenced by his partners' directly. Sometime, they did not want to write Email, but they have to write response Emails to his partners. Unfortunately, previously examined data often do not allow us to analyze this interaction precisely. However, we have the data (Short Message account bills) obtained from a mobile phone operator which provides a very attractive proxy for studying the interaction of human activity. Moreover, we also obtain data from 'tianya' which is one of the most popular on-line social systems in China which can be used for study human comment dynamics. Quantitative understanding of complex human behavior, such as human communication, human comment dynamics is one of the most important aims of my research.

1.3 Outline

In chapter 2, we consider complete synchronization in small-world networks of identical Rössler oscillators. By applying a simple but effective dynamical optimization coupling scheme, we realize complete synchronization in networks with undelayed or delayed couplings, as well as ensuring that all oscillators have uniform intensities during the transition to synchronization. Further, we obtain the coupling matrix with much better synchronizability in a certain range of the probability p for adding long-range connections. Direct numerical simulations fully verify the efficiency of our mechanism. This part of work has been published in Chaos [Y. Wu, et al. 2008].

In chapter 3, the response of scale-free networks with community structure to external stimuli is studied. By disturbing some nodes with different strategies, we find that the robustness of this kind of network can be enhanced due to the existence of communities in the networks. Some of the response patterns are found to coincide with topological communities. We show that such phenomena also occur in the cat brain network which is an example of a scale-free like network with community structure. Our results provide insights into the relationship between network topology and the functional organization in complex networks from another viewpoint. This part of work has been published in Physica A [Y. Wu, et al. 2009].

In chapter 4, here we present clear empirical evidences from Short Messages (SM) correspondence that observed human actions are the result of interplay of three basic ingredients: Poisson initiation of tasks and decision-making for task execution in individual human and the interaction among individuals. This interplay leads to new types of inter-event time distribution, neither completely Poisson nor power-law, but a bimodal combination of them. We show that the events can be separated into bursts which are generated by frequent mutual interactions following independent, random initiations by the individuals. We introduce a minimal model of two interacting priority-queues incorporating the three basic ingredients which fit well the distributions using the parameters extracted from empirical data. The model can also embrace a range of realistic social interacting systems such as email and letter communications when taking the time scale of processing into account. Our findings provide insight into various human activities both at the individual and network level. This part of work has been submitted [Y. Wu, et al. 2010a]..

In chapter 5, human comment is studied using data from 'tianya' which is the most popular on-line social systems in China. We found that the time interval between two consecutive comments on the same topic, called inter-event time, follows a power-law distribution. This result shows that there was no characteristic decaying time on a topic. It allows for very long

periods of no comment that separate bursts of intensive comments. Furthermore, the frequency of different ID comments on a topic also follows a power-law distribution. It indicates that there were some "hubs" in the topic who lead the direction of the public opinion. Based on the personal comments habit, a model was introduced to explain the phenomena. The numerical simulations of the model fit well with the empirical results. Our findings are helpful for discovering regular patterns of human behavior in on-line society and the evolution of the public opinion in the virtual as well as realistic society. This part of work has been submitted [Y. Wu, et al. 2010b].

In chapter 6, it is a conclusion of the whole thesis and some outlook. Appendix A is about “Enhanced synchronizability in scale-free networks” which is published in Chaos [M, Chen, 2009].Appendix B is about “Matrix measure criterion for synchronization in coupled map networks” which is published in Phys. Rev. E [P. Li, 2009]. I am a co-worker in appendix A and appendix B.

Chapter 2 Synchronization in small world networks

2.1 Introduction

In the past decade, the dynamics of complex networks has been extensively investigated, with special emphasis on the interplay between the complexity in the overall topology and the local dynamical properties of the coupled oscillators [D. J. Watts 1998, A. L. Barabasi 1999, S. H. Strogatz, 2001, I. Z. Kiss, R. Albert, 2002, S. Strogatz, 2003, L. F. Lago-Fernandez, 2000, A. Arenas, 2004a, 2004b]. As a typical kind of dynamics on complex networks, synchronization, especially the ability of networks to become synchronized (synchronizability), has attracted a lot of interest in multidisciplinary fields.

The works on synchronizability in networks with a given topology can be divided into two classes according to the coupling matrix. One is the static mechanism, where the coupling matrix remains fixed during the transition to synchronization. The character is that the coupling matrix unidirectional affects synchronization [G. Osipov, 2007, M. Barahona, 2002, T. Nishikawa, 2003, G. A. Polis, 1998, V.Latora, 2001, M. Chavez]. It has been recently shown that for randomly enough unweighted and weighted networks [C. S. Zhou, 2006a], the synchronizability is controlled by $S_{\max}/S_{\min}$, where $S_{\max}$ and $S_{\min}$ are the maximum and minimum of the intensities S_i, defined by the sum of the couplings for oscillator i. For unweighted scale-free networks (SFNs) generated by the Barabási–Albert [A. L. Barabási 1999] model, $S_{\max}/S_{\min} = K_{\max}/K_{\min} \approx N^{1/2}$, where N is the network size, $K_{\max}$ and $K_{\min}$ are the maximal and minimal degrees, respectively. From the degree [A. E. Motter, 2005a, 2005b] and load [M. Chavez 2005, 2006] based weighted networks, the synchronizability becomes optimal when the intensities of all oscillators become uniform.

The other is the dynamical mechanism, where the coupling matrix evolves in time by introducing adaptive strengths between connected oscillators. The adaptation process can enhance synchronization by modifying the coupling matrix. However, during the transition to synchronization, the dynamical mechanism [C. S. Zhou, 2006b, Q. Ren, 2007] cannot ensure uniform intensities even for small-world networks (SWNs), which is not consistent with the necessary condition for the optimal synchronizability in the static mechanism. Zhou and Kurths [C. S. Zhou, 2006b,] proposed a dynamical mechanism using local information among each oscillator and its neighbors. In the corresponding networks the connections between different oscillators are strengthened. The adaptive process drives the network into the direction of a more homogeneous topology, ongoing with an enhanced ability for synchronization. Thereby it is possible to synchronize networks that exceed by several orders of magnitude the size of the largest comparable random graph that is still synchronizable [T.

Gross, 2007]. For simplicity, we call this mechanism the ZK method. It shows that the ZK method is very effective to realize synchronization in SFNs, and can enhance the synchronizability in SFNs substantially. After the adaptation of the couplings, the weights of incoming links V_i scale with the degree k of the corresponding oscillator X_i as $V(k) \approx k^{-\theta}$, and the synchronizability is characterized by $S_{\max}/S_{\min} \approx N^{\beta/2}$ with $\beta = 1-\theta$ and $\theta = 0.54 \pm 0.01$ for SFNs of Rössler oscillators, and the average intensity $S(k)$ over oscillators with degree k increases as $S(k) \approx k^{\beta}$ [C. S. Zhou, 2006b,].

In this chapter we consider complete synchronization in SWNs, especially the Newman–Watts (NW) model [M. E. J. Newman, 1999], by introducing a simple but effective dynamical mechanism. Our aims are to (i) realize complete synchronization in SWNs with undelayed or delayed couplings, whose oscillators all have uniform intensities during the transition to synchronization, and (ii) to assign the coupling matrix with enhanced synchronizability in certain cases.

By applying the dynamical optimization (DO) mechanism, we will achieve the above aims. The DO mechanism adjusts the coupling strengths based on the 'winner-take-all' strategy. It realizes complete synchronization in SFNs with undelayed couplings, as well as enhances the synchronizability greatly [M. Chen, 2009].

In this chapter, we extend the DO mechanism to NW networks with undelayed or delayed couplings. We show that the DO mechanism is more effective in realizing synchronization in NW networks than the ZK method. Since the DO mechanism can ensure the uniform intensities of all oscillators, it can also effectively realize synchronization in NW networks with delayed couplings. But the ZK method cannot realize synchronization in networks with delayed couplings. Moreover, in a certain range of the probability p for adding long-range connections, we design a coupling matrix for NW networks, which has much better synchronizability than unweighted networks, degree based weighted networks and the ZK method.

This chapter is organized as follows: In section 2.2, by applying the DO mechanism, we can realize complete synchronization in NW networks of identical Rössler oscillators, as well as ensure the uniform intensities of all oscillators during the transition to synchronization. In Sec. 2.3, we enhance the synchronizability in NW networks by designing the coupling matrix. We draw up our conclusions in the last section.

2.2 Synchronization in small world network

Our general model for networks consisting of N coupled identical Rössler oscillators with a

time-varying coupling matrix is given by

$$\dot{X}_i = F(X_i) + \sum_{j=1}^{N} G_{ij} H(X_j, X_i) \quad \cdots\cdots \quad 2.1$$

Where X_i is the state, $F(X_j)$ is the dynamics of the individual oscillator X_i, $H(X_j, X_i)$ is the inner coupling function, $G = (G_{ij})$ is the outer coupling matrix. $G_{ij} = A_{ij} W_{ij}$, where $A = (A_{ij})$ is the binary adjacency matrix, W_{ij} is the coupling strength of the incoming link (X_i, X_j) pointing from oscillator X_j to oscillator X_i if they are connected, $G_{ii} = -\sum_{j \in K_i} A_{ij} W_{ij}$, K_i is the neighbor set of oscillator X_i.

In this chapter we consider complete synchronization in network in two cases. (i) One case is the network with undelayed couplings, where the function $H(X_j, X_i) = H_0(X_j) - H_0(X_i)$, and H_0 is the output function for each oscillator. (ii) The other case is the network with delayed couplings, in which the function $H(X_j, X_i) = H_0[X_j(t-\tau)] - H_0[X_i(t)]$ with a time delay $\tau > 0$.

Our aim is to realize complete synchronization in network, as well as ensure that all oscillators in network have uniform intensities during the transition to synchronization. Recently, we have already obtained some results on this problem. For different variants of the Kuramoto model, we have proposed a *dynamical gradient network* approach to realize phase synchronization [M. Chen, 2008]. It shows that all the oscillators have uniform intensities during the transition to synchronization. However, the DGN approach is very special in two aspects. One is that it should assign a scale potential to each oscillator within any time interval, which depends on the extent of the local synchronization among itself and its neighbor oscillators. The other is that the incoming link to be adjusted by the DGN approach is often not mostly effective. Inspired by the idea of the DGN approach [M. Chen, 2008], we have further introduced a DO mechanism for SFNs [M. Chen, 2009]. It reflects the 'winner-take-all' strategy, where the incoming link to be adjusted is always chosen as a pair of oscillators with the weakest synchronization. This means that the DO mechanism is more effective than the DGN approach. We also show that the DO mechanism has much better synchronizability in SFNs than the ZK method [M. Chen, 2009].

In this chapter, we apply the DO mechanism to SWNs. Here we first introduce the idea of the DO mechanism. The DO mechanism is to increase the strength of only one incoming link of each oscillator by a small amount ε, at every time step $t_n = t_0 + nT$ for $n \geq 1$, where t_0 is the transient time, and $T > 0$ is the length of time intervals. For oscillator X_i and its neighbor oscillator X_j, the total synchronization difference.

$$E_n(i, j) = \int_{t_{n-1}}^{t_n} \Phi(X_i, X_j) dt \quad \cdots\cdots \quad 2.2$$

Within the interval $[t_{n-1}, t_n)$, is evaluated, where Φ is a synchronization error function. For complete synchronization in SWNs, the function Φ is a non-negative error function if oscillators i, j are not synchronized, and satisfies $\Phi(X_i, X_j) = 0$ if oscillators i, j are synchronized. To check complete synchronization in network, the function Φ is chosen as

$$\Phi(X_i, X_j) = \left|X_i - X_j\right| + \left|y_i - y_j\right| + \left|z_i - z_j\right| \cdots\cdots\cdots\cdots\cdots\cdots\cdots\cdots\cdots\cdots\cdots\cdots\cdots\cdots\cdots\cdots 2.3$$

The total synchronization difference $E_n(i, j)$ reflects the competition ability of the incoming link (X_i, X_j) within the time interval $[t_{n-1}, t_n)$. For oscillator X_i, the incoming link with the weakest synchronization, i.e., $(X_i, X_{j^n_{\max}})$, is the winner within the interval $[t_{n-1}, t_n)$, where the index $j^n_{\max}$ is decided by the following dynamical optimization problem:

$$j^n_{\max} = \arg\max_{j \in K_i} E_n(i, j) \cdots\cdots\cdots\cdots\cdots\cdots\cdots\cdots\cdots\cdots\cdots\cdots\cdots\cdots\cdots\cdots\cdots\cdots\cdots\cdots 2.4$$

The solutions of the optimization 2.3 within different intervals are also different, which depends on the dynamics of oscillators. The connection strength is then adjusted dynamically by:

$$W^{n+1}_{ij^n_{\max}} = W^n_{ij^n_{\max}} + \varepsilon, \quad W^{n+1}_{ij} = W^n_{ij}, j \neq j^n_{\max} \cdots\cdots\cdots\cdots\cdots\cdots\cdots\cdots\cdots\cdots\cdots\cdots\cdots\cdots\cdots\cdots 2.5$$

Where $\varepsilon > 0$ is a small value, and W^n_{ij} is the coupling strength in the interval $[t_{n-1}, t_n)$.

From Eqs. 2.4 and 2.5, we strengthen the incoming link with the weakest synchronization, namely, the link with the maximal competition ability. For complete synchronization in SWNs with undelayed couplings, the additional term $\varepsilon(X_{j^n_{\max}} - X_i)$ can be regarded as the negative feedback term for the unidirectional synchronization from oscillator $X_{j^n_{\max}}$ to oscillator X_i. This could make the synchronization difference between oscillator X_i and its neighbor $X_{j^n_{\max}}$ be smaller, which implies the synchronization in SWNs be realized.

Note that the intensities of all oscillators in network are uniform, since at each step the intensity of each oscillator increases by the same amount ε. This is consistent with the necessary condition for optimal synchronizabiliy in the static mechanism [M. Chavez, 2005, 2006, A. E. Motter, 2005a, 2005b, X. Wang, 2007].

In order to show the effectiveness of the DO mechanism, our analysis and simulations are based on SWNs generated by the NW model. The initial network is a K nearest neighbor coupled network consisting of N oscillators arranged in a ring, with each oscillator X_i being adjacent to its neighbor oscillators $X_{i\pm1}, \cdots, X_{i\pm K/2}$, and with K being even. Then one adds with probability p a connection between a pair of oscillators. In the following, network is a network of Rössler oscillators

$$X = (x_i, y_i, z_i), \quad F(X_i) = [-0.97y_i - z_i, 0.97x_i + 0.15y_i, z_i(x_i - 8.5) + 0.4]$$

the function $H_0(X_i) = (x_i, 0, 0)$. In order to show complete synchronization, we define the average synchronization error as

$$E = \frac{1}{N}\sum_{i=1}^{N} \left\| X_i - \overline{X} \right\| \quad ,$$

where $\overline{X} = (\overline{x}, \overline{y}, \overline{z})$ is the mean-field of all X_i. In our simulations, the initial coupling strengths for all incoming links are zero, the transient time is $t_0 = 100s$, the length of time intervals is T=1 s, and the small value is $\varepsilon = 0.001$. Further, initial conditions for all oscillators are randomly chosen from the chaotic attractor. The solution of network is solved by using the Euler method with the time step h=0.01 s, and our ending condition for the DO mechanism is $E < 10^{-5}$.

In this chapter we consider complete synchronization in NW networks in two cases. One case is the network with undelayed couplings, where the function $H(x_j, x_i) = H_0(x_j) - H_0(x_i)$. From recent works [C. S. Zhou, 2006, Q. Ren. 2007], the dynamical mechanism can realize complete synchronization both in SFNs with undelayed couplings and in SWNs with

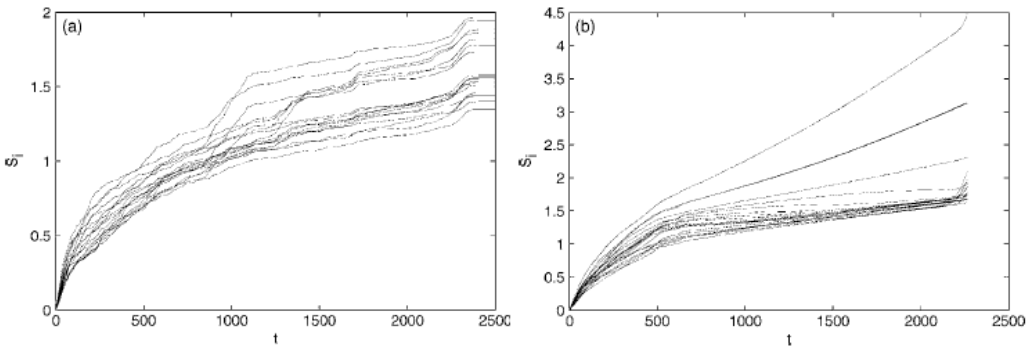

Fig. 2.1 The intensities S_i as a function of time t for arbitrarily 20 oscillators in networks with undelayed couplings (a), or delayed couplings (b), by the ZK method. The parameters are $N = 500, K = 4, p = 0.0003, \gamma = 0.0002, \tau = 0.01$

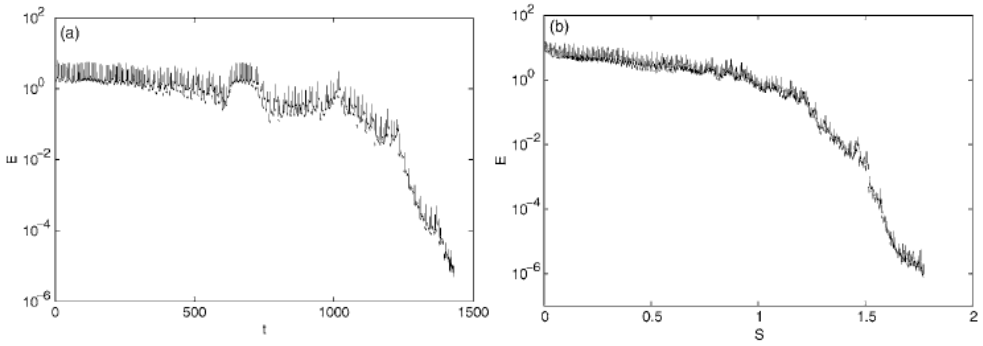

Fig. 2.2 The average synchronization error E in networks with undelayed couplings as a function of (a) time t, and (b) the intensity S, by the DO mechanism. The parameters are $N = 500, K = 4, p = 0.0003, T = 1s, \varepsilon = 0.0001$.

undelayed couplings. However, even for NW networks with homogeneous degrees, the dynamical mechanisms cannot ensure uniform intensities if all oscillators have different initial conditions. We plot the intensities S_i, defined by the sum of the coupling strengths of neighbor oscillators of oscillator I (i.e. $S_i = \sum_{j \in K_i} G_{ij}$).for 20 arbitrarily chosen oscillators in NW networks according to the ZK method (Fig. 2.1(a)). When the adaptation parameter is chosen as $\gamma = 0.002$ in the ZK method, we find that the ZK method cannot ensure uniform intensities during or after the adaptation. Based on the DO mechanism, complete synchronization in NW networks are realized effectively Fig2.2(a), and the intensities are always uniform during the transition to synchronization. From Fig. 2.2(b)，the intensity $S = S_i$ is also a good indicator for synchronization in networks. As S increases to a critical value, a network becomes synchronous. (ii) The other case is the network with delayed couplings, in which the function $H(x_j, x_i) = H_0[x_j(t-\tau)] - H_0[x_i(t)]$ with a time delay $\tau > 0$. Even for a small time delay τ such as $\tau = 0.01s$, the ZK method

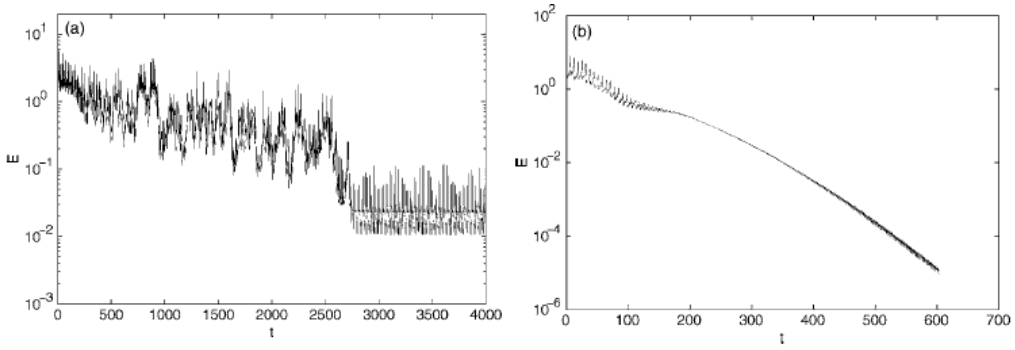

Fig. 2.3 The average synchronization error E in networks with delayed couplings as a function of time t. (a) The ZK method $\tau = 0.01s$,(b) The DO mechanism($\tau = 2s$). The parameters $N = 500, p = 0.003, \gamma = 0.002, T = 1s, \varepsilon = 0.001$.

cannot realize synchronization in NW networks (Fig. 2.3(a)). The synchronization error between two connected oscillators is about $10^{-2} \times 500 = 5$ for networks with N=500. Due to the DO mechanism, complete synchronization can be realized effectively when the time delay $\tau = 2s$ (Fig. 2.3(b)). The synchronization error is about $10^{-5} \times 500 = 0.005$. Hence the DO mechanism is more effective than the ZK method. The main reason is that the DO mechanism ensures that the intensities are always uniform during the transition to synchronization. But the ZK method cannot ensure uniform intensities even for the small time delay Fig. 2.1(a). Though the difference of intensities between oscillators is small initially, it becomes large as time increases. The uniformity of intensities is the necessary condition for the existence of a synchronous manifold in NW networks with delayed couplings. After the adaptation, the synchronous manifold is given by $X_i(t) = X_0(t), i = 1,2,\cdots,N$, where $X_0(t)$ is the solution of the isolated dynamics $\dot{X}_0(t) = F[X_0(t)] + S_0\{H_0[X_0(t-\tau)] - H_0[X_0(t)]\}$， $S_0 = \varepsilon n_0$ is the

ultimate intensity, and n_0 is the ending adjustment step.

2.3 Synchronizability of small world networks

In this section we discuss the synchronizability of NW networks. We first briefly review the stability of networks,

$$\dot{X}_i = F(X_i) + \sigma \sum_{j=1}^{N} G_{ij}^0 [H_0(X_j) - H_0(X_i)]$$

where H_0 is the output function, and σ is the overall coupling strength in networks. Without loss of generality, we assume that the coupling matrix $G^0 = (G_{ij}^0)$ is asymmetric. The coupling matrix $G^0 = (A_{ij} W_{ij}^0)$ is similarly defined as the matrix G in network. The variation equation for the synchronous state $\{X_i = s, \forall i\}$ is given by $\dot{\xi}_i = [DF(s) - \sigma\lambda_l DH_0(s)]\xi_i$, where $\dot{s} = F(s)$ is the dynamics of the isolated oscillator, D is the Jacobian operator,

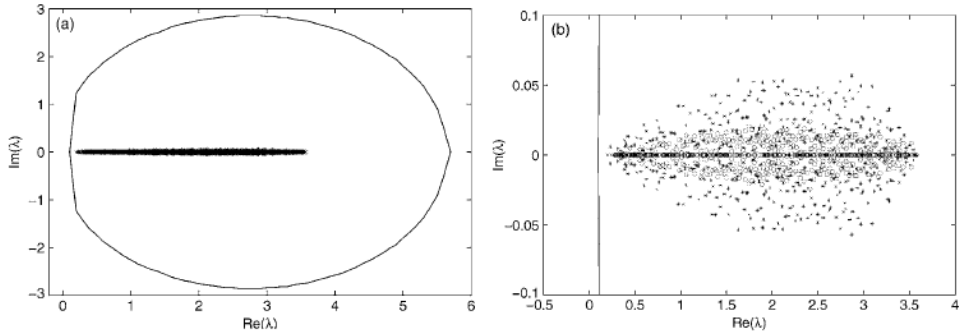

Fig. 2.4 (a) and (b) Distribution of eigenvalues of the Laplacian matrix of σG_{norm} in network with undelayed couplings (o) and delayed couplings (*), Solid line: The stability region R. The parameters are $N = 500, K = 4, p = 0.003, T = 1s, \varepsilon = 0.001, \sigma = 2, \tau = 1s$

and λ_l is a complex eigenvalue of the Laplacian matrix $L(=-G^0)$, satisfying $\mathrm{Re}(\lambda_1) \le \mathrm{Re}(\lambda_2) \le \cdots \le \mathrm{Re}(\lambda_N)$. The largest Lyapunov exponent（LLE）, $\Lambda(\alpha, \beta)$, of the master stability equation $\dot{\eta} = [DF_0(s) - (\alpha + i\beta)DH_0(s)]\eta$ is a function of the parameters α and β, which is known as the master stability function（MSF）[J. F. Heagy, 1995, L. M. Pecora, 1998]，Let R be the region in the complex plane where the MSF provides a negative LLE (Fig. 2.4). The region R bounded by the solid line. The condition for complete synchronization in network is that the set is entirely contained in R [J. F. Heagy, 1995, L. M. Pecora, 1998]. Here we only consider the case where the region R is bounded. For the networks of Rössler oscillators in this chapter, the stability region R is shown by the solid line in Fig. 2.4(a). In order to judge whether the set $\{\sigma\lambda_l, \lambda_l \neq 0\}$ is in the stability region in the case of the complex eigenvalues of the Laplacian matrix L, one should minimize the ratio $\mathrm{Re}(\lambda_N)/\mathrm{Re}(\lambda_2)$ for a fixed value of the max $|\mathrm{Im}(\lambda_l)|$, and one should minimize max$|\mathrm{Im}(\lambda_l)|$ for a fixed value of the ratio $\mathrm{Re}(\lambda_N)/\mathrm{Re}(\lambda_2)$. Summing up the above minimization, a good

condition is that $\mathrm{Re}(\lambda_N)/\mathrm{Re}(\lambda_2)$ and $\max|\mathrm{Im}(\lambda_l)|$ are simultaneously minimized [M. Chavez, 2006, D. Huang, 2005].

In this section we analyze the synchronizability in NW networks by applying the DO mechanism. From our recent work [M. Chen, 2009] the DO mechanism can ensure uniform intensities of all oscillators in networks, regardless of the initial conditions of the oscillators in networks with undelayed or delayed couplings. Here we design the coupling matrix G_0 in network through the adaptation of the coupling strengths in network. After the adaptation by the DO mechanism, the coupling matrix G_0 in network is assigned by the following matrix: $G_0 = G_{norm} = G_{end}/S_0$,where G_{end} is the coupling matrix of network after the adaptation. For the coupling matrix $G_0 = G_{norm}$, all eigenvalues are fully contained within the unit circle centered at 1[M. Chavez, 2006, D. Huang, 2005]. So $0 \le \mathrm{Re}(\lambda_l) \le 2, |\mathrm{Im}(\lambda_l)| \le 1$, and the largest $\mathrm{Re}(\lambda_N)$ still never diverge. During the transition to synchronization in network, $S_{\max}/S_{\min}$ always equals 1 in the DO mechanism.

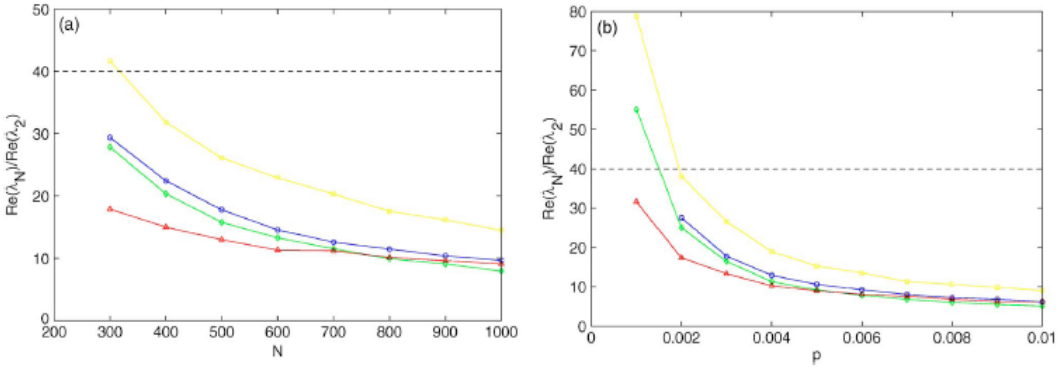

Fig. 2.5 (Color online) The ratio $\mathrm{Re}(\lambda_N)/\mathrm{Re}(\lambda_2)$ as a function of network size N for a fixed probability $p = 0.003$, and the probability p for a fixed size N=500 (b). Yellow line (): type I networks; green line (): type II networks; blue line (): type III networks; red line (): type IV networks; black dashed line: the maximal ratio $\mathrm{Re}(\lambda_N)/\mathrm{Re}(\lambda_2)$ in the region R. The parameters are $K = 4, \gamma = 0.002, T = 1s, \varepsilon = 0.001$. All the estimates are averaged over 20 realizations of networks.

It should be pointed out that max $|\mathrm{Im}(\lambda_i)|$ is sufficiently small due to the DO mechanism (the maximal value is less than 0.1). Even for a large coupling strength $\sigma = 2$, all the nonzero eigenvalues of the Laplacian matrix of σG_{norm} are located in a narrow region around the real axes in the stability region R (Fig. 2.4(a)). Hence the ratio $\mathrm{Re}(\lambda_N)/\mathrm{Re}(\lambda_2)$ indicates the synchronizability in networks. In order to show the enhanced synchronizability in NW networks, we compare the synchronizability in the unweighted network (type I network: $W_{ij} = 1$), the degree based weighted network (type II network: $W_{ij}^0 = 1/k_i$), network with adaptive couplings by the ZK method(type III network), and network with the coupling matrix being designed by network with undelayed couplings (type IV networks.)

We find that for a fixed small probability p such as p=0.003 for adding long-range connections, the synchronizability in type III networks is better than that in type I networks, but it is worse than that in type II networks, no matter how large the size N of the networks in Fig 2.5, Table I. However, we find that type IV networks have a better synchronizability than both type II networks and type III networks when the size is not too large. Of course, the smaller the probability p, the larger the size of type IV networks with better synchronizability than both type II networks and type III networks. For the fixed size N=500, we observe similar results in a certain range of the probability p (Fig. 2.5, Table II). From Fig. 2.5 and Tables I and II, we see that the synchronizability in type IV networks is better than those in type II networks and type III networks in some cases. It is reasonable that type IV networks have better synchronizability than type III networks. This is because the DO mechanism ensures uniform intensities of all oscillators in type IV networks. Now we further analyze the reason why type IV networks have better synchronizability than type II networks in a certain range of the probability p.

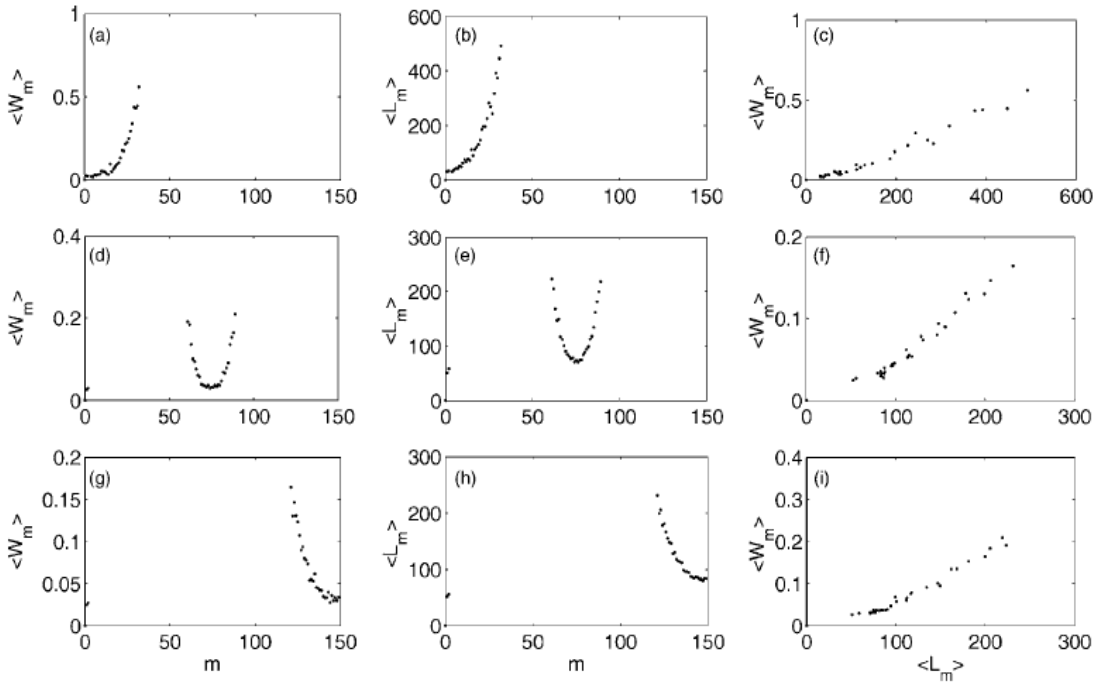

Fig. 2.6 The dependence of $\langle W_m \rangle$ on m in (a), (d) and (g) of $\langle L_m \rangle$ on m in (b), (e), and (h), and the relationship between $\langle W_m \rangle$ and $\langle L_m \rangle$ in (c), (f) and (i), respectively. $n_1 = 0, n_2 = 30$ [(a),(b) and (c)]; $n_1 = 60, n_2 = 90$ [(d),(e)and (f)]; $n_1 = 120, n_2 = 150$ [(g),(h) and (i)]. The parameters in type V networks are $N = 300, K = 4, p = 0.2, T = 1s, \varepsilon = 0.001$

TABLE I. The ratio $\mathrm{Re}(\lambda_N)/\mathrm{Re}(\lambda_2)$ as a function of network size N for a fixed probability p=0.003.

	N							
Type	300	400	500	600	700	800	900	1000
I	41.66	31.83	26.10	22.91	20.34	17.55	16.17	14.51
II	27.84	20.36	15.77	13.29	11.53	9.96	9.08	7.97
III	29.38	22.44	17.61	14.56	12.60	11.49	10.42	9.68
IV	17.88	15.00	12.99	11.31	11.22	10.17	9.63	9.08

TABLE II. The ratio $\mathrm{Re}(\lambda_N)/\mathrm{Re}(\lambda_2)$ as a function of the probability p for a fixed size N=500.

	p								
Type	0.002	0.003	0.004	0.005	0.006	0.007	0.008	0.009	0.01
I	38.04	26.53	18.98	15.25	13.52	11.38	10.63	9.88	9.01
II	24.98	16.45	11.32	9.16	7.85	6.78	6.03	5.50	5.07
III	27.52	17.77	12.92	10.61	9.22	8.02	7.23	6.80	6.18
IV	17.37	13.33	10.26	8.96	8.06	7.55	6.79	6.22	6.19

In order to do so, we slightly modify NW networks. The initial network is a K-nearest-neighbor coupled network consisting of N oscillators arranged in a ring, with each oscillator X_i being adjacent to its K neighbor oscillators $X_{i\pm1},\cdots X_{i\pm K/2}$, and with K being even. Then one adds with probability p a long-range connection between a pair of oscillators with indices satisfying $n_1 \le \min\{|i-j|, N-|i-j|\} \le n_2$, where $0 \le n_1, n_2 < N/2$ are two positive integers. This kind of network is called type V networks. Based on type V networks, we adjust the coupling strengths by the DO mechanism. After the adaptation, we define the average coupling strength $\langle W_m \rangle$ over the K_W links having the same $m \le \min\{|i-j|, N-|i-j|\}$.

$$\langle W_m \rangle = \frac{1}{k_W} \sum G_{ij}$$

Frther, for the unweighted type V networks, the average load $\langle L_m \rangle$ over the k_L links having the same m is given by

$$\langle L_m \rangle = \frac{1}{k_L} \sum L_{ij}$$

where the load L_{ij} of the link connecting oscillators X_i and X_j quantifies the traffic of the shortest paths passing that link. Here the size of type V networks is N=300 and the probability p=0.2. For different n_1 and n_2, we plot the relationship between $\langle W_m \rangle$ and m (Fig. 2.6 (a), (d), (g)), and the relationship between $\langle L_m \rangle$ and m (Fig. 2.6(b) (e), and (h)),

respectively. From these subfigures, we conclude that $\langle W_m \rangle$ has a similar dependence on m as $\langle L_m \rangle$, which is further verified by the relationship $\langle W_m \rangle \approx \langle L_m \rangle$ Fig. 2.6 (c), (f), (i). This implies that the adaptation due to the DO mechanism ay lead to a similar synchronizability as the load based weighted networks. This may in part explain why type V networks have a better synchronizability than type II networks n a certain range of the probability p for adding long range connections.

2.4. Conclusion

This chapter considers complete synchronization in small world networks of identical Rössler oscillators. Differing from the exiting dynamical mechanism, we apply a simple but effective DO mechanism to networks with undelayed or delayed couplings. We realize complete synchronization in networks, as well as ensure that all oscillators have uniform intensities during the transition to synchronization. The uniformity of the intensities is consistent with the necessary condition for the optimal synchronizability in the static mechanism. Further, we design a coupling matrix with much better synchronizability in a certain range of the probability p for adding long-range connections.

The DO mechanism can also be applied to the phase synchronization in SWNs with non-identical oscillators. For example, we consider the phase synchronization in the Kuramoto model [Q. Ren, 2007, M. Chen, 2008, Y. Kuramoto, 1984, J. Acebron, 2005]. In this case, $X_i = \theta_i, F(X_i) = w_i$, w_i are frequencies uniformly distributed in the interval $[-\Delta, \Delta]$, with $\Delta > 0$, $H(X_j, X_i) = \sin(\theta_j - \theta_i)$ for the undelayed couplings and $H(X_j, X_i = \sin[\theta_j(t-\tau) - \theta_i])$ for the delayed couplings, the error function $\phi(X_i, X_j) = 1 - r_n(i, j)$ with $r_n(i, j)e^{\xi\psi_n(i,j)} = (e^{\xi\theta_j} + e^{\xi\theta_i})/2$ and $\xi^2 = -1$ where $0 \le r_n(i, j) \le 1$ measures the extent of the synchronization of oscillators i , j, and $\Psi_n(i, j)$ stands for an average phase. Hence $\phi(X_i, X_j)$ are non-negative oscillators X_i, X_j are not synchronized, and $\phi(X_i, X_j) = 0$ if oscillators X_i, X_j are synchronized. Of course, our mechanism can be applicable to the synchronization in networks with non-identical chaotic oscillators such as Rössler oscillator provided that the term of "phase" in networks is well-defined [G. Osipov, 2007].

Chapter 3 Response of scale-free networks with community structure to external stimuli

3.1 Introduction

Many natural systems are found, on one hand, to be able to react to small selected stimuli with large alterations, whereas, on the other hand, they can with stand large environmental variations (sometimes even unpredictable ones) with minimal changes or loss of functionality. This implies two complementary attributes of dynamical systems: sensitivity and robustness. Sensitivity implies the possibility of a large response to small stimuli and robustness implies the possibility of a small response to large stimuli. Not only biological systems but also several man-made complex systems, such as power grids or communication systems require this combination of traits to optimize the system's performance. Recently, the focus on understanding the interplay between dynamical behavior and their topologies has attracted a lot of interest [S. Boccaletti, 2006, T. C. Jarrett, 2006, J. A. Acebrn, 2007, E. A. Variano, 2004, C. Piccardi, 2008, A. Arenac, 2008, S. N. Dorogovtsev, 2008]. Recent research [B. Shargel, 2003] shows that the observed network topologies which are often scale-free or scale-free like [A. L.Barabasi] are not necessarily optimal in their connectivity and connectivity-related attributes. Moreover, it is manifesting [B. R. Bollobas, 2003] that scale-free networks are fragile to intentional attack but resilient to random failures, in the face of node removal. We ask why so many networks found in nature have a scale-free (like) architecture with a lack of optimal network connectivity? In this paper, we study the properties which determine the efficiency of networks by analyzing the response of such systems to external perturbations.

To describe a complex system, one can take the units of response as nodes and the interactions between them as edges and then generate a network model. It is well known that many complex networks exhibit not only short average distances, but also a high clustering coefficient, the ‘small-world’ property [D. J. Watts, 1998]. Moreover, several of them can be approximated well by a power-law degree distribution, $P(k) \propto k^{-\gamma}$, the ‘scale-free’ property [A. L. Barabasi, 1999]. Many real-world networks exhibit not only the ‘small-world’ and ‘scale-free’ property, but also have a community structure which is defined as collections of nodes within which the connections are dense, but between the communities the connections are sparse. Community structures [L. Danon, 2008, A. Arenas, 2004] are supposed to play an important role in many real networks. For example, communities in a citation network might represent related papers on a single topic [S. Redner, 1998]; communities on the web might represent pages on related topics [G. W. Flake, 2002]; communities in a biochemical network or neuronal system might correspond to special functional units [P. Holme,2003, O. Sporns,

2004]. Therefore, it is important to study the response of a scale-free network with community structure.

In this chapter, we use the dynamical model presented by Bar-Yam and Epstein [Y. Bar-Yam, 2004] to study the response of scale-free networks with community structure to external stimuli. Our investigation reveals that the community characteristic of the networks is crucial to enhance its robustness. Some of the response patterns are found to coincide with the topology communities. As an example of scale-free like networks with community structure, such phenomena also occur in mammal brain networks.

This chapter is organized as follows: In Section 3.2, the model of the network is introduced. The dynamical attractor network model is presented in Section 3.3. Numerical simulations and a detailed analysis are presented in Section 3.4. In Section 3.5, we study the response of the cat brain network to stimuli as an example. Finally, our conclusions are given in Section 3.6.

3.2 The model of the network

In order to create a scale-free network with community structure, we use a modified procedure of the algorithm proposed in [C. G. Li, 2005]. We assume that there are $M(M > 2)$ communities in the network. This model is defined by the following scheme:

Step 1: Initialization: Start from a small number $m_0(m_0 > 1)$ of fully connected nodes in each community. There are n_0 random links between every two communities.

Step 2: Growth: At each time step, a new node is added to the network. We assume that the probability P(I) of which community I the new node is added to depends on the number of nodes in the communities n_I , i.e.:

$$P(I) = \frac{n_I}{\sum_I n_I}$$

The new node will be connected to $m(m_0 \geq m \geq 1)$ nodes inside the same community I through m intra-community links (defined as the links that connect nodes in the same community), and with probability α connected to $n(m \geq n \geq 1)$ nodes (none with probability $1-\alpha$) to the other $M-1$ communities through inter-community links (defined as the links that connect nodes among different communities). We assume that the probability $P(i,I)$ that a new node will be connected to node i in community I which is selected before depends on the inner-degree S_{iI} (define as the number of intra-links connected to node i) of that node, i.e.:

$$P(i,I)=\frac{S_{iI}}{\sum_k S_{kI}}$$ We also assume that the probability $P(j,K)$ that a new node will be connected to node i in community $K(K\neq 1)$ depends on the inter-degree l_{jK} (defined as the number of inter-links connected to the node), i.e.:

$$P(j,K)=\frac{l_{jK}}{\sum_{m,N,N\neq K} l_{mN}}$$

We call this network a community-scale-free (CSF) network (compare with scale-free network (SF)). It is shown in Fig. 3.1 that such a CSF network has also a power-law degree distribution $P(k)\propto k^{-\gamma}$.

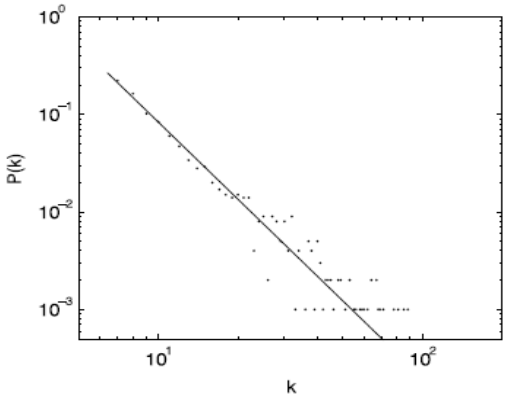

Fig. 3.1 The degree distribution of CSF. $N=1000, M=5, n=6, m=1, \alpha=1, \gamma=3$

3.3 The dynamic model

To investigate the response of CSF networks, we choose a conventional multi-attractor network model; which describes a dynamical system. The node states $s_i=\pm 1, i\in 1,2\cdots,N$ are binary. The states of the network system are then composed by the set of the node states s_i. The dynamical attractor system evolves as follows:

$$s_i(t+1)=sign(\sum_{j=1}^{N} A_{ij}s_j(t))$$

where $A=(A_{ij})_{N\times N}$ is the connection matrix whose elements A_{ij} are positive if there is a link going from node i to node j with $i\neq j$ and zero otherwise ($A_{ii}=0$) (A is symmetric if the network has no weights and no directions). This model can also be interpreted as social opinion models of binary states, such as yes (+1) or no (-1). It is known [J. J. Hopfield, 1982] that there are multiple attractors generated by this model. Any attractor with a non-empty attracting basin is stable to perturbation and thus can represent a functional state of the system.

External stimuli are modeled by flipping the signs of a specified set of nodes. When the states

of some nodes are changed, the system either evolves back to its initial state or switches to other attractors. The response of the network system is described as a process of switching between the attractors. The size of the basin of attraction, i.e., the number of nodes whose states can be changed before the dynamics of the network fails to bring the systems back to its original states, indicates the degree of stability of the system. The system is said to be sensitive to a certain disturbance if it changes its current state to another one, and vice versa. We calculate the size of the basin of attraction in different cases of stimuli to reveal the sensitivity and robustness of the network [L. K. Gallos, 2005, G. Bianconi, 2006].

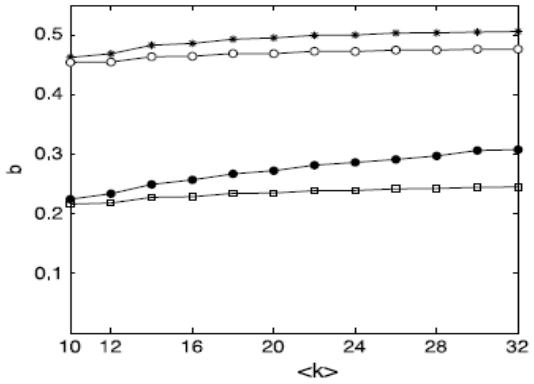

Fig. 3.2 Size of the basin of attraction (fraction of total nodes, b) as a function of the average degree $\langle k \rangle$,* CSF network and random stimulus, ◦ SF network and random stimulus, • CSF network and directed stimulus, SF network and directed stimulus, $\langle k \rangle = m$ in SF, $\langle k \rangle = m + \alpha n$ in CSF, $N = 1000, M = 4$.

3.4 Numerical simulations and analysis

We study the CSF networks mentioned in Section 3.2 and the Barabási-Albert model of SF networks. Without loss of generality, we can randomly choose two states to represent the functional states of the system. To ensure that these states are stable, we adopt the Hebbing imprinting rule $J_{ij} = \sum_{\alpha} s_i^{\alpha} s_j^{\alpha}$ to construct the desired attractors. For sufficiently many links and for a broad range of network topologies, this form of non-zero links will make the pre-selecting functional states into stable attractors of the network dynamics [J. J. Hopfield, 1982]. For the sake of convenience, we consider two attractors S1 and S2 (S1=(+1,+1,……,+1), S2=(-1,-1,……,-1)). as the stable states between which the system can switch. Initially, all the nodes are set to be in the state +1, that is, $s_i = +1, i = 1,2,\cdots,N$. We suppose, at some time t, such environment changes or new information arises, which induce the states of some nodes being selected to flip to the opposite state $S_{k_i} = -1, i = 1,2,\cdots,r_s$, where r_s is the number of the nodes whose states are flipped. Then after a period of transient time, the system evolves into a stable state which is either its original state or another attractor. To explore the changes of the system state, 100 simulations are performed for each different

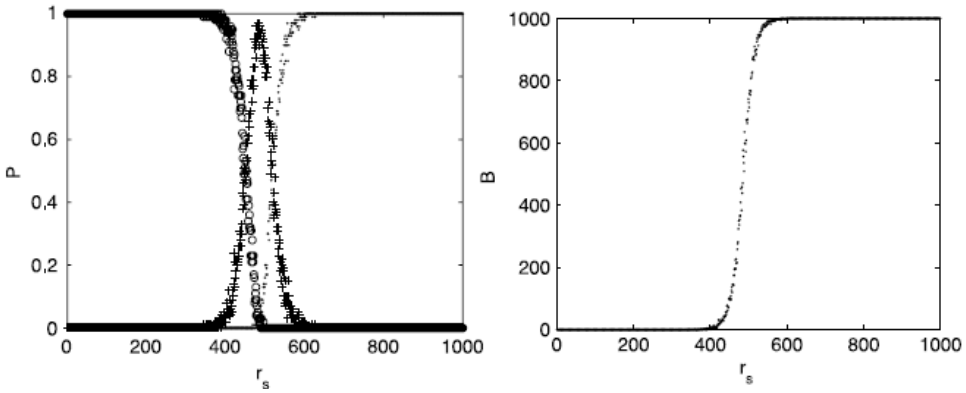

Fig. 3.3 CSF networks: $N = 1000, m = 4$. (a) The probability P that the system evolves into S1, S2 or other steady states under different disturbances r_s: oall the nodes were in status +1, i.e. the system evolves back to its initial state. C some of the nodes were in status +1, others were in status -1; all the nodes were in status -1, i.e. all the nodes were influenced. (b) The average number of influenced nodes B in the long-time behavior for different r_s.

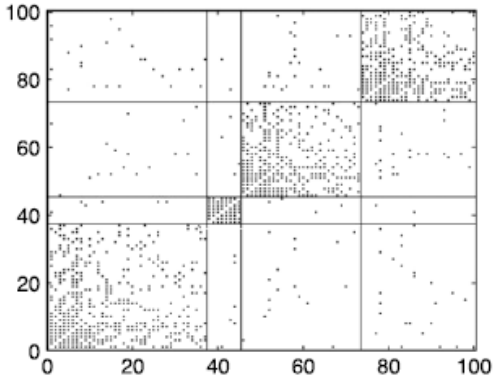

Fig. 3.4 Connection matrix A of the CSF network, $\bullet: A_{ij} = 1, blank: A_{ij} = 0$. The parameters of the CSF network $N = 100, M = 4, M = 6, n = 1$.

average degree. We find (Fig. 3.2) that for the two basic types of stimuli: direct stimuli (changes are made to the most highly connected nodes, the hubs) and random stimuli (changes are made to randomly chosen nodes), CSF networks are more robust than SF networks. Therefore, the community structure enhances the robustness of the networks. In order to see how the community structure influences the robustness of the network, we randomly chose a CSF network to investigate the probability P that the system evolves into S1, S2 or other steady states under different random disturbances.

It is shown in Fig. 3.3 that the CSF network maintains the original states under a small perturbation, which illustrates its robustness to some extent, until the strength of perturbation (numbers of flips r_s) exceeds a critical value. For intermediate stimuli, the system converges to mixed steady states in which some node states are +1 but the others are -1. By increasing the stimuli continuously, all of the nodes are influenced and the system evolves into an all -1

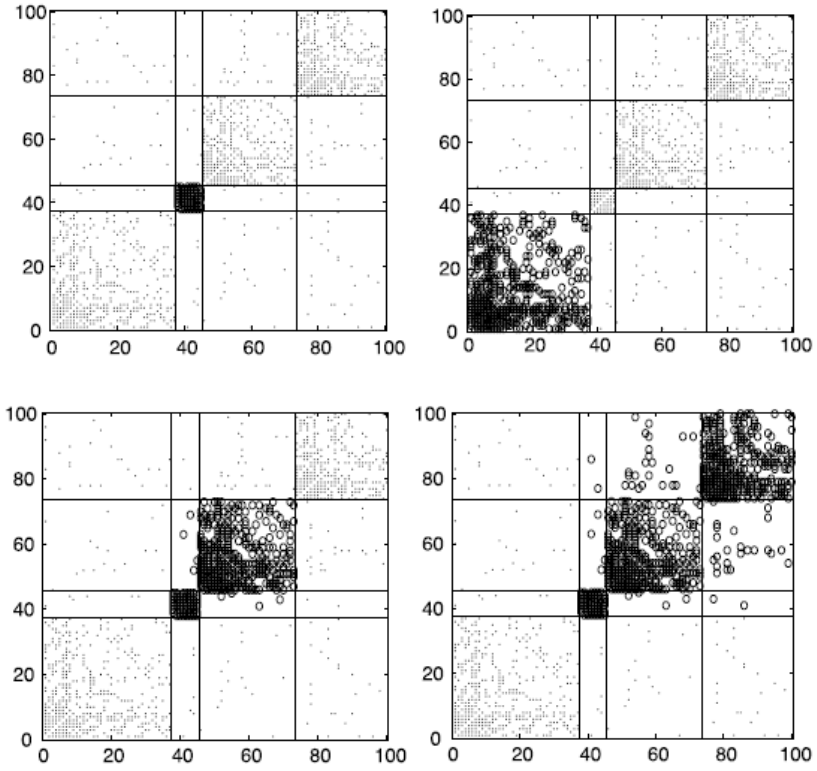

Fig. 3.5 The pattern of R with different initial conditions: $\circ : R_{ij} = -1, \bullet, R_{ij} = 1, blank : R_{ij} = 0$, The parameters of the CSF network $N = 100, M = 4, m = 6, n = 1, \alpha = 1, r_s = 48$

state (S2), which is an extreme response. It should be noted that there are two phase transition points in the process of response. The first one corresponds to the transition of the system from a normal state to partial destruction. The second one corresponds to the transition from partial destruction to complete destruction.

It is interesting to ask: why is the response of a CSF network different from a SF network without modular structure, though the degree distribution of the CSF is also scale-free? In the following, we explore the response patterns for r_s in the intermediate region i.e. in the region between both phase transitions. We randomly choose some nodes to be flipped and identify whose states are changed in the network as the system evolves into a steady state, which illustrates the response to stimuli. To describe the response patterns, a new variable is defined as follows:

$$R_{ij} = \begin{cases} +1, \textit{if } A_{ij} > 0 \textit{ and } s_i = -1, s_j = -1 \\ -1, \textit{if } A_{ij} > 0 \textit{ and } s_i, s_j \textit{ are not in status } -1 \textit{ at the same time} \\ 0, \textit{if } A_{ij} = 0 \end{cases}$$

R indicates which part of the network was influenced. In order to see the patterns clearly, we use a small size network here as an example. The connection matrix is shown in the Fig. 3.4.

We have also found similar results in much larger CSF networks and smaller networks. It is shown in Fig. 3.5 that for certain r_s in the intermediate region; some patterns of R appear with large probability, which almost correspond to the topological communities. Clearly, the community structure plays a crucial role in response to the stimuli. When some segments of the network are destroyed, the community structure can prevent the damage from spreading to other segments. A similar impact of clustering has been also found in Ref. [M. Kaiser, 2007]. This phenomenon can be explained by the underlying structure of communities which has a high density of connections inside the communities and sparse connections with the outside nodes. Therefore, those nodes which connect two communities can hardly be affected by the negative nodes with respect to our majority opinion-like model. In this sense, the network structure coincides well with the dynamical pattern. By detecting some special patterns appearing with high probability, our results are expected to provide a new approach for community detection.

3.5 Response of cat brain networks to stimuli

As an example, the response of cat brain networks to stimuli is analyzed here. The cerebral cortex of a cat can be percolated into 53 areas, linked by about 830 fibers of different densities into a weighted complex network as shown in Fig. 3.6 [C. S. Zhou, 2006]. This network displays a heterogeneous structure, where some nodes have only 2 links while others have up to 35 connections. It is clear that the size of the network is too small to claim that the degree distribution is scale-free. Nevertheless, the distribution is very close to that of networks of the same size and density generated by scale-free models. Moreover, the cortical network of cats exhibits a hierarchically clustered organization. There exists a small number of topological clusters that broadly agree with four functional cortical sub-divisions: visual cortex (V,16 areas), auditory (A, 7(SM,16 areas) and fronto-limbic (FL,14 areas). In addition, this network also displays typical small-world properties, i.e. short average path length and high clustering coefficient [O. Sporns, 2004, C. C. Hilgetag, 2000, 2004, E. D. Bullmore, 2009].

We perform simulations on this network by applying the same dynamics as in our CSF model (Section 3.3). The responsively under different external perturbations can be found in Fig. 3.7 and Fig. 3.8, which is similar to the case of our network model. It can provide insights into the relationship between network topology and functional organization of the cat brain networks from another viewpoint [L. Zemanova, 2006]. Furthermore, we make the stimuli acting on large-intensity nodes or on small-intensity nodes (directed stimuli) other than random stimuli and then see the response pattern of the network. We define the intensity c_i of node i as

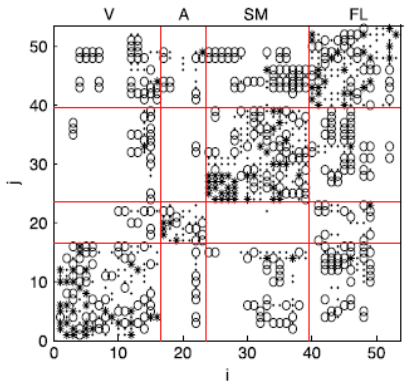

Fig. 3.6 Connection matrix A of the cortical network of cat brain. The different symbols represent different connection weights: 1 (o sparse), 2 (. intermediate), 3 (* dense).

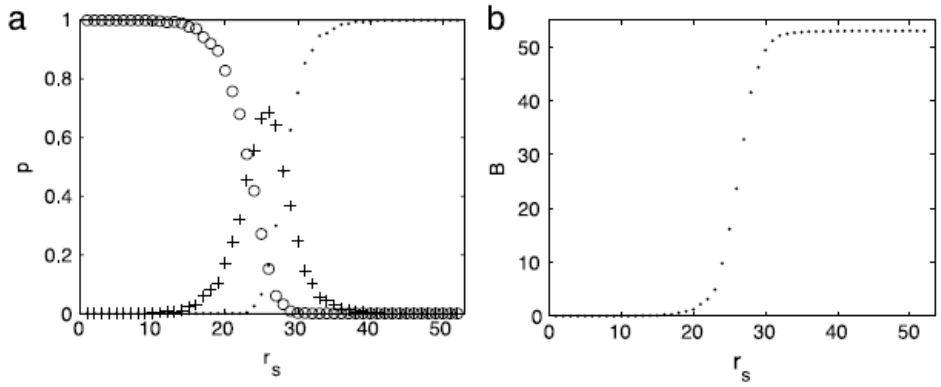

Fig. 3.7 Cat brain network (a) probability P that the system evolves into S1, S2 or other steady states under different disturbances r_s : o: all the nodes were in status +1, i.e. the system evolves back to its initial states. +: some of the nodes were in status +1, others were in status -1, • : all the nodes were in status -1, i.e. all the nodes were influence. (b) The average number of influenced nodes B in the long-time behavior for different r_s

follows: $c_i = \sum_{j=1, j\neq i}^{N} A_{ij}$

In particular, for unweighted networks, the intensity of a node is the degree of this node. It is known that scale-free networks are more robust to random attacks, while more sensitive to directed disturbance to the large-degree nodes. As shown in Fig. 3.8, the brain network can be partially disturbed when $30 > r_s > 16$ directed stimuli are acting on small-degree nodes (shown in Fig. 3.9(b)). On the other hand, the system can be entirely disturbed when $r_s > 24$ for large-node perturbation (shown in Fig. 3.9(a)). It is manifest that the robustness for directed stimuli acting on large-degree nodes is stronger case for directed stimuli on small-degree nodes. This enhanced robustness is also better than the case for random stimuli, which is different from the result in Refs. [Y. Bar-Yam, 2004, S. J. Wang, 2007] for scale-free networks.

Compared with the robustness of the classical scale-free network model, a complex brain network is likely to be more robust for direct stimuli. It should be noted that the brain network displays not only heterogeneity on the degree distribution but also hierarchical clustering characteristic. These special properties may play an important role in the response to stimuli. However, more evidence should be presented in future studies.

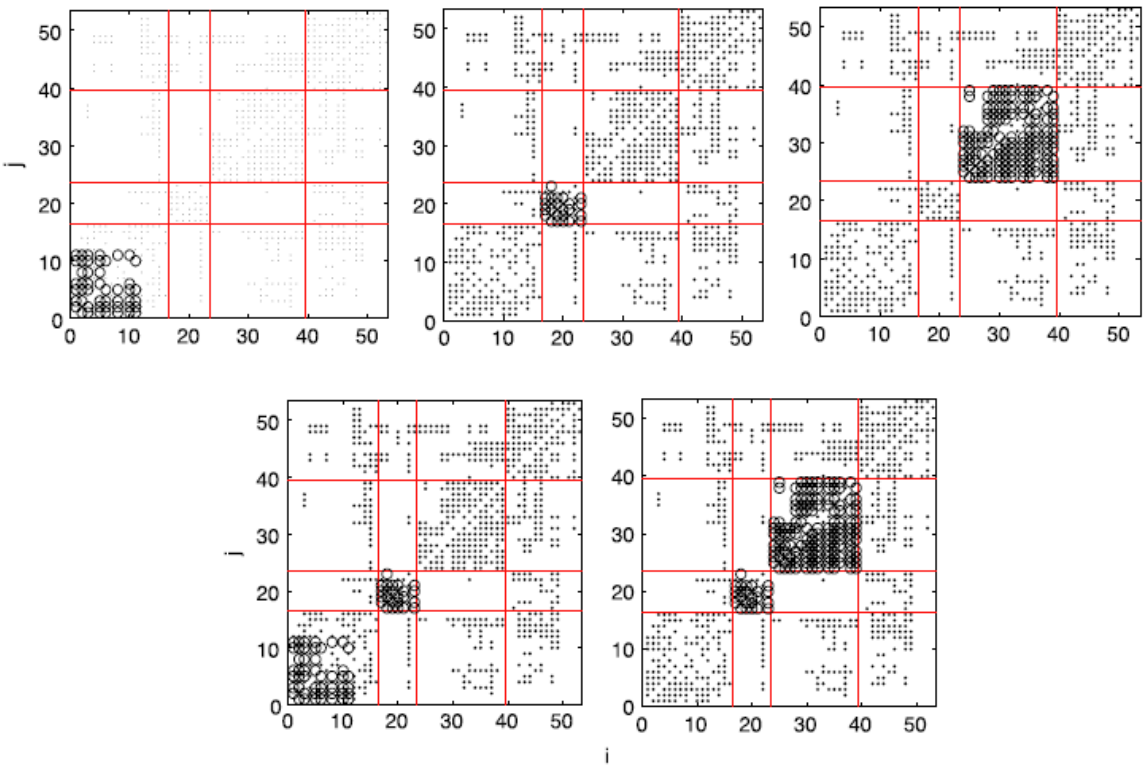

Fig. 3.8 Cat brain networks. The pattern of R with different initial conditions:

$R_{ij} = -1, \cdot R_{ij} = 1$, blank: $R_{ij} = 0. r_s = 25.$

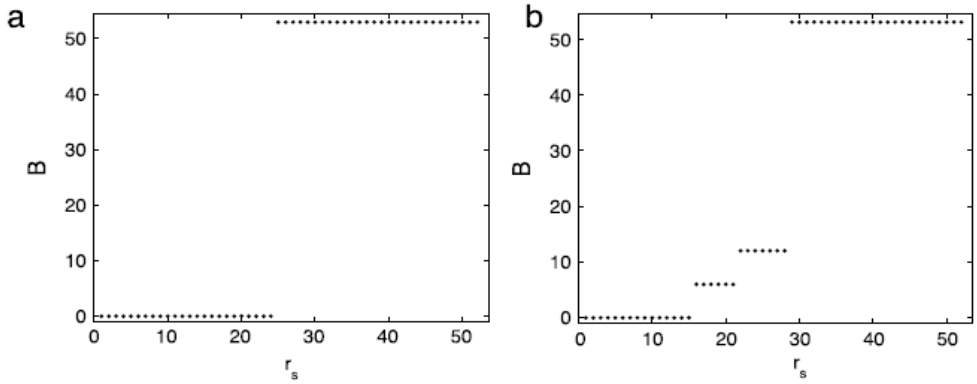

Fig. 3.9 The number of nodes (B) whose states are changed in long-time behavior for different stimuli. (a) the responses for directed stimuli acting on large-degree nodes, (b) The responses for directed stimuli acting on small-degree nodes.

3.6 Conclusion

In this letter, we investigate the relationship between dynamics of complex networks and their topology properties by studying the response of the whole system. An adaptive system should be robust for large stimuli, which makes the system stable. Additionally, it also should be sensitive for small stimuli, which makes the system react rapidly on the new external changes. According to the analysis of the response of scale-free networks with community structure, we find that the hierarchical characteristic of the networks enhances their robustness to external stimuli. Switching patterns are found to coincide with the topology communities. We verify our results in a real-world -cat brain network which has similar topological properties as our model. We show that the robustness for directed stimuli acting on large-degree nodes is better than in the case of directed stimuli on small-degree nodes, which is different from the response in the scale-free networks. Our results provide new insights into the relationship between network topology and the functional organization of the cat brain networks from another viewpoint.

Chapter 4 Modelling the human communication dynamics

4.1 Introduction

Humans participate in various activities every day in an apparently random manner. By assuming that human actions are Poisson processes [F. A. height, 1967, Reynolds, 2003] in which independent events occur at a constant rate λ and the inter-event time τ between two consecutive actions of an individual follows an exponential distribution $P(\tau) = \lambda e^{-\lambda\tau}$, one could perform a quantitative analysis of collective social activities as diverse as disease spreading, emergency response, resource allocation, in particular phone line availability and bandwidth allocation in the case of Internet or Web use.

The recent proposal that human activities are somewhat generically non-Poissonian with power-law waiting times or inter-event times $P(\tau) \propto \tau^{-\gamma}$ due to various possible mechanisms [A. L. Barabasi, 2005, J. G. Olivera, 2005, A. Vazquez, 2005, 2006, J. P. Eckmann, 2004, J. Candia, 2007, A. Gabrielli, 2007, R. D. Malmgen, 2008, 2009, X. P. Han, 2008] should significantly change the quantitative understanding of collective social dynamics, especially when taking into account the complex network structure in social interactions [M. E. J. newman, 2003, D. Rybski, 2009], if those observed non-Poisson activities are solely the behaviour of individual agents. While the power-law waiting time has been regarded as the result of the priority-queuing mechanism of decision-making in individuals [A. L. Barabasi, 2005, J. G. Olivera, 2005, A. Vazquez, 2005, 2006, J. P. Eckmann, 2004, J. Candia, 2007], the inter-event time of a certain type of activity of an individual, such as the interval between sending two consecutive emails, is influenced by the actions of this agent and the other communication partners.

We can distinguish at least two types of communications: (1) initiation by the individual and (2) response to other interacting individuals. Therefore, to distinguish, when possible, what are the properties of separated individuals and what are the consequences of the interactions among individuals, is of paramount importance to elucidate the challenging problem of mutual interplay between individual and collective human dynamics. In particular, are there Poisson processes at all in individual activity, and how do they express themselves when interacting with the decision-making mechanism of individuals and the interaction among individuals? Unfortunately, previously examined data often do not allow us to evaluate precisely both the waiting times and the inter-event times, and a detailed analysis of the relationship between individual and collective human activities is still lacking apart of some simple models of coupled priority queues [J. G. Oliveita, 2009, B. Min, 2009].

Here we address this important problem from both data analysis and modelling. The system we consider is Short Messages (SMs) correspondence; one of the most frequently used communication systems in modern society. Usually, people can only send emails when sitting before the computer. On the contrary, people can send and receive SMs almost anytime and anywhere. The time required to composite a short message is usually much shorter than Email, making it quite possible to get promotes response. But it is also flexible that a short message can be totally ignored without response or can be put into the waiting list as a task with lower priority. These features imply a nontrivial interplay between the activity of single individuals and the interaction with the network neighbours in SMs communication. The system thus provides a very attractive proxy for studying the interaction of human activity.

Here we present clear empirical evidence from Short Messages (SM) correspondence that observed human actions are the result of interplay of three basic ingredients: Poisson initiation of tasks and decision-making for task execution in individual human and the interaction among individuals. This interplay leads to new types of inter-event time distribution, neither completely Poisson nor power-law, but a bimodal combination of them. We introduce a minimal model of two interacting priority-queues incorporating the three basic ingredients which fits well the distributions using the parameters extracted from empirical data. The model can also embrace a range of realistic social interacting systems such as email and letter communications when taking the time scale of processing into account. Our findings provide insight into various human activities both at the individual and network level.

4.2 Empirical result

4.2.1 Data description

The data investigated in this work was obtained from a mobile phone operator. It contains three charging accountant bills from three companies over one month period. Each record comprises a sender mobile phone number, a recipient mobile phone number and a time stamp with a precision of one second. The detailed information about the data is listed in Table 4.1.

Table 4.1. Information of the data sets.

Name of the company	The total number of the records	The number of the users	the number of the active users*
A	548,182	44,430	9,567
B	643,502	72,146	12,162
C	398,185	31,096	7,727

*Who sends more than 5 SMs and receives more than 5 SMs is a active user

For the purpose of retaining customer's anonymity, each subscription is identified by a surrogate key such that it is not possible to recover the actual phone numbers from it. There is no other information available for identifying or locating customers; this guarantees that their privacy is respected.

The inter-event time in our analysis is the time interval between sending two consecutive messages. For active users with at least several messages per day, the longest waiting time during a day is limited to 5-6 hours, on average shorter than the time interval between the last message of one day and the first message of the next day (8-9 hours). We thus exclude the time intervals crossing two days from the analysis, which have negligible effects on our results. Note that such time intervals associated to sleep break may not be so neatly separated for inactive users, and for many other human activity occurring at slower scales.

4.2.2 Bimodal distribution

While the degree, the number of partners of a user can be quite heterogeneous in SMs networks [Y. Wu, 2007], we have found that many users mainly have heavy communication with just one of their friends (see Fig. 4.1); thus in this work we will mainly focus on such pairs of users, with a typical one shown in Fig. 4.2. At a first glance, the burst-silence patterns in individuals (Fig. 4.2(a)) are similar to many other human activities [A. L. Barabasi, 2005, J. G. Olivera, 2005, A. Vazquez, 2005, 2006, J. P. Eckmann, 2004, J. Candia, 2007, A. Gabrielli, 2007, R. D. Malmgen, 2008, 2009, X. P. Han, 2008]. However, the distributions $P(\tau)$ of the

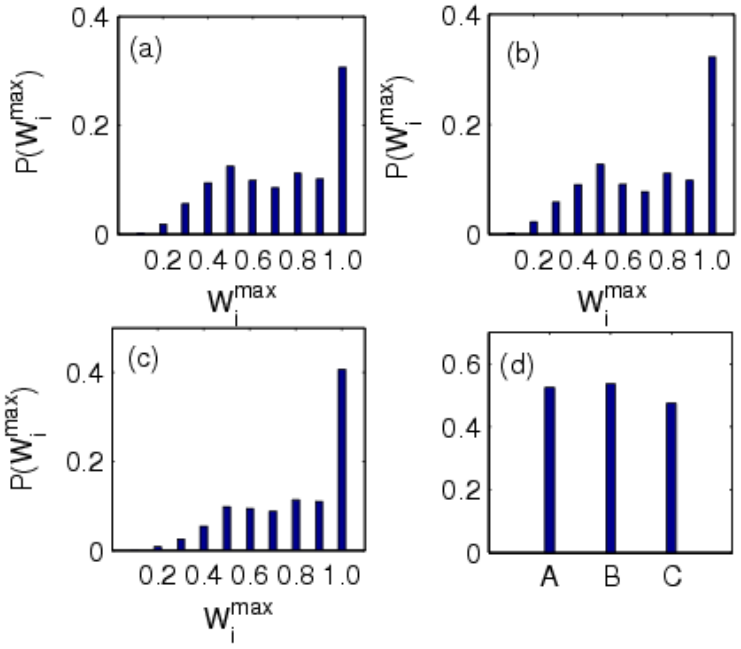

Fig. 4.1 Intensity of communication of the users is highly heterogeneous among their network neighbors. (a)-(c) The distribution of $W_i^{\max}$ in each company. (d) The ratio of active users who send more than 90% SMs to only one friend in each company.

inter-event time τ, the interval between sending two consecutive messages, are bimodal rather than power-law (Fig. 4.2(c,d)): they are power-law in the range of 2-20 minutes, followed by an exponential tail extending to 5-6 hours, which can be well described as:

$$P(\tau) \propto \begin{cases} \tau^{-\gamma}, \tau < \tau_0 \\ e^{-\beta\tau}, \tau > \tau_0 \end{cases} \quad (1)$$

In this bimodal distribution, the exponential tail is connected to the power-law with a hump well above the straight line extrapolation of the power-law. This feature is significantly

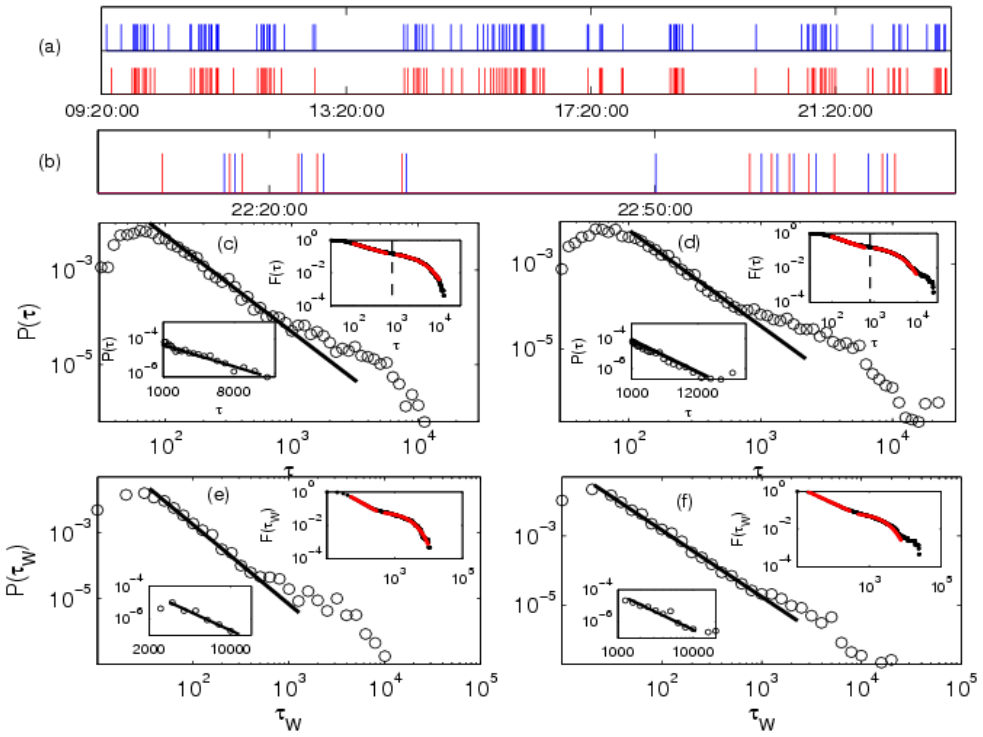

Fig. 4.2 Typical patterns of SMs activity of a pair of users. The users send more than 95% of the messages to each other. (a) Succession of events by user A (blue) and B (red). The horizontal axis denotes time (in 1 second) and each vertical line corresponds to an event of sending a short message. (b) An enlargement of a short period where the events of A (blue) and B (red) are put together, showing clearly a sending-response pattern by the alternating blue and red colours. The interval between two consecutive lines with the same colour is the inter-event time τ and that between two consecutive lines with different colours is the waiting time τ_w. (c) and (d) are the distributions $P(\tau)$ of the inter-event times τ for the users A and B, respectively. $P(\tau)$ is binned in the log-log scale. The upper inset displays the corresponding accumulative distribution $F(\tau)$. The vertical dotted line indicates $\tau_0 = 780$, which is determined in the SI to separate the event sequence into independent bursts. The lower inset shows the exponential tails of $P(\tau)$ in the linear-log plot. The straight lines are the power law and exponential fitting functions, which are correspondingly shown by the red line and red curve in the upper inset. The exponents are: $\gamma_A = 1.79 \pm 0.01, \beta_A = (3.78 \pm 0.02) \times 10^{-4}$ and $\gamma_B = 1.93 \pm 0.05, \beta_B = (3.90 \pm 0.03) \times 10^{-4}$ (e) and (f) as (c) and (d), but for the distributions $P(\tau_w)$ of the waiting times τ_w. The exponents are $\gamma_{wA} = 2.12 \pm 0.01, \beta_{wA} = (4.34 \pm 0.04) \times 10^{-4}$, $\gamma_{wB} = 1.90 \pm 0.02, \beta_{wB} = (3.63 \pm 0.03) \times 10^{-4}$.

different from the usually truncated power-law with the form $\tau^{-\gamma}e^{-\beta\tau}$, where the exponential tail is below the straight line of the power-law and is often considered as finite size effects [A. Vazquez, 2006]. Note that in a recent report of SM statistics [W. Hong, 2009], the distributions have been regarded as power-law for the tails also, without paying special attention to the humps and the underlying mechanisms.

We can see that the burst-silence patterns of the two users appear to be synchronized (Fig. 4.2(a)). A clear sending-response pattern is observed by alternating colours when we join the events of both users (Fig. 4.2(b)), and we obtain the waiting time τ_w between two consecutive events with different colours. Similar to the inter-event time τ, the distributions $P(\tau_w)$ also display pronounced bimodal features (Fig. 4.2(e,f)), in contrast to the prediction of power-law tails from the priority-queuing mechanism [A. L. barabasi, 2003, A. Vaquez, 2006].

The bimodal feature of the distribution is found to be general, including those users with many active partners. The exponents γ, γ_w and β, β_w differ from user to user (see Fig. 4.3).

These results are significantly different from previous observations of power-law heavy tails in other human dynamics, such as e-mails. The clearly distinguished distributions at small and large intervals imply that there are different processes underlying the observed patterns.

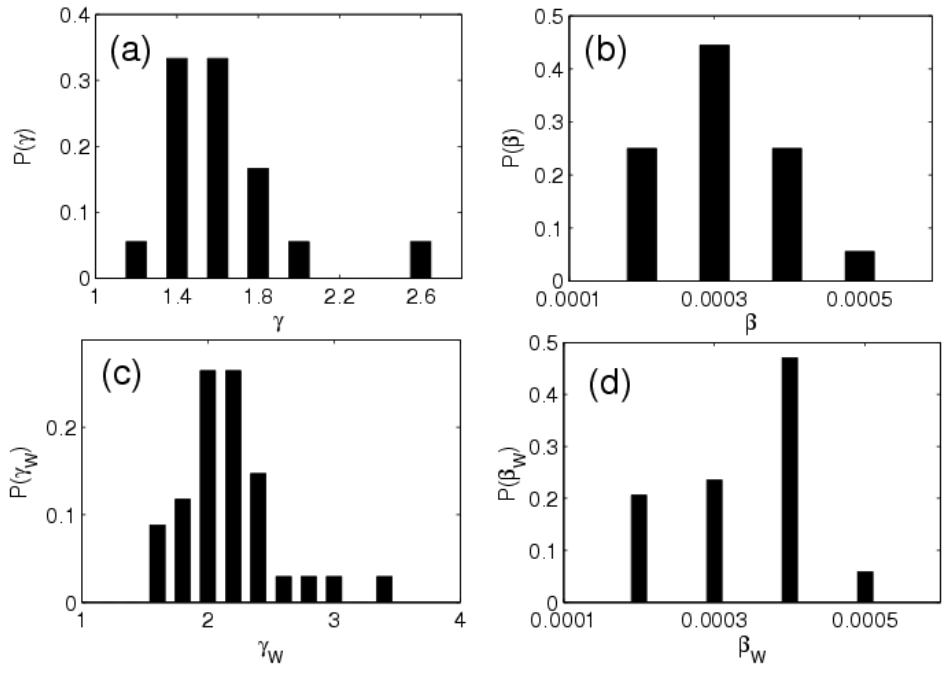

Fig. 4.3 The histogram of the exponents. (a) γ, (b) β, (c) γ_w and (d) β_w for 36 most active users having the total number of messages $N \geq 800$, considered for good statistics.

Fig.4.2(b) shows that a burst is initiated by one of the users, which is then followed by frequent mutual communications. SMs or emails suggests that quite likely the initiation of communication over a topic could require a few dense mutual responses. The pronounced exponential tails in the distributions imply that the initiation of communication of the two users could be regarded as independent Poisson processes, which is consistent with the intuition of initiating relatively independent topics of communications in a random manner.

4.3 Our model

4.3.1 Model description

The model we proposed here differs significantly from previous models of interacting queues. When considering two users as motivated by the empirical observation, it is a minimal model that incorporates the basic ingredients we observed in the data. In the following we present more detailed information and analysis of the model. The model consists of two main parts:

(i) Priority-queue of tasks of individuals.

Consider two individuals A and B, each with a priority list of L tasks. The L tasks correspond to different activity, ranging from sending SMs, shopping, sending emails to attending meetings, etc. A short message task, in particular, sending a message, is marked as I-task, while the others are denoted as O-tasks. At each *processing step,* i.e. every t_p seconds (1 second is the sampling precision in our SMs data and in many previous data of email communications), a task is executed and removed from the list, and a new task is added. As we will discuss later on, the introduction of the processing time t_p is very important because (1) it is obviously not realistic to consider the sampling time of 1 second as the time of actions, as has been done in previous analysis of email communications [A. Vazquez, 2006]; (2) without introducing t_p the model cannot fit to the data while using all the other parameters from the data; and (3) the introduction of t_p enables us to explain the observation of power-law inter-event time in email communications. Of course, in reality the processing time is different for different types of tasks and fluctuates for tasks of the same type, but for simplicity we assume that it is the same for different tasks. We have also simulated the model with a random distribution of t_p and obtain very similar fitting to the data.

The tasks on the list compete with each other for the agent's time and attention. Each task is assigned a priority x chosen from a uniform distribution $x \in (0,1)$. The probability to choose a task for execution is a function of the priority x i.e., $\prod(x) \propto x^{\alpha}$, where the parameter α can be used to indicate different habits of individuals in the execution of tasks. This part of the model is the same as the standard model proposed in [A. L. Barabasi, 2005].

To account for random initiation of communication observed in the data, the I-tasks are added

to the list with a probability $\lambda_p = \lambda t_p$ at each processing step. λ is the rate of initiating an I-task in the sampling time unit of 1 second, as obtained from the data. I-tasks can also be added to the list of one individual as a result of the communication from the other individual, which will be discussed in more detail in the following.

(ii) The interaction between individuals.

An interaction occurs when A or B (or both) selects an I-task in the list. For example, when A selects an I-task, A sends a short message to B. B then decides whether to reply a SM to A or not. According to our experience, SMs are mostly replied, but not always, which is consistent with the high response rates $P_{A,B}$ which would be obtained from the data later on. We assume that each received message is replied with the probabilities P_A, P_B for the two users A and B, respectively. If B decides to reply, an I- task with random priority x is added to the task list of B to wait for execution according to the priority-dependent selection scheme in *(i)*. When the I-task is executed by B, it is A's turn to decide whether to reply, with the probability P_A. Depending on the product $P_A P_B$, there are a number of consecutive mutual communications until someone decides not to reply, governing the number of messages sent by a user during a burst of communication. The same procedure happens if B initiates the communication. If A and B execute the I-task at the same time, one task is randomly ignored. But this happens with only a very small probability. The priority-queue in our model is substantially different from previous priority-queuing models [1] mainly by introducing a processing time t_p, by distinguishing the interacting I-task from the other tasks, and by adding the I-tasks with a small probability λ. The interaction between the individuals in our model is also different from previous models [J. G. Oliveita, 2009, B. Min, 2009], where the interaction follows the AND-protocol (both individuals select the I-tasks) or the OR-protocol (one individual selects the I-task and the other is forced to execute the I-task). In both protocols, the I-tasks are executed simultaneously by the two individuals, and a new I-task is added to each list immediately after the interaction. The interaction in our model shows some similarity to the OR-protocal, but the receiver may choose not to reply at all, or put the message in the priority-queue list to reply later. These new features will generate different inter-event time patterns compared to previous models, which can provide a rather comprehensive understanding of SMs and other types of interacting human activity.

There are three important parameters in our model, $P_i, \lambda_i,$ and α_i. P_i is the probability that a passivity I-task is added to the list of an agent when the other agent executes an I-task, λ_i is the rate of adding initiative I-tasks and α_i controls the probability $\prod(x) \propto x^{\alpha}$ to select a task for execution according to the priority x.

4.3.2 Estimating important parameters from data

The most important concept in our work, as suggested by the bimodal distribution of the inter-event time, is to associate the power-law distribution at small intervals and the exponential distribution at large intervals to different communication modes, one is correlated, passive and frequent sending-response in the bursts and the other one is random initiation of the bursts. Without relying on the contents of the communications, we are able to separate events into independent bursts and estimate important parameters from the data, in particular, the probability of response and rates of random initiation of bursts for the two users ($P_i, \lambda_i, i = A, B$), which can be used in our model simulations. Here we present the detailed methods of burst separation and parameter estimation.

1) The parameter P_A, P_B

A straightforward method to separate the bursts is to consider a crossover time τ_0. The mutual communications between the two users A and B become very evident by alternating red and blue colors when we join the events of the two users together (Fig.4.2(b)). With such a joint sequence of events from the two users, we can take two events (regardless of the color) with an interval larger than τ_0 as the ending of one burst and the beginning of another one, so that the whole sequence is broken into bursts with various sizes. At first place, we take some values of τ_0 around the crossover point from the power-law to exponential distribution in Fig. 4.2(c,d) (e.g. $\tau_0 = 600 \sim 900$), and we do not worry about the exact value of τ_0, because later on a more accurate τ_0 will be determined with the additional requirement that the separated bursts are best approximated as random processes (see next section). Important here is that we obtain a reliable and consistent estimation of the response rates P_A, P_B using a range of τ_0. After we separate the bursts using certain τ_0, we can divide them into two groups: one is initiated by user A and the other by B, by examining whether the first message (called initiative message) of the burst is blue or red. For each group, we can get the number of bursts where the *i*-th message in the burst is sent by A or by B, and denote them with bars of blue and red colors (Fig. 4.4 (a,b) for the two groups, respectively). From Fig.4.4 (a), it is clearly seen that after the initial message from A to B (the first blue bar), the next SMs are almost the response of B to A (red), and then the response of A to B, etc. There are a few mutual communications after the initial message. We can estimate the ratio of response for the two users from the two groups: $P_A^{A\to B}(i) = n_{i+1}(blue)/n_i(red)$ and $P_B^{A\to B}(i) = n_{i+1}(red)/n_i(blue)$ from Fig. 4.4(a), and likewise $P_A^{A\to B}(i) = n_{i+1}(red)/n_i(blue)$ and $P_B^{B\to A}(i) = n_{i+1}(red)/n_i(blue)$ from Fig. 4.4(b). Here the superscripts $A \to B$ and $B \to A$ denote the two groups of bursts initiated by A and B, respectively.

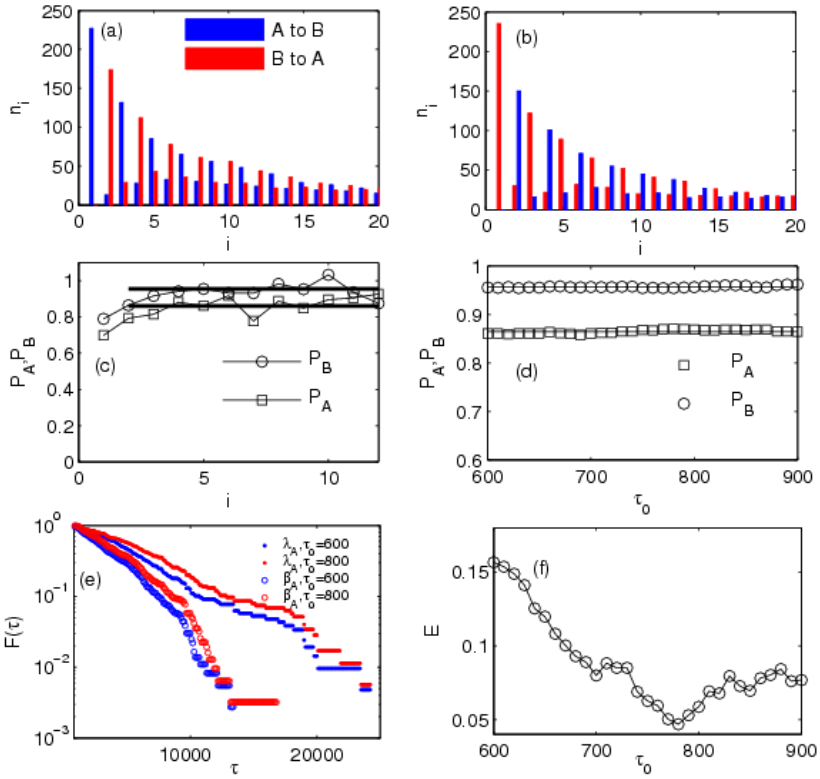

Fig. 4.4 Separation of bursts and estimation of parameters from data. (a) and (b) Communication patterns within the separated bursts (obtained at certain τ_0) that are initiated by user A and B, respectively. The index i denotes the position of the message in a burst, and the height of the bar (n_i) is the number of bursts having a message at position i by user A (blue) or user B (red). (c) The response probability of the two users estimated at position i. (d) The average response probability estimated at different τ_0. (e) Accumulative distributions of the interval τ_λ between two consecutive initiative messages by the same user A and the interval τ_δ between two consecutive bursts either initiated by A or response to the initiative message of B. Linear approximation of these plots in linear-log scale gives the rates λ_A, δ_A, which decreases at larger τ_0. The plots are similar for user B (not shown). (f) Relative error $E(\tau_0)$ displays a minimum where the initiations of bursts in the two users are best approximated by independent Poisson random processes.

The average of the two groups, $P_{A,B}(i) = (P_{A,B}^{A\to B}(i) + P_{A,B}^{B\to A}(i))/2$, is roughly independent of the position i of the message in the bursts (Fig. 4.4(c)), which means that when A (B) receive a SM from B(A), he/she responds with an almost constant probability. Further averaging over the positions i ($i = 3-10$) improves the statistics and these averaged values are almost constant with respect to τ_0 (Fig. 4.4(c)). This is because the pattern of communication in the middle of the bursts is rather independent of the definition of the bursts at different τ_0 which only affects the first and the last few positions of some bursts. We take the average in the range $\tau_0 = 600-900$ as the response probability $P_{A,B}$ of the two users, giving $P_A = 0.865, P_B = 0.957$ for the example presented here.

2) The parameter λ_A, λ_B

After identifying the bursts with a given τ_0, we pay attention to the statistics of the bursts. We can easily distinguish whether a burst is initiated by user A or B by the color of the first message leading a burst, and compute the rates of initiation as λ_A, λ_B (by definition, the number of initiations divided by time). At the meanwhile, we can sort the separated bursts into two groups (G_A, G_B) of a new type. The group G_A for user A includes the bursts initiated by user A (the first message is blue) and the responses to the initiative messages of B (the first message is blue and the second message red). And similarly we obtain G_B for user B and get the rates of such bursts as δ_A, δ_B respectively. If the bursts were separated properly, we would expect that the initiation of communications by A and B are independent Poisson processes. Neglecting the very small portion of messages that are not sent to each other, the number of bursts in the group G_A should include the number of initiations messages by A himself and the responses to those initiative messages by B with the probability P_A. Thus the rates of the two independent processes are related as $\delta_A = \lambda_A + P_A\lambda_B(1-\lambda_A) \cong \lambda_A + P_A\lambda_B$ ($\lambda_A\lambda_B << 1$). Likewise, for the user B we have $\delta_B \cong \lambda_B + P_B\lambda_A$.

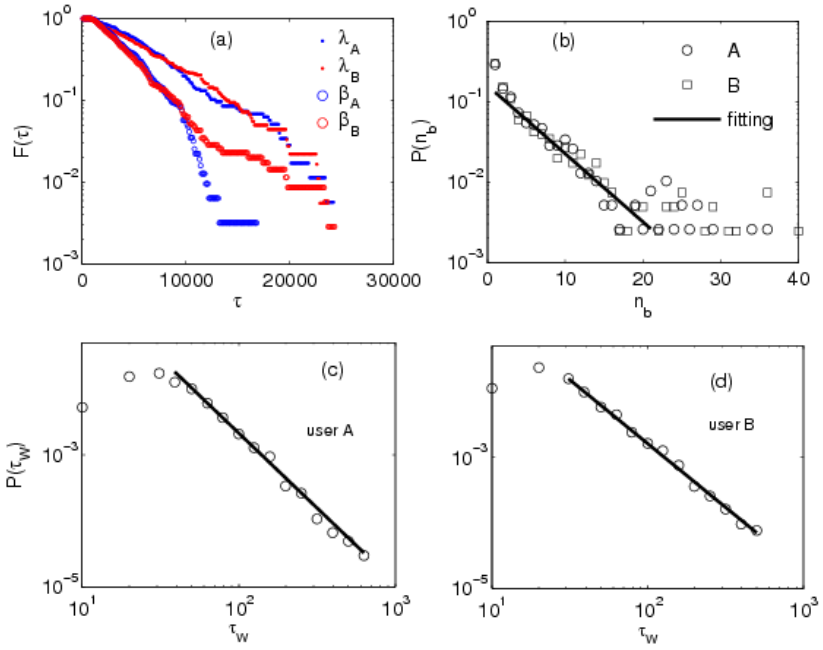

Fig. 4.5 Separation of the initiative and passivity messages with the most suitable τ_0. (a) Accumulative distributions $F(\tau)$ for the interval between two consecutive bursts that are initiated by the same user A (with rate λ_A) and the interval between two consecutive bursts that can be either initiated by A or the response to an initiative message of B (with rate δ_A). These rates of the two users satisfy the relationships $\delta_A \cong \lambda_A + P_A\lambda_B$ and $\delta_B \cong \lambda_B + P_B\lambda_A$, implying that the initiation of communications in the two users are independent Poisson processes. (b) The distribution of the size n_b of the separated bursts. The solid line is the exponential fitting $(P_AP_B)^{n_b}$. (c,d) Distributions $P(\tau_w)$ of the waiting time τ_w obtained only from the messages within the separated bursts, for the user A and B, respectively. The solid lines are the power law fitting with $\gamma_{wA} = 2.05 \pm 0.01, \gamma_{wB} = 1.89 \pm 0.01$.

While the estimation of the response rates $P_{A,B}$ using the messages within the bursts is rather insensitive to the choice of τ_0, as discussed Section 4.3, the rates $\lambda_{A,B}, \delta_{A,B}$ decrease when a larger τ_0 is employed.

In our analysis, due to the small number of bursts in the data, the rates are not calculated directly by the number of bursts. Rather we examine the interval τ_λ between two consecutive bursts initiated by the same user (related to $\lambda_{A,B}$) and the interval τ_δ between two consecutive bursts that can be either initiated by the user or the responses to an initiative message of the other user (related to $\delta_{A,B}$), and we obtained the accumulative distributions of these intervals τ_λ and τ_δ, respectively (Fig.4.4(e), only user A is shown). The distributions display a linear dependence in the linear-log plots which support the hypothesis that the initiation of bursts can be well approximated by a random Poisson process. By fitting exponential functions to these distributions we can overcome strong finite size effects in the data and obtain more reliably the rates $\lambda_{A,B}, \delta_{A,B}$. The assumption of independent Poisson processes in the two users is used as the criterion to select the most suitable τ_0. This means that the two relationships are best satisfied,

$$\begin{cases} \delta_A = \lambda_A + P_A \lambda_B, \\ \delta_B = \lambda_B + P_B \lambda_A, \end{cases} \qquad 4.1$$

which corresponds to the minimum of the relative error function:

$$E(\tau_0) = \left(\left| \delta_A(\tau_0) - [\lambda_A(\tau_0) + P_A \lambda_B(\tau_0)] \right| + \left| \delta_B(\tau_0) - [\lambda_B(\tau_0) + P_B \lambda_A(\tau_0)] \right| \right) / \left(\delta_A(\tau_0) + \delta_B(\tau_0) \right). \qquad 4.2$$

For the pair of users considered here, we found that E is minimal at $\tau_0 = 780$ (Fig. 4.4 (f)), and the corresponding rates are $\lambda_A = 1.490 \times 10^{-4}, \lambda_B = 1.587 \times 10^{-4}, \delta_A = 2.708 \times 10^{-4}, \delta_B = 2.906 \times 10^{-4}$.

With the bursts obtained using this optimal τ_0, we examine the distribution of the waiting time τ_w for the two users (the interval between two consecutive lines with different colors in the bursts). As shown in Fig. 4.5(c,d), the waiting time displays power-law distribution. The interval between the last message of one burst and the first message of the next burst, if they have different colors, are not considered as waiting time, because in our framework of analysis, we regard the two bursts as independently initiated communications, although we cannot fully exclude the possibility that the next burst is indeed the response to the first one. If we take these long intervals into the distribution of the waiting time, we observe a pronounced bimodal feature as in distribution of inter-event times (Fig. 4.2(e,f)). The separation procedure proposed here is heuristic because the waiting times in the bursts and those relatively small

intervals of random initiation are unavoidably overlapping. The separation is meaningful when the crossover time is clearly smaller than the characteristic Poisson interval, $\tau_0 << 1/\beta$, which is the case for most of the active users in the data set, with clear bimodal distributions of the inter-event times.

4.4 Fitting the model to the data

We simulated the model using the parameters $\lambda_A, \lambda_B, P_A, P_B$ extracted from the data by separating the events into independent bursts (see Sec. 4.3). For the parameters α_i used in priority-queues, we take $\alpha_i = 1/(\gamma_{wi} - 1)$, where γ_w is the exponent in the power-law distribution of the waiting time τ_w within the bursts in the data (Fig. 4.5(c,d)). This is based on the theoretical formula developed in [A. L. Barabasi, 2005] for this priority-queue model where it is predicted that $\gamma_w = 1 + 1/\alpha$. With these parameters, the model is simulated to generate the same number of events as in the data. We find that the distribution of the inter-event times from the model cannot fit to that of the data when $t_p = 1$, but moves closer, when t_p increase and then deviates again. We monitor the quality of fitting by the relative difference E between the accumulative distributions $F^M(\tau)$ of the model and $F^D(\tau)$ of the data, binned in the log-log scale with K bins:

$$E = 2\frac{\sum_{k=1}^{K}\left|\ln(F^M(k)) - \ln(F^D(k))\right|}{\sum_{k=1}^{K}[\ln(F^M(k)) + \ln(F^D(k))]}. \qquad \text{(S3)}$$

E has a minimum at $t_p \sim 10$, where the model fit well the distributions of the inter-event and waiting times from the data (Fig. 4.6).

4.5 Analysis of the model

4.5.1 The effect of the parameters

In the following we present a more detailed analysis of the model in order to understand the bimodal inter-event distributions. An important ingredient in our model is the interaction between the individuals with response rates $P_{A,B}$. Without loss of generality and for simplicity of discussion, we assume that the parameters of the two queues are the same, in particular, $P_A = P_B = P_1$. We also take $t_p = 1$ for the analysis in this subsection. The effect of P_1 on the distribution of inter-event time τ is shown in Fig. 4.7 when the other two parameters λ and α are fixed. At the extreme case $P_1 = 1$ the process happens as follows: A sends a message, B receives it and waits for a time τ_{wB} to reply to A, and then A receives it and waits for a time τ_{wA} to send back again. The time interval between sending two SMs by A (or B), i.e., the inter-event time, is $\tau = \tau_{wA} + \tau_{wB}$. Here each of the priority-queue of A or B is the same as the original model [A. L. Barabasi, 2005] where the waiting time is a

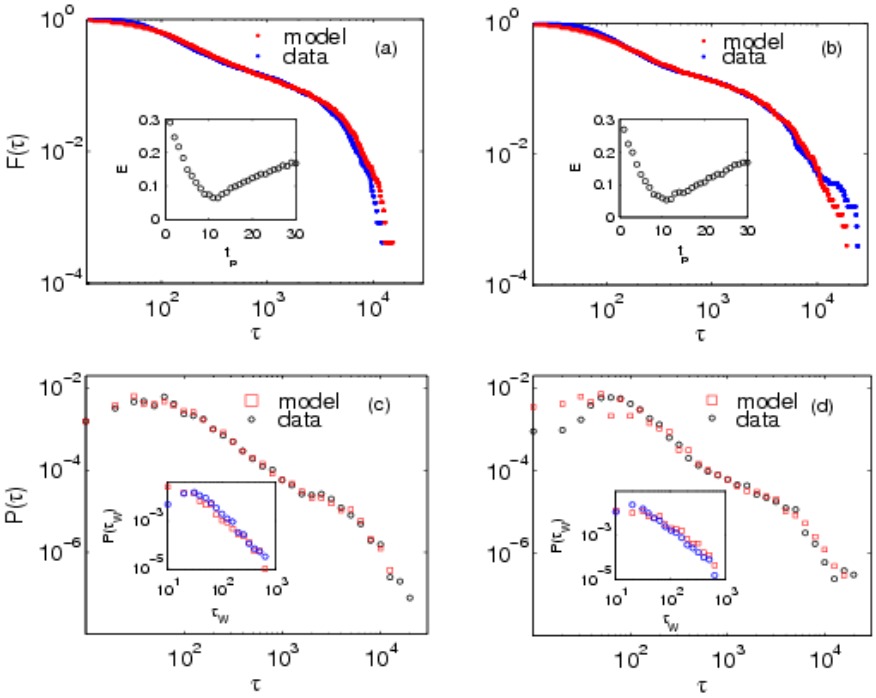

Fig. 4.6 Fitting of the model to data. The model is simulated for various processing time t_p, using all the other parameters obtained from the data, to generate the same number of events as in the data. The relative difference E between the accumulative distributions $F(\tau)$ of the inter-event times τ in the model and data, is obtained as a function of t_p (averaging over 10 realizations of independent model simulations) (insets of (a, b)). E is minimal at $t_p = 10$ for both users, yielding very accurate fitting of $F(\tau)$ (a,b), $P(\tau)$ (c, d) and $P(\tau_w)$ (insets of (c, d)), except for a few points with the minimal and maximal intervals mainly due to finite size fluctuations.

power-law $P(\tau_{wi}) \propto \tau^{-\gamma_{wi}}$.

The distribution of τ as a sum of the two queues is also a power-law, taking the form $P(\tau) = \tau^{-\gamma_{\min}}$, where $\gamma_{\min}$ is the smaller value of the exponents γ_{wA} and γ_{wB} in the queues A and B [5]. Here in our discussion, the parameters of the two queues are identical, so that $P(\tau) \propto \tau^{-\gamma}$ ($\gamma = \gamma_w = 1 + 1/\alpha$). Since the I-tasks due to communication are created with a much higher probability than the Poisson rate λ, the inter-event time pattern will be dominated by the power-law, as seen clearly in Fig. 4.7. Note that the case of $P_1 = 1$ in our model corresponds to a model previously proposed to explain the power-law inter-event times in email communication from the power-law waiting times due to priority-queuing mechanism [A. Vazquez, 2006]. There it was assumed that email communication is the process that A sends an email to B as a response to an email B sent to A and vice versa in an endless manner [A. Vazquez, 2006]. This is in contrast with the intuition about email communication where we do have mutual responses, but do not reply every email (thus $P_1 < 1$), and we also initiate independent communications in addition to passive responses.

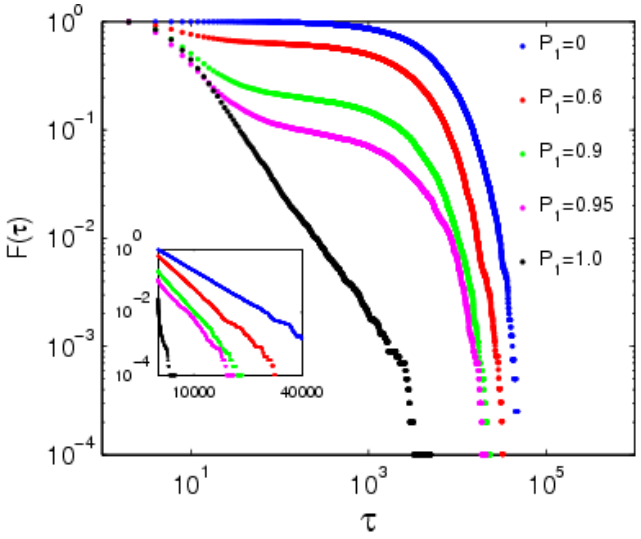

Fig. 4.7 Effect of interaction on human activity patterns in the model. The cumulative distribution $F(\tau)$ of the inter-event times obtained at various response rates P_1. The other parameters are fixed as $\lambda = 1.5\times10^{-4}, \alpha = 1.0, t_p = 1$. The inset shows the exponential tails in the linear-plot.

It is important to emphasize that the activity patterns are very sensitive to P_1. As seen in Fig. 4.7, when P_1 is only slightly smaller than 1.0 (e.g., $P_1 = 0.95$), the distribution is no loner a complete power-law, but clearly bimodal with a pronounced exponential tail. This happens because frequent mutual communication will be terminated: the probability to get bursts of large size decreases exponentially ($\prod(n_b) \propto P_1^{2n_b}$). This means that the mechanism of mutual response as proposed in [A. Vazquez, 2006] cannot explain the power-law behavior in the email communication when P_1 is not exactly 1.0, and we need to seek an alternative, more natural explanation which allows generating a power-law distribution with $P_1 < 1$. This will be discussed in more detail soon.

A value of P_1 close to but less than 1.0 is important for a pronounced bimodal distribution. The bursts have an average size $\overline{n}_b = 1/(1-P_1^2)$. Here a large number of SMs are replied, but they are put into the waiting list with a random priority x, and the inter-event time for these events follows a power-law distribution $P(\tau) \propto \tau^{-r}$. The cut-off of the power-law distribution by the finite event size $\overline{n}_b$ leads to a crossover waiting time τ_0, with the relationship $\int_{\tau_{0p}}^{\infty} P(\tau)d\tau = 1/\overline{n}_b$, where $\tau_{0p} = \tau_0 / t_p$ is the cut-off in the unit of processing step. Taking the power-law distribution $P(\tau) \propto \tau^{-\gamma}$, we get

$$\tau_0 \propto t_p(\overline{n}_b)^{1/(\gamma-1)} \propto t_p(1-P_1^2)^{-1/(\gamma-1)}. \qquad 4.1$$

Thus the crossover time τ_0 is on average larger if P_1 is closer to 1.0 because there will be larger number of SMs in a burst. As a result we observe a regime of power-law distribution of the inter-event time: there are many more short and intermediate intervals than we can expect

from the Poisson processes only. The bursts and the power-law regime will not be clearly observable when P_1 becomes smaller, since $\bar{n}_b = 1/(1-P_1^2)$ becomes too small and the distribution is dominated by the exponential function, e.g., when $P_1 = 0.6$.

As seen from the inset of Fig. 4.7, the inter-event time distributions display pronounced exponential tails when $\lambda << 1$, with the exponent β depending on the value of $P_1 < 1$. The exponential tails can be understood as follows: (1) The two users initiate communications independently with the rate λ, and respond to each other with the probability P_1. Consequently in the event sequence of an individual, we observe independent bursts either initiated by the individual or the response to the other with the rate $\delta = \lambda + P_1\lambda$, and the interval between the first message of two consecutive bursts is τ_δ. In the inter-event distribution $P(\tau)$, the tail corresponds to long intervals between the last message of one burst and the first message of the next burst, $\tau = \tau_\delta - \tau_b$, where τ_b is the total time spent in the first burst. The interval within the burst follows the power-law distribution, and $\tau_b = n_b \int^{\tau_0} P(\tau)\tau d\tau \sim \tau_0$. As a result, for those long intervals we have $\tau \approx \tau_\delta$, corresponding to the exponential tails with the exponent $\beta \approx \delta = \lambda + P_1\lambda$ when $P_1 < 1$.

4.5.2 From bimodal to truncated power-law distribution

A pronounced bimodal distribution with clear power-law and exponential parts can be observed when the cut-off time $1 << \tau_0 << 1/\beta$, where $1/\beta$ is the characteristic interval of the Poisson process to initiate the bursts. The distribution will shift to a truncated power-law if the extrapolation of the power-law moves above the exponential tails, i.e., $a\tau^{-\gamma} > be^{-\beta\tau}$ for $\tau > \tau_0$, where a *and* b are the normalization constants. This happens when $\tau_0 > (\ln(b/a) + \gamma)/\beta \approx 1/\beta \sim 1/\lambda$. This analysis shows that when the cutoff time τ_0 become comparable to the characteristic interval size $1/\lambda$ of the Poisson process of random initiation of communication, the bimodal distribution will move to a truncated power-law better described by the form $\tau^{-\gamma}e^{-\beta\tau}$. In email communication, such an exponential cut-off has been understood from the viewpoint of mathematics [A. Vazquez, 2006]: the scaling $P(\tau) \sim \tau^{-\gamma}$ cannot hold for infinitely long times because the resulting probability density cannot be normalized for $\gamma \leq 1$. Therefore, a natural cut-off should emerge for large τ. In our framework, however, the power-law and the exponential distributions are explained by different processes, associated to interaction between individuals and random initiations of individuals, respectively. There is indeed a cut-off of the power-law, but it is resulted from the finite number of mutual communications within a burst due to the fact that the response rate $P_1 < 1$. Clearly, these new interpretations provide a much deeper understanding of interacting human activity.

4.6 Discussion

4.6.1 Extension to other human activity

The three ingredients clearly identified from the empirical data of SMs communication, the task execution basing on the priority-queuing and random initiation of tasks of individuals and the interaction among individuals, are common in many other interacting human activities, including previously analyzed email and letter based communications. Therefore, our model should be able to explain some basic observations of these systems as well.

Indeed, in the letter communication, the waiting time distributions without separating the initiative and passivity messages do show clear bimodal features with humps in the exponential tails (e.g., see Fig. 4 (a,b) in [A. Vazquez, 2006], similar to but not as pronounced as that in SMs (Fig. 1(e,f)). In Ref. [A. Vazquez, 2006] it has been pointed out that the inter-event time distribution appears to be a power law, but not stationary, mainly due to non-stationary activity of letter communications over a long time span (over 70 years for Einstein and Darwin). When a shorter period of 10 years is examined, an exponential distribution is observed for the inter-event time. In our model, this could be understood by a relatively small response rate P_1 as intuitively expected for letter communication. For example, we will no longer observe pronounced long bursts if we take $P_1 = 0.7$ where the average size of the burst $\bar{n}_b \approx 2$; consequently, there will not be a clear regime of power-law distribution, and the inter-event time distribution will be best described as an exponential function.

As for email communication, previous data show that the inter-event intervals extend to $\sim 10^4$ seconds similar to SMs, but the inter-event distribution has been described as a power-law. While a close inspection of the distributions in the previously published results (e.g., Fig. 2(b) in Ref. [A. Vazquez, 2006]) does indicate the bimodal feature, it is not as pronounced as in SMs. Two assumptions used in the previous analysis of the email communication [A. Vazquez, 2006] are not realistic. (1) Email communication is the process that user A sends an email to B as a response to an email B sent to A and vice versa, so that all the messages are replied (i.e., $P_1 = 1$) and (2) The sampling time of 1 second is taken as the time unit of the action. Clearly our model of interacting queues with $P_1 < 1$ provides a more natural and realistic description of email communication. In this case, if we take a small rate $\lambda \sim 10^{-4}$ corresponding to $\sim 10^4$ seconds of longest intervals in emails, the inter-event time distribution would display a very pronounced bimodal feature even though P_1 is rather close to 1.0 if the processing time is considered to be 1 second ($t_p = 1$) (see Fig. 4.7). This happens because $\tau_0 << 1/\lambda$. As discussed in Sec. 4.4, when τ_0 becomes larger and comparable to $1/\lambda$, the bimodal distribution will shift to a power law. This can be achieved when t_p is

increased, as seen in Fig. 4.8. The distributions in Fig. 4.8(c) and (d) are very similar to previously reported email activities (e.g., Fig. 2(b) in Ref. [A. Vazquez, 2006] and Fig. 2(a) in Ref. [A. L. Barabasi, 2005]). No doubt, with additional tuning of the parameter α in the priority queue to adjust the exponent γ, our model should be able to fit well the email communication as well.

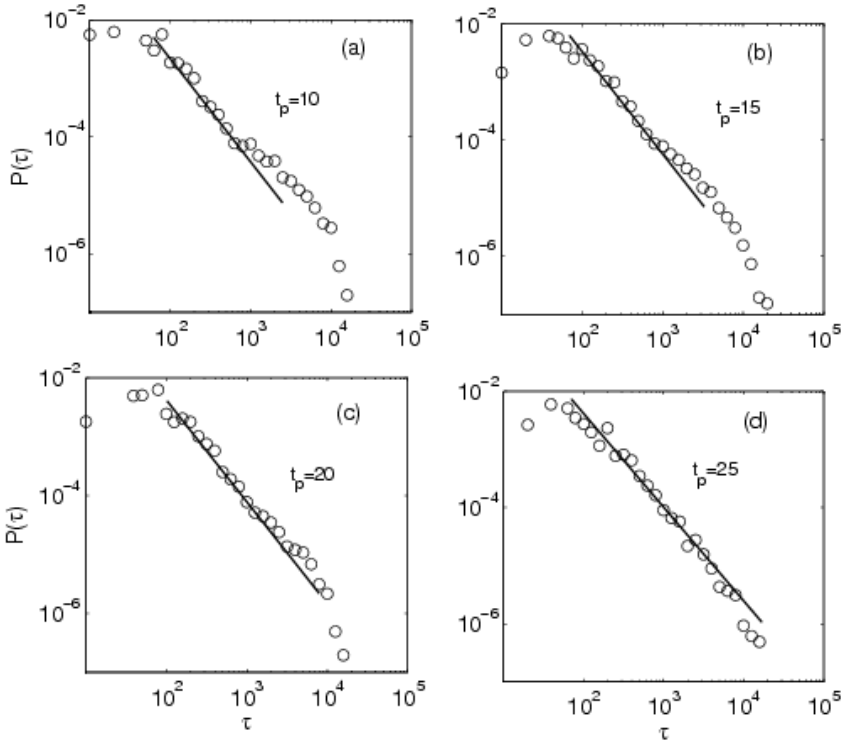

Fig. 4.8 Change of distribution of the inter-event time τ with respect to t_p. The other parameters are fixed as $\lambda = 1.5 \times 10^{-4}, \alpha = 1.0$.

4.6.2 Extension of our analysis and modelling

Several variations of the model could be considered to describe realistic situations in more detail. Here we assume that whether a message will be replied by user B is independent of the priority x_A of this task in the list of A. In reality, a more urgent message would get more attention and be responded with higher probability or priority. We could introduce a transmission/correlation of priority between the queues. The two-user model can be easily extended to a network of users where the users can have different number of communication partners and response rate. The comparison of the network model to the activity patterns of users with several or many regular partners (users with $W_i^{\max}$ clearly smaller than 1, see Fig. 4.2) will be carried out in the near future. The algorithm for the separation of the events into independent bursts will have to be developed for that case. We envisioned that we will be able to identify the bursts associated to different network neighbours.

4.7 Conclusion

Our findings reveal that there is a generic Poisson process in individual human behaviour which is connected to the power-law like bursts through the interaction with the other individuals, resulting in the interplay between the cut-off time τ_0 and the characteristic Poisson interval $1/\beta$ which are generally influenced by the network topology and the processing time t_p in various human activities. This picture has significantly changed the current competing views of human activity, either following Poisson or power-law statistics. Our findings open a new perspective in understanding human behaviour both at the individual and network level which is of utmost importance in areas as diverse as rumour and disease spreading, resource allocation and emergency response, economics, etc [A. Vazquez, 2009, J. L. Iribarren, 2009, D. Rybski, 2009]. The method of separation of the bursts into independent bursts should be useful for the analysis of some other bimodal natural phenomena, such as the inter-event times in human dialogue [D. G. Xenikos, 2009] and earth-quakes [S. Hainzl, 2006, S. Touati, 2009].

Chapter 5 Human comment dynamics in on-line social systems

5.1 Introduction

Recently, understanding regularity in complex human dynamics has attracted more and more attention in various fields. The classical view has assumed that human activities are homogeneous Poisson processes [Haight, 1967]. Such processes have a well-known statistical property: the time interval between two consecutive events, called the inter-event time τ, follows an exponential distribution, $P(\tau) \propto \lambda e^{-\lambda\tau}$. Recent evidences [A. L. Barabási 2005, J. G. Oliveira, 2005, A. Vázquez, 2006, U. Harder, 2006, J. P. Eckmann, 2004, J. Candia, 2007, R. D. Malmgen, 2008, W. Hong, 2009, X. P. Han, 2008, A. Vázquez, 2007a, A. Grabowski, 2007, F. Z. Wang, 2009, D. Rybskia, 2009, A. Carbone,, 2007] from various deliberate human activity patterns, including email and letter communications, library usage, broker trades, web browsing, etc., have shown that various human activities are non-Poissonian, with bursts of frequent actions separated by long periods of inactivity, leading to power-law heavy tails in the distribution of the inter-event time $P(\tau) \propto \tau^{-\gamma}$. These findings are very important in areas as diverse as disease spreading, resource allocation and emergency response, etc. Several mechanisms proposed to explain the origin of bursts and heavy tails are limited in applications. More evidences about non-Poissonian human dynamics are needed. And the general origin of the heavy tails is still far from being clearly understood.

As an important part of modern life, human behavior on the internet also attracts more and more research interest. Dezsõ et al. found that the time interval between consecutive visits by the same user to the site http://www.origi.hu follows a power-law distribution [Dezsõ, 2006]. They also showed that the exponent characterizing the individual user's browsing patterns determines the power-law decay in a document's visitation. A. Chmiel [A. Chmiel, 2009] investigated flows of visitors migrating between different portal sub-pages. A model of portal surfing is developed where the browsing process corresponds to a self-attracting walk on weighted networks with a short memory. A. Grabowski [A. Grabowski, 2009] found that the distribution of human activity (e.g. the total number of books read or songs played in on-line social systems) has the form of a power-law. All these findings indicate that human behavior on the internet is typically non-Poissonian. It is very interesting and important to further study the scaling about the human dynamics on the internet.

In this chapter, based on the data collected from 'tianya' which is one of the most popular on-line social systems in China, we show that the inter-event time between two consecutive comments on the same topic follows a power-law distribution. Meanwhile, the distribution of the number of comments in the same topic from different users also follows a power-law. This

means that there were some "hubs" in the topic who lead the direction of the public opinion. Furthermore, the power-law distribution of the inter-event time shows that there is no characteristic decay time on a topic. A topic may be ignored for a long time, and is revisited and intensively commented again sometimes. To obtain more insights into these observations of the human dynamics in on-line social systems, we propose a model basing on the attraction mechanism. Our findings may be helpful to distinguish different types of public opinions in the virtual society in the future.

This chapter is organized as follows: In section 5.2, the original of the data and the detailed information about the data are introduced. The statistic results are presented in section 5.3. The model and numerical simulations are presented in section 5.4. Finally, our conclusions are given in section 5.5.

5.2 Data description

Our data were obtained from "tianya"(http://www.tianya.cn/), which is one of the most popular on-line social systems in China. Every user is assigned a different identity name (ID). An ID can build a topic, and the other IDs can comment on it. They can discuss different opinions and communicate in the topic. Until 2010/02/11, there were 33,296,350 IDs in "tianya", and there were about 200,000 IDs on average on-line at the same time. The topics and the public opinion in "tianya" reflect part of the public opinions in the real society in China. We randomly sample some topics which were commented more than 3,000 times as our dataset. The types of the topics are different, from public news to personal stories, indicates that our results are general for different topics. The format of the data is shown in Table 5.1.

User (ID)	Comment time	Topic
ID 1	2009/02/12, 12:10:01	Topic A
ID 2	2009/02/12, 12:11:05	Topic A
……	……	Topic A
ID 3	2009/02/15, 10:10:03	Topic A
ID 2	2009/02/12, 11:02:01	Topic A

Table 5.1 The detailed format of one topic

5.3 Statistic results

The inter-event time plays an important role in many human collective behaviors. For example, the power-law distribution of the inter-event time about sending two consecutive E-mails can advance the spreading of the computer virus [A. Vázquez, 2007b]. The non-Poissonian distribution of arriving rate has also impact on the classical queue theory. Here, we also focus on the inter-comment time on the same topic, i.e., the time interval between two consecutive comments on the same topic. Although the inter-comment time has some relationship with inter-visit time on a website [Dezsõ, 2006], it is obviously different from inter-visit time because comment behavior is only a very little part of the web visiting behavior. Human comment dynamics on the web can reflect how individuals comment with each other while human dynamics of visiting a website cannot. Four different topics were taken as examples. The detailed information about the topics is given in Table 5.2. Duration is the time interval between the topics creation and data collection. Total clicks, total comments and total number of IDs are counted during the whole duration.

	A	B	C	D
Total clicks	792,429	618,885	223,961	524,512
Total comments	5,549	9,822	5,757	7,186
Total number of IDs	3,965	1,760	3,959	2,663
Duration (s)	24,989,467	464,957	829,408	1,082,256

Table 5.2 The detailed information about four randomly selected topics

The distribution of the inter-comment time is shown in Fig. 5.1. It is clearly seen that all the distribution are power-law, although the topics differ by contents and popularity. The exponent varies for the different topics. These results show that the human comment process is non-Poissonian as the human dynamics of the letter and E-mail communication, web browsing, on-line movie watching and broker trades. The heavy tail of the distribution allows for long periods of inactivity that separate bursts of intensive activity. Here, it also means there is no characteristic decay time in the human comment dynamics. A topic can be revisited, reactivated and commented frequently after a very long time. For example, topic A was created 8 months ago and it is still often commented now. A large population would read the topic and their opinions may be influenced by it.

There were thousands of IDs taking part in the discussion in one topic (Table 5.2). It is an

interesting question to ask: do they contribute to the topic equally or are there some "hub" IDs who are more important in the topic? In order to answer this question, we study the number of times n_i an ID participates in a topic. The distributions are shown in Fig. 5.2.

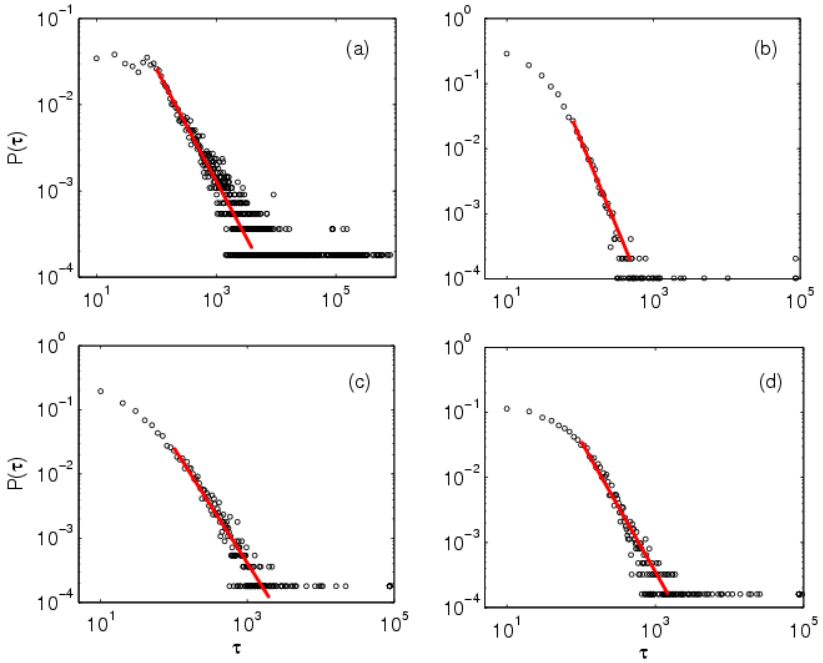

Fig. 5.1 The inter-comment time distribution of four different topics. The red line is the fitting function. (a) Topic A, slope $\gamma = 1.30 \pm 0.01$, (b) Topic B, slope $\gamma = 2.73 \pm 0.02$, (c) Topic C, slope $\gamma = 1.79 \pm 0.01$, (d) Topic D, slope $\gamma = 2.0 \pm 0.02$,

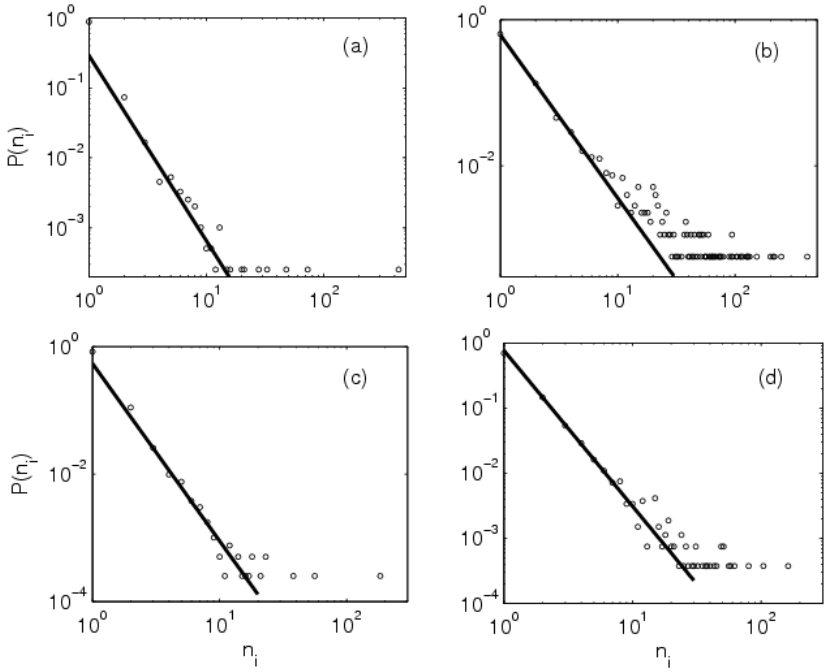

Fig. 5.2 The distribution of frequency of different ID comments on a topic. The black line is the fitting function. (a) Topic A, slope $\gamma = 2.56 \pm 0.01$, (b) Topic B, slope $\gamma = 2.24 \pm 0.02$, (c) Topic C, slope $\gamma = 2.78 \pm 0.02$, (d) Topic D, slope $\gamma = 2.39 \pm 0.01$.

It is evident that they are power-law $P(n_i) \propto n_i^{\alpha}$ in all the four topics. The exponents are slightly different but all in the range $2 \le \alpha \le 3$. The power-law distributions mean that most of the users only comment once or very few times in a topic. But there are also some users who comment many times in a topic. We may call these types of users as audiences and actors, respectively. The actors play a crucial role in leading the direction of the public opinion formation of the topic followed by the audiences. This could be useful for some commercial applications. For example, the topic could be about some negative news of a company, which maybe created by its competitor and the "hubs" could belong to or depend on this competitor. In such a case, the guidance of the opinion by the hubs will be harmful for this company.

5.4 Model and simulation

We propose a model in order to get a better understanding of our empirical observations from section 5.3. Based on our intuitive experience on comment habit, we can see that the number of the comments grows one by one. After the topic was created by a user a, some other users b and c et al. will comment on it later on. Then a would respond to their comments. b and c may come back to respond to the response to their original comments, and the process continues. Comment behavior can be regarded as a kind of communication. Someone who comments a topic before would come back to read the response of others to his comment. And he would comment again with higher probability than other IDs. This discussion indicates that the more times we participate in a topic; the higher is the probability that we make comments again. So our model is defined by the following scheme:

Step 1: Growing. A topic is created at $t = 0$. There is an ID commenting on the topic at each time step in the following time. In other words, the number of the comments increases one by one. This is a simplification of the real situation where the time needed to make a comment varies due to various lengths of the comments.

Step 2: Comment habit. A new comment is created with probability P by a new ID who has never commented in the topic in the past time and with probability $1-P$ by other old IDs. The old IDs do not contribute equally to the creation of a new comment. Rather, the probability that a new comment is created by ID i is a function of the topic attraction of this ID: ,

$$\prod(i) = \frac{A_i(t)}{\sum A_i(t)}$$

where $A_i(t)$ is the attraction of user i at time t reflected by the number of comments n_i made by the ID in the past, i.e., $A_i(t) = A_0 + n_i(t)$. Here A_0 represents the initial attraction,

which is different for different topics. $n_i(t)$ is the number of comments user i wrote until t.

Mathematically, the model is similar to growing networks in Ref. [S. N. Dorogovtsev, 2000] , where an existing node is selected to be connected to a new node with a probability depending on the degree k_i as

$$\prod(i) = \frac{(B + k_i(t))}{\sum(B + k_i(t))} \quad .$$

Basing on the analysis of the growing network in this work, we obtain that the distribution of $n_i(t)$ is a power-law $P(n_i) \propto (n_i)^{-\alpha}$ at a large enough time t and with the exponent $\alpha = 2 + A(0)$.

To compare our model with data, let us take topic C in our data as an example. Here $\alpha_c = 2.78$, and we take $A(0) = \alpha(c) - 2 = 0.78$ in the model simulation. There were 5,757 comments and totally 3,959 IDs made comments in topic C. As a result, there are 3,959 comments which are made by new IDs when they first join the topic. Thus, we can estimate that $P = 3959/5757 = 0.687$. We then simulate the model with $A(0)$ and P obtained in this way. The results are shown in Fig. 5.3(a). The distribution of the simulation is indeed a power-law with the similar exponent as found from the data.

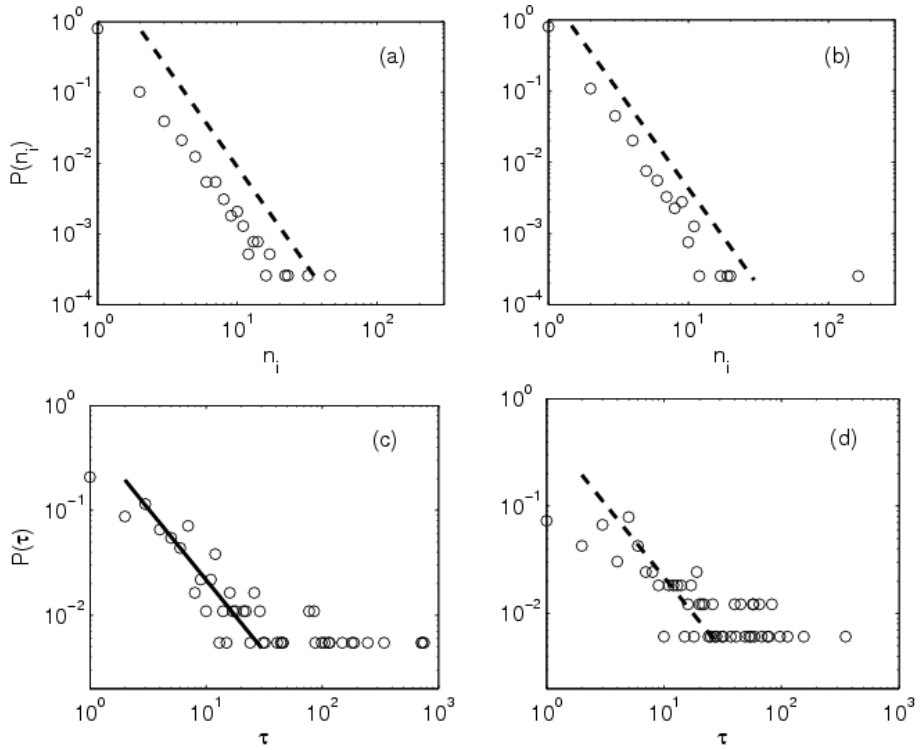

Fig. 5.3 The simulation result of the model. (a-b) The distribution of frequency of different ID commenting on a topic in the model, the slope of the dash line is the same as in correspondence Fig. 5.2(c), Parameter (a) $A(0) = 0.78, P = 0.687$, (b) $A(0) = 0.78, P = 0.687, A(0)_1 = 35$, (c-d) Inter-comment time distribution of the most activity ID. (c) Data, exponent of the line is $\beta = 1.36$, (d) Model, the slope of the dash line is the same as in Fig. 5.3 (c)

Comparing to the model to the empirical data in Fig. 5.2, we note that there are a few IDs with extremely large n_i in the data. Basing on our experience with on-line comments, this could result from the fact that some users, for example, the author and his strong supporters, have different behavior in the topic. They comment the topic with higher probability than others. This could be accounted in the model with larger $A(0)$ for these users. We test this by assuming that there was a user whose $A(0) = 35$ which is much larger than others, so that most of the comments by the old users of the topic in the early stage are from this particular user. The result is shown in Fig. 5.3(b). We can see that indeed there is an ID whose n_i is much larger than the others, as observed in the data. So the difference between the data and the power-law fitting can be account by different initial attraction of some special users. This type of users is the "hubs" who could deliberately try to lead the public opinion formation of the topic. They play an important role in the topic, in other words, they are "opinion leader".

It is very hard to know exactly the time used for a comment because the size of the comments can be very different. Therefore the model cannot simulate the distribution of the inter-event time directly. But we can do it in another way. We assume one comment takes one time step, i.e. the number of the comments between two comments can be taken as the time interval between the two comments. In this way, we can study the inter-event time between two consecutive comments made by the same ID. For example, the time interval between Ith and Jth comment was $\tau' = J - I$. We analyze the most active user to have good statistics. Furthermore, it is important to understand his behavior as an ``opinion leader". We find that his inter-event time distribution is also power-law, as shown in Fig. 5.3 (c). Meanwhile, the corresponding result of the model is shown in Fig. 5.3 (d). Strikingly, the result of the model fits well with the real data. It clearly implies that individual user's behavior is non-Poissonian. He/She may not take part in the discussion for a long time and may make comments in the topic frequently in a short time. From the analysis above, our model can well describe most important features in the human comment dynamics in the on-line social systems.

5.5 Conclusion

In this chapter, we present clearly new evidence that human comment behavior in on-line social systems, a different types of interacting human dynamics, is non-Poissonian. The inter-comment time follows a power-law distribution as many other human dynamics. A model based on the personal attraction was introduced to explain the human comment behavior. Numerical simulations of the model fit well with the empirical results. Our work would be useful to understand human comment behavior in realistic society, for example, human discussion behavior in a meeting, group communications in trunked mobile telephone

[D. G. Xenikos, 2009]. We expect that quantitative understanding of the human comment dynamics, when combined with additional content analysis, will open a new perspective on how to distinguish fraud public opinion from realistic opinion.

Chapter 6 Conclusion and outlook

In the past decade, as a typical kind of dynamics in complex networks, synchronization, especially the ability of networks to become synchronized, has attracted a lot of interest in multidisciplinary fields. From now on, several schemes including both static and dynamical mechanism were proposed to enhance the synchronizability of networks. However, the synchronizability was still far from being optimal. In this thesis, first, I studied a dynamical optimization coupling scheme to realize complete synchronization in networks with undelayed or delayed couplings. Moreover, the coupling matrix obtained from our method has much better synchronizability in a certain range of the probability p for adding long range connections in NW small world models than that obtained from degree based or ZK method. Our method can also be applied to the phase synchronization in SWNs with nonidentical oscillators and other topologies.

Second, scale-free networks with community structure are very common in nature. However, the response of scale-free networks with community structure to external stimuli is never been studied until now. By using the dynamical model present by Bar-Yam and Epstein [Y. Bar-Yam, 2004], we shown that the community characteristic of the networks is crucial to enhance their robustness. Some of the response patterns are found to coincide with the topology communities. As an example of scale-free like networks with community structure, such phenomena also occur in cat brain networks.

Third, interacting human activities which would be a new type of nonlinear dynamics in complex networks were studied both by data and the model. By analyzing the Short Message charging accountant bills, we found a new type of human activity pattern. The inter-event time distribution follows a bimodal distribution which is different from exponential or power-law that was found before. We showed that the new type of human activity pattern is the result of interplay of three basic ingredients: Poisson initiation of tasks and decision-making for task in individual human as well as the interaction among individuals. We introduce a model which fits well the distributions using the parameters extracted from the empirical data. The model was general for it can also embrace email and letter communications when taking the time scale of processing into account. Our method is also useful for understanding bimodal phenomena in other complex systems.

Fourth, human comment dynamics in on-line social systems, as new types of human dynamics, was studied both by data and the model. People who comments a topic before preferred to come back to read the response of others to his comment. This comment habit leads to power-law distribution of the number of times an ID participates in a topic. Basic on the personal attraction comment habit, a model was proposed to explain the complex

dynamics of human comment behavior. We expect that quantitative understanding of the human comment dynamics, when combined with additional content analysis, will open a new perspective on how to distinguish fraud public opinion from realistic opinion.

From now on, human communication dynamics and human comment dynamics which were new types of nonlinear dynamics were analyzed and modeled in detailed. However, understanding human dynamics was only in the individual level or small network level until now. It is more important to understanding human dynamics in large networks level. The following problem will be interesting and important for me to consider in the future.

1) Until now, the study of human correspondence dynamics is only studied based on one individual or a pair of users. The detailed correspondence interaction among human which is a kind of nodes of complex networks, however, are poorly study. Quantitative understanding of human correspondence dynamics on complex networks, especially human phone calls and short message dynamics, is very important for designing efficacy phone served systems. In the future, I will try to get more data from mobile phone operator to study human correspondence in the network level.

2) The interactions of human activities are also important to study other human collective behavior, such as rumor spreading. The classic view of rumor spreading models assumes that human spread rumor to his/her friends randomly and independently. Indeed, some types of rumor spreading dynamics are correlated directly with human correspondence patterns. Meanwhile, human correspondence patterns are influenced by the rumor spreading, too. The interplay between the events and human behavior are very interesting and important to study.

3) Interestingly, bimodal patterns seem to be quite universal in a wide range of complex systems, including human dialogue [D. G. Xenikos, 2009], trading [E. Scales, 2005] and financial activity [E. Scales, 2004] in social systems, tsunami [E. L. Geist, 2008], rainfall [T. M. Heneker, 2001], forest fries [J. Benavent-Coral, 2007], earthquakes [S. Haizl, 2006, S. Touati, 2009], in nature. However, a bimodal distribution is found and analyzed only in the earthquake systems very recently. The bimodal feature of other complex systems is still poorly found and understood.

4) How to distinguish fraud public opinion from realistic opinion is not only from a scientific viewpoint, but also from a commercial application. The classic view only focuses on the contents. Moreover, combined with additional quantitative understanding of the human comment dynamics, it will open a new perspective. Besides the features of human comment dynamics, we study in Chapter 5, more properties of human comment dynamics are needed to understand, such as the detailed behavior of each user, the difference dynamics in different time periods. I expect that fraud public opinion could be distinguished from real opinion when

data mixing methods are used in the future.

5) I expect not only fraud opinion, but also fraud click in the internet can be distinguished after quantitative understanding of the human dynamics. Distinguishing the fraud click in the internet has more applications. Fraud click is the most barriers in google Ads and other Ads as well as some on-line vote systems.

References

Order by the letter of family name

J. Acebron, L. L. Bonilla, C. J. P. Vicente, F. Ritort, and R. Spigler, Rev. Mod. Phys. 77, 137, 2005.

J. A. Acebrn, S. Lozano, A. Arenas, Phys. Rev. Lett. 99, 128701, 2007.

C. Anteneodo, Phys. Rev. E, 80, 041131, 2009

R. Albert, H. Jeong and A. L. Barabási, Nature, 406, 378, 2000

R. Albert and A. L. Barabási, Rev. Mod. Phys. 74, 47, 2002.

U. Alon, Science, 301, 1866, 2003

A. Arenas, A. Fernández, S. Gómez, New. Jop. Phys, 10, 053039, 2008.

A. Arenas, A. Díaz-Guilera, J. Kurths, Y. Moreno, C. S. Zhou, Phys. Rep. 469, 93, 2008.

A. Arenas, A. Díaz-Guilera, C. J. Perez-vicente, Phys. D, 244, 27, 2004a

A. Arenas, A. Díaz-Guilera, C. J. Perez-vicente, Phys. Rev. Lett, 96, 114102, 2006

A. Arenas, L. Danon, A. Díaz-Guilera, etc. Eur. Phys. J. B. 38, 373, 2004b

A. L. Barabási and R. Albert, Science 286, 509, 1999

A. L. Barabási, Nature, 435, 207, 2005

A. Barrat, M. Barthelemy, A. Vespignani, Phys. Rev. Lett, 92, 228701, 2004.

A. Barrat, M. Barthelemy and A. Vespignani, 'Dynamic processes on complex networks', Cambridge University Press, 2008

Y. Bar-Yam, I.R. Epstein, Proc. Natl. Acad. Sci. USA 101, 4341, 2004.

M. Barahona and L. M. Pecora, Phys. Rev. Lett. 89, 054101, 2002.

J. Benavent-Coral, C. Rojo, el, tc. Ecol. Model., 205, 336, 2007

G. Bianconi, M. Marsili, Phys. Rev. E, 73, 066121, 2006.

M. Boss, H. Elsinger, M. Summer, S.Thurner, Quantitative Finance, 4, 677, 2004.

S. Boccaletti, V. Latora, Y. Moreno, M. Chavez, D.-U. Hwang, Phys. Rep. 424, 175, 2006.

B. R. Bollobás, J. G. Oliver, Internet Math. 1 (1), 1-35, 2003.

A. Z. Broder, S. R. Kumar, F. Maghoul, etc, Comput. Netw, 33, 309, 2000.

J. Buhl, J. Gautrais, N. Reeves, et al, Eur. Phys. J. B. 49, 513, 2006

E. Bullmore, O. Sporns, Nature Reviews, Neuroscience 10, 186, 2009.

M. Byungjoon, K.-I. Goh, and I.-M. Kim, Phys. Rev. E, 79, 056110, 2009

J. Candia, etc. J Phys A 41, 2240156, 2007

A. Carbone, H. E. Stanley, Phys. A, 384, 21, 2007

A. Cardillo, S. Scellato, V. Latora and S. Porta, Phys. Rev. E, 73, 066107, 2006

M. Chavez, D. Huang, A. Amann, H. G. E. Hentschel, and S. Boccaletti, Phys. Rev. Lett. 94, 218701, 2005.

M. Chavez, D. Huang, A. Amann, and S. Boccaletti, Chaos, 16, 015106, 2006.

M. Chen, Y. Shang, Y. Zou, and J. Kurths, Phys. Rev. E 77, 027101, 2008.

M. Chen, Y. Shang, C. Zhou, Y. Wu, and J. Kurths, Chaos, 19, 013105, 2009.

M. Chen, Phys. Rev. E 76, 016104, 2007.

A. Chmiel, K. Kowalska, J. A. Holyst, Phys. Rev. E 80, 066122, 2009.

L. Danon, A. Arenas, A. Diaz-Guilera, Phys. Rev. E, 77, 036103, 2008

Z. A. Dezsõ, A. Lukács, A. Rácz. etc, Phys. Rev. E, 73, 066132, 2006.

L. Donetti, P. I. Hurtado, and M. A. Munoz, Phys. Rev. Lett. 95, 188701, 2005.

S. N. Dorogovtsev, A.V. Goltsev, J. F. F. Mendes, Rev. Modern Phys. 80, 1275, 2008.

S. N. Dorogovtsev, J. F. F. mendes, A. N. Samukhin, Phys. Rev. Lett. 85(21), 4633(4), 2000

J. P. Eckmann, E. Moses, D. Sergi, Proc Natl Acad Sci USA , 101, 14333, 2004.

A. K. Erlang, Nyt. Tidsskrift for Matematik B 20, 1909

R. Ferrer and R. V. Solé, Proceedings of the Royal Society of London B, 268, 2261, 2001

G. W. Flake, S. R. Lawrence, C. L. Giles, F. M. Coetzee, IEEE Comput. 35, 66 2002.

L. K. Gallos, P. Argyrakis, Phys. Rev. E 72, 017101, 2005.

A. Gabrielli, G. Caldarelli, Phys. Rev. Lett, 98, 208701, 2007

E. L. Geist, T. Parsons, Geophys. Rev. Lett. 35, L02612, 2008

A. Grabowski, Phys. A, 385, 363, 2007

A. Grabowski, Eur. Phys. J. B, 69, 603, 2009.

G. Grinstein and R.Linsker, Phys. Rev. Lett, 97, 130201, 2006

R. Guimera, S. Mossa, A. Turtschi, and L. A. N. Amaral, Proc Natl Acad Sci USA, 102, 7794, 2004.

T. Gross and B. Blasius, arXiv:0709.1858v1, 2007.

T. Gross, L. Rudolf, S. A. Levin, U. Dieckmann, Science, 325, 745, 2009

T. Gross, I. G. Kevrekidis, Euro. Lett. 82, 38004, 2008

T. Gross, C. Dommar DLima, B. Blasius, Phys. Rev. Lett, 96, 208701, 2006

X. P. Han, T. Zhou, B. H.Wang, New J. Phys, 7, 073010, 2008

S. Hainzl, F. Scherbaum, C. Beauval, Bulletin of the Seismological Society of America, 96, 313, 2006

F. A. Haight, handbook of the Poisson Distribution, Wiley, New York, 1967

U. Harder, M. Paczuski, Phys. A, 361, 329, 2006

J. F. Heagy, T. L. Carroll, and L. M. Pecora, Phys. Rev. Lett. 74, 4185, 1995.

T. M. Heneker, M. F. Lambert, G. Kuczera, J. Hydrol, 247, 54, 2001

C. C. Hilgetag, G. Burns, M. A. O'Neill, J. W. Scannell, M. P. Young, Philos. Trans. Soc. Lond. B, 355, 91, 2000.

C. C. Hilgetag, M. Kaiser, Neuroinformatics 2, 353, 2004.

W. Hong , X. P. Han, T. Zhou, B. H.Wang, Chin Phys Lett, 26, 028902, 2009.

P. Holme, M. Huss, H. Jeong, Bioinformatics 19, 532, 2003.

J. J. Hopfield, Proc. Natl. Acad. Sci. 79, 2554, 1982.

D. Huang, M. Chavez, A. Amann, and S. Boccaletti, Phys. Rev. Lett. 94, 138701, 2005.

T. C. Jarrett, D.J. Ashton, M. Fricker, N.F. Johnson, Phys. Rev. E 74, 026116, 2006.

M. Kaiser, M. Görner, C.C. Hilgetag, New. J. Phys. 9, 110, 2007.

K. Klemm, V. M. Eguíluz, R. Toral, and M.S. Miguel, Phys. Rev. E, 67, 026120, 2003

I. Z. Kiss, Y. Zhai, and J. L. Hudson, Science, 296, 1676, 2002.

Y. Kuramoto, Chemical Oscillations, Waves, and Turbulence Springer, Berlin, 1984.

V. Latora and M. Marchioric, Phys. Rev. Lett. 87, 198701, 2001.

L. F. Lago-Fernández, R. Huerta, F. Corbacho, and J. A. Siguenza, Phys. Rev. Lett. 84, 2758, 2000.

C. G. Li, P. K. Maini, J. Phys. A 38, 9741, 2005.

P. Li, M, Chen, Y. Wu, J. Kurths, Phys. Rev. E, 79, 067102, 2009

F. Liljeros, C. R. Amaral, R. Raghavan et al, Nature, 411, 907, 2001

R. D. Malmgen, D. B. Stouffer, A. E. Mottter, A. L. N. Amaral, Proc Natl Acad Sci USA 105, 18153, 2008.

R. D. Malmgen, D. B. Stouffer, el. Tc, Science, 325, 1696, 2009.

S. Maslov, K. Sneppen, A. Zaliznyak, Phys. A, 333, 529, 2004.

A. E. Motter, C. S. Zhou, and J. Kurths, Phys. Rev. E 71, 016116, 2005a.

A. E. Motter, C. S. Zhou, and J. Kurths, Europhys. Lett. 69, 334, 2005b.

M. E. J. Newman and D. J. Watts, Phys. Lett. A 263, 341, 1999.

M. E. J. Newman, Phys. Rev. E, 64, 016131, 2001a.

M. E. J. Newman, Phys. Rev. E, 64, 016132, 2001b.

M. E. J. Newman, Proc Natl Acad Sci USA, 98, 404, 2001c.

M. E. J. Newman, S. Forrest, J. Balthrop, Phys. Rev. E, 66, 035101, 2002

T. Nishikawa, A. E. Motter, Y. Lai, and F. C. Hoppensteadt, Phys. Rev. Lett. 91, 014101, 2003.

G. Osipov, J. Kurths, and C. S. Zhou, Synchronization in Oscillatory Networks Springer-Verlag, Berlin, 2007.

J. G. Oliveira, A. L. Barabási, Nature, 437, 12511, 2005.

J. G. Oliveira, A. Vazquez, Phys. A, 388, 187, 2009

C. Piccardi, R. Casagrandi, Phys. Rev. E 77, 026113, 2008.

G. A. Polis, Nature, 395, 744, 1998.

L. M. Pecora and T. L. Carroll, Phys. Rev. Lett. 80, 2109, 1998.

H. Ren, Graph Theory, China, 2009

Q. Ren and J. Zhao, Phys. Rev. E 76, 016207, 2007.

S. Redner, Eur. Phys. J. B 4, 131, 1998.

R. Steuer, T. Gross, J. Selbig, B.Blasius, Proc Natl Acad Sci USA 103, 11868, 2006

D. Rybskia, S. V. Buldyrevb, S. Havlin, etc, Proc Natl Acad Sci USA, 106, 12640, 2009

Reynolds, P. Call Center Staffing, The call Center School Press, Lebanon, Tennessee, 2003.

E. K. Scalas, T. Kirchler, M. Huber, A. Tedeschi,, Phys. A, 366, 463, 2006.

E. Scales, R. Gorenflo, H. Luckock, el, tc. Fina. Lett, 3(1), 38, 2004a

E. Scales, R. Gorenflo, H. Luckock, el, tc. Quantitaitve Finance, 4, 695, 2004b

P. Sen, S. Dasgupta, A. Chatterjee, etc, Phys. Rev. E, 67, 036106, 2003

B. Shargel, H. Sayama, I. R. Epstein, Y. Bar-Yam, Phys. Rev. Lett. 90, 068701, 2003.

J. Sienkiewicz, J. A. Holyst, Acta Phys Polon B, 36, 1771, 2005.

O. Sporns, D.R. Chialvo, M. Kaiser, C.C. Hilgetag, Trends Cogn. Sci. 8, 418, 2004a.

O. Sporns, J.D. Zwi, Neuroinformatics 2, 145, 2004b.

R. V. Solé, M. Rosas-Casals, B. Corominas-Murtra, and S. Valverde, Phys. Rev. E, 77, 026102, 2008.

S. H. Strogatz, Nature, 410, 268, 2001.

S. H. Strogatz, Sync: The Emerging Science of Spontaneous Order Hyperion, New York, 2003.

A. Vázquez, Phys. Rev. lett, 95, 248701, 2005

A. Vázquez, J. G. Oliverira, Dezsõ, etc. Phys. Rev. E 73, 036127, 2006.

A. Vázquez, Phys. A, 373, 747, 2007a

A. Vázquez, A. Rácz, A. Lukács, A. L. Barabási, Phys. Rev. Lett, 98, 158702, 2007b

E. A. Variano, J. H. Mccoy, H. Lipson, Phys. Rev. Lett. 92, 188701, 2004.

F. Z. Wang, S. J. Shies, S. Havlin, and H. E. Stanley, Phys. Rev. E, 79, 056109, 2009

S. J. Wang, A.C. Wu, Z. X. Wu, X. J. Xu, Y. H. Wang, Phys. Rev. E 75, 046113, 2007.

X. Wang, Y. Lai, and C. Lai, Phys. Rev. E 75, 056205, 2007.

D. J. Watts and S. H. Strogatz, Nature, 393, 440, 1998.

Y. Wu, Y. Shang, M. Chen, C. S. Zhou, J. Kurths, Chaos, 18, 037111, 2008

Y. Wu, P. Li, M. Chen, JH. Xiao, J. Kurths, Phys. A, 388, 2987, 2009

Y. Wu, C. S. Zhou, JH, Xiao, J. Kurths, H. J. Schellnhuber, submitted 2010a

Y. Wu, C. S. Zhou, M. Chen, JH, Xiao, J,Kurths, submitted 2010b

D. G. Xenikos, Phys. A, 388, 4910, 2009

G. Yan, T. Zhou, B. Hu, etc, Phys. Rev. E, 73, 046108, 2006

S. H. Yook, H. Jeong, A. L. Barabási and Y. Tu, Phys. Rev. Lett, 86, 5835, 2001.

L. Zemanova, C.S. Zhou, J. Kurths, Physica D, 224, 202, 2006.

C. S. Zhou, A. E. Motter, and J. Kurths, Phys. Rev. Lett. 96, 034101, 2006a.

C. S. Zhou and J. Kurths, Phys. Rev. Lett. 96, 164102, 2006b.

C. S. Zhou, L. Zemanova, G. Zamora-Lopez, C.C. Hilgetag, J. Kurths, Phys. Rev. Lett 97, 238103, 2006c.

Acknowledgement

My deepest gratitude goes first and foremost to my supervisor Professor. Jugen. Kurths who gave me a perfect and comfortable condition to finish my PHD study. All I have learned from him will become priceless treasure throughout my whole career.

Second, I would like to express my heartfelt gratitude to my collaborators who helped me much and make the things easy. In particular, thanks to Dr. Changsong Zhou, who guide me to study human dynamics, which eventually become the main focus of my PHD study. To be specific, results presented in Chapter 2 were obtained in collaboration with Yun Shang, Maoyin Chen, Changsong Zhou, results presented in Chapter 3 with Ping Li, Maoyin Chen, Jinghua Xiao, results presented in Chapter 4 with Changsong Zhou, Jinghua Xiao, Hans Joachim Schellnhuber, results presented in Chapter 5 with Changsong Zhou, Maoyin Chen, Jinghua Xiao.

Before I went to Potsdam, I was a graduate student under Prof. Jinghua Xiao. He is my first supervisor of research. Most of my knowledge about what is research and how to do research were learned from him.

Last my thanks would go to my beloved family especially my parents, sister and my girlfriend for their loving considerations and great confidence in me all through these years. I also owe my sincere gratitude to my friends and my fellow classmates who gave me their help.

Enhanced synchronizability in scale-free networks

Maoyin Chen,[1] Yun Shang,[2] Changsong Zhou,[3] Ye Wu,[4] and Jürgen Kurths[4]
[1]*Tsinghua National Laboratory for Information Science and Technology, Tsinghua University, Beijing 100084, China and Department of Automation, Tsinghua University, Beijing 100084, China*
[2]*Institute of Mathematics, AMSS, Academia Sinica, Beijing 100080, China*
[3]*Department of Physics, Hong Kong Baptist University, Kowloon Tong, Hong Kong*
[4]*Institut für Physik, Potsdam Universität, Am Neuen Palais 10, D-14469, Germany*

(Received 11 August 2008; accepted 8 December 2008; published online 16 January 2009)

We introduce a modified dynamical optimization coupling scheme to enhance the synchronizability in the scale-free networks as well as to keep uniform and converging intensities during the transition to synchronization. Further, the size of networks that can be synchronizable exceeds by several orders of magnitude the size of unweighted networks. © *2009 American Institute of Physics*. [DOI: 10.1063/1.3062864]

Works on synchronizability in networks with a given topology can be divided into two classes according to the coupling matrix. One class is the static mechanism, where the coupling matrix remains fixed during the transition to synchronization. This mechanism includes the degree and load based weighted networks. The other class is the dynamical mechanism, where the coupling matrix evolves in time by introducing adaptive strengths between connected oscillators. The adaptation process can enhance synchronization by modifying the coupling matrix, but the resulting networks have nonuniform intensities even for networks with homogeneous degrees. In this paper, we introduce a modified dynamical optimization mechanism to enhance the synchronizability in the scale-free networks as well as to keep uniform and converging intensities during the transition to synchronization. Further, the size of networks that can be synchronizable exceeds by several orders of magnitude the size of unweighted networks.

I. INTRODUCTION

In the past few years, the dynamics of complex networks has been extensively investigated.[1–4] As a typical dynamical process on networks, synchronization, especially the ability of networks to obtain synchronization (synchronizability), has attracted a lot of interest.[5–22] Recent studies have revealed that unweighted small-world and scale-free networks are more synchronizable than unweighted regular networks.[5,6] But the assumption that local units are symmetrically coupled with undirected couplings does not match the properties of real networks (such as unequal connection weights and asymmetry of the couplings).[7,8] Recent efforts have been focused on achieving efficient synchronization by introducing connection weights and directionality into networks.[9–15,18–21]

From Ref. 20, works on the synchronizability in networks with a given topology can be divided into two classes according to the coupling matrix. One class is the static mechanisms, where the coupling matrix is invariant.[6,9–17] For randomly enough unweighted and weighted networks, the synchronizability is controlled by $S_{\max}/S_{\min}$, where $S_{\max}$ and $S_{\min}$ are, respectively, the maximum and minimum of intensity S_i, which is defined by the sum of the coupling strengths of oscillator i.[14] For unweighted Barabási–Albert (BA) networks,[14] $S_{\max}/S_{\min}=k_{\max}/k_{\min}\sim N^{1/2}$, where $k_{\max}$ and $k_{\min}$ are the maximal and minimal degrees, respectively. Hence, the synchronizability can be enhanced if intensities become more homogeneous. From the degree based weighted networks,[11,13] one necessary condition for the optimal synchronizability R_{opt} is that the intensities become uniform.

The other class is the dynamical mechanisms, where the coupling matrix is variant by introducing adaptive strengths into networks of identical oscillators[18] and nonidentical oscillators.[19] The adaptation process can enhance the synchronization by modifying the coupling matrix, but the resulting networks have heterogeneous intensities due to heterogeneous degrees. For BA networks, after the adaptation, the synchronizability is characterized by $S_{\max}/S_{\min}\sim N^{\beta/2}$ with $\beta=1-\theta$ and $\theta\sim 0.5$.[18] Inspired by the static mechanisms,[11,13] one necessary condition for the optimal synchronizability is that intensities become uniform. However, even for networks with homogeneous degrees, the mechanisms[18,19] cannot ensure uniform intensities due to different initial conditions of oscillators.[20] Therefore, a problem naturally arises: *By the dynamical mechanism, how can we realize the synchronization in networks as well as ensure uniform intensities during the transition to synchronization and enhance the synchronizability, regardless of heterogeneous degrees and initial conditions of oscillators*?

II. THE MODIFIED DYNAMICAL OPTIMIZATION MECHANISM

Recently, we have already obtained some results on the above problem. For different variants of the Kuramoto model, we have proposed a dynamical gradient network (DGN) approach to realize phase synchronization.[21] It is shown that all the oscillators have uniform intensities during the transition to synchronization. However, the DGN approach is very special in two aspects. One is that it should assign a scale potential to each oscillator within any time interval, which depends on the extent of the local synchronization among itself and its neighbor oscillators. The other is

that the adjustment of the respective link by the DGN approach is often mostly ineffective. Inspired by the DGN approach,[21] we have further introduced the original dynamical optimization (DO) mechanism for small-world networks (SWNs).[20] The main idea in the original DO mechanism is to increase the coupling strength of only one incoming link of oscillator i by a small value in different intervals with a fixed length. It reflects the "winner-take-all" strategy, where the incoming link to be adjusted is always chosen as a pair of oscillators with the weakest synchronization. This means that the original DO mechanism is more effective than the DGN approach. We previously showed that the original DO mechanism has much better synchronizability in SWNs.[20]

Unfortunately, there exists one main shortcoming in the original DO mechanism.[20] That is, the coupling strength between two connected oscillators is an increasing function of time as well as the intensities are diverging to infinity. Basically, this means that full synchronization is trivially obtained for some kinds of networks, such as any variant of the Kuramoto model[21] and networks of Rössler oscillators coupled through full states. The above networks always converge to a fully synchronized regime if the couplings (or intensities) are sufficiently large. However, for some kinds of networks such as networks of Rössler oscillators coupled through partial states,[22] the synchronization cannot be realized if the couplings (or intensities) are largely enough. In our recent work,[20] we have to end the original DO mechanism provided that the synchronization error is small enough. If not, the couplings (or intensities) are so large that the synchronization can be destroyed and the synchronization error becomes large again. Obviously, it is reasonable to introduce one dynamical mechanism with limited couplings (or intensities) even if time increases to infinity. Here we modify the original DO mechanism such that the intensities are converging and the ultimate intensity can be adjusted.

We consider networks consisting of N coupled oscillators

$$\dot{\mathbf{x}}_i = \mathbf{F}(\mathbf{x}_i) + \sum_{j\neq i, j=1}^{N} G_{ij}(\mathbf{H}(\mathbf{x}_j) - \mathbf{H}(\mathbf{x}_i)), \quad 1 \leqslant i \leqslant N, \tag{1}$$

where $\mathbf{x}_i$ is the state, $\mathbf{F}$ is the dynamics of individual oscillator, $\mathbf{H}$ is the output function, and $G=(G_{ij})$ is the coupling matrix. $G_{ij}=A_{ij}W_{ij}$, where $A=(A_{ij})$ is the binary adjacency matrix, W_{ij} is the coupling strength of the incoming link (i,j) pointing from oscillator j to oscillator i if they are connected, $G_{ii}=-\Sigma_{j\in K_i}A_{ij}W_{ij}$, and K_i is the neighbor set of oscillator i. In unweighted networks, $W_{ij}=1$ is uniform for all the incoming links.

In the original DO mechanism,[20] we increase the coupling strength of only one incoming link of oscillator i by a small value, at the time step $t_n=t_0+n\tau$, where $n\geqslant 1$ is the positive integer, t_0 is the transient time, and $\tau>0$ is the duration time. This adaptation results from the competition between neighbor oscillators within the interval $[t_{n-1},t_n)$. For oscillator i and one neighbor $j\in K_i$, a total synchronization difference, i.e., $E_n(i,j)=\int_{t_{n-1}}^{t_n}\phi(\mathbf{x}_i,\mathbf{x}_j)dt$, within the interval $[t_{n-1},t_n)$ is evaluated, where ϕ is a non-negative error function, and satisfies $\phi(\mathbf{x}_i,\mathbf{x}_j)=0$ if oscillators i,j are synchronized. For oscillator i, the incoming link with the weakest synchronization, i.e., $(i,j^n_{\max})$, is the winner within the interval $[t_{n-1},t_n)$, where the index $j^n_{\max}$ is decided by the optimization problem

$$j^n_{\max} = \arg\max_{j\in K_i} E_n(i,j). \tag{2}$$

If several neighbors have the same synchronization difference, we choose only one randomly. In the original DO mechanism, the coupling strength is adjusted dynamically by[20]

$$\begin{aligned} W^{n+1}_{ij^n_{\max}} &= W^n_{ij^n_{\max}} + \varepsilon, \\ W^{n+1}_{ij} &= W^n_{ij}, j \neq j^n_{\max}, \end{aligned} \tag{3}$$

where the incremental coupling $\varepsilon>0$ is a small value, and W^n_{ij} is the coupling strength in the interval $[t_{n-1},t_n)$. Obviously, the intensities are diverging as time tends to infinity.

In order to ensure that the intensities converge to a limited value as time tends to infinity, we adjust the coupling strength by

$$\begin{aligned} W^{n+1}_{ij^n_{\max}} &= W^n_{ij^n_{\max}} + \chi_n, \\ W^{n+1}_{ij} &= W^n_{ij}, j \neq j^n_{\max}, \end{aligned} \tag{4}$$

where $\chi_n>0$ is the incremental coupling. Here we give some basic rules for choosing the incremental coupling χ_n, which make the ultimate intensities be uniform and convergent. (i) The incremental couplings χ_n for all oscillators are identical at the time step t_n, which make the intensities S_i be uniform during the transition to synchronization. (ii) The incremental coupling χ_n is limited by the fixed constant ε, which implies that at the time step t_n the incremental coupling χ_n should not be large. (iii) The incremental coupling χ_n is a nonincreasing function on the time step n, and the ultimate intensity $\bar{S}=\Sigma_{i=1}^{\infty}\chi_i$ exists. This requirement means that after the time step t_n, the total intensity $\Sigma_{i=1}^{n}\chi_i$ is convergent and χ_n approaches zero as the time step n tends to infinity. (iv) The ultimate intensity $\bar{S}$ can be adjusted. This is consistent with realistic cases where the intensities (or couplings) for synchronization are in a certain range (such as networks of Rössler oscillators coupled through partial states). We can further discuss the relationship between network synchronization and network topology by adjusting the ultimate intensity $\bar{S}$.

Summing up the above analysis, the term $\varepsilon e^{-n/n_0}$ is one suitable choice of the incremental coupling χ_n. Hence, we choose $\chi_n=\varepsilon e^{-n/n_0}$. We then adjust the coupling strength by

$$\begin{aligned} W^{n+1}_{ij^n_{\max}} &= W^n_{ij^n_{\max}} + \varepsilon e^{-n/n_0}, \\ W^{n+1}_{ij} &= W^n_{ij}, j \neq j^n_{\max}, \end{aligned} \tag{5}$$

where n_0 is a suitable positive integer. Here we call this mechanism [namely, Eqs. (2) and (5)] the modified DO mechanism.

In this paper, the initial coupling strengths in networks are assumed to be zero.[23] Hence, the intensities are uniform

at the time step t_n, since the intensity of each oscillator increases by the same amount $\varepsilon e^{-n/n_0}$ at the time step t_n. Further, the intensity S_i for oscillator i is bounded by the limit $\bar{S}=\lim_{n\to\infty}S_i$, where

$$\bar{S}=\varepsilon e^{-1/n_0}/(1-e^{-1/n_0}). \quad (6)$$

We can adjust the ultimate intensity by the suitable parameter n_0. For a fixed ε, when n_0 is larger (smaller), the intensity $\bar{S}$ is larger (smaller).

III. ENHANCED SYNCHRONIZABILITY IN SCALE-FREE NETWORKS

We briefly review the stability of networks

$$\dot{\mathbf{x}}_i=\mathbf{F}(\mathbf{x}_i)+\sigma\sum_{j\neq i,j=1}^{N}G_{ij}^0(\mathbf{H}(\mathbf{x}_j)-\mathbf{H}(\mathbf{x}_i)),\quad 1\leqslant i\leqslant N, \quad (7)$$

where σ is the overall strength. For a generally asymmetric matrix $G^0=(G_{ij}^0)$, the variational equation on the synchronous state $\{\mathbf{x}_i=\mathbf{s},\ \forall i\}$ is $\dot{\mathbf{u}}_i=[D\mathbf{F}(\mathbf{s})-\sigma\lambda_l D\mathbf{H}(\mathbf{s})]\mathbf{u}_i$, where D is the Jacobian operator, and λ_l is the complex eigenvalue of the Laplacian matrix L $(=-G^0)$, satisfying $\mathrm{Re}(\lambda_1)\leqslant\mathrm{Re}(\lambda_2)\leqslant\cdots\leqslant\mathrm{Re}(\lambda_N)$. The largest Lyapunov exponent (LLE), i.e., $\Lambda(\epsilon,\eta)$, of the master stability equation $\dot{\mathbf{v}}=[D\mathbf{F}(\mathbf{s})-(\epsilon+i\eta)D\mathbf{H}(\mathbf{s})]\mathbf{v}$ is a function of ϵ and η, which is the master stability function (MSF).[22] Let $\mathcal{R}$ be the region in the complex plane where the MSF provides a negative LLE. The synchronization condition is that the set $\{\sigma\lambda_l:\lambda_l\neq 0\}$ is entirely contained in $\mathcal{R}$.[22] Here we only consider the case where the region $\mathcal{R}$ is bounded, which is shown by the dashed line in Figs. 4(a) and 4(c). A better synchronizability is achieved if simultaneously the ratio $\mathrm{Re}(\lambda_N)/\mathrm{Re}(\lambda_2)$ and $\max|\mathrm{Im}(\lambda_l)|$ are minimized.[10,12]

In this paper, we have two aims based on networks (1) and (7). One is to realize the synchronization in network (1), in which all the oscillators have uniform intensities during the transition to synchronization. The other is to examine the synchronizability in network (7) when the coupling matrix G^0 is assigned by the coupling matrix from the synchronization in network (1), during or after the adaptation. Our analysis and simulation are based on BA networks.[4] Initially, M oscillators with labels $i=1,\ldots,M$ are fully connected. At every time step a new oscillator is introduced to be connected to M existing oscillators. The probability that the new oscillator is connected to oscillator i depends on degree k_i, i.e., $\Pi_i=k_i/\Sigma_j k_j$. Here we choose Rössler networks to illustrate the effectiveness of our mechanism: $\mathbf{x}_i=(x_i,y_i,z_i)$, $\mathbf{F}(\mathbf{x}_i)=(-0.97y_i-z_i,0.97x_i+0.15y_i,z_i(x_i-8.5)+0.4)$, $\mathbf{H}(\mathbf{x}_i)=(x_i,0,0)$, and $\phi(\mathbf{x}_i,\mathbf{x}_j)=|x_i-x_j|+|y_i-y_j|+|z_i-z_j|$. In order to measure the synchronization, we define the average error as $E=(1/N)\Sigma_{i=1}^N|\mathbf{x}_i-\bar{\mathbf{x}}|$, where $\bar{\mathbf{x}}=(1/N)\Sigma_{i=1}^N\mathbf{x}_i$ is the global mean field.

In our simulations the initial conditions for oscillators are randomly chosen from Rössler attractor (here, $t_0=0$). The parameter n_0 in Eq. (5) is $n_0=1200$. Hence, the limit $\bar{S}$ is about 1.2 if the value $\varepsilon=0.001$. From Fig. 1, the synchronization in network (1) is realized effectively. From Eqs. (2) and (5), all the oscillators have uniform intensities during the transition to synchronization, regardless of heterogeneous degrees and initial conditions. It is consistent with the necessary condition for the optimal synchronizability in the static mechanisms.[11,13] But this is totally different from the dynamical mechanisms.[18,19] The average intensity $S(k)$ over oscillators with degree k increases as $S(k)\sim k^\beta$ with $\beta\sim 0.5$.[18]

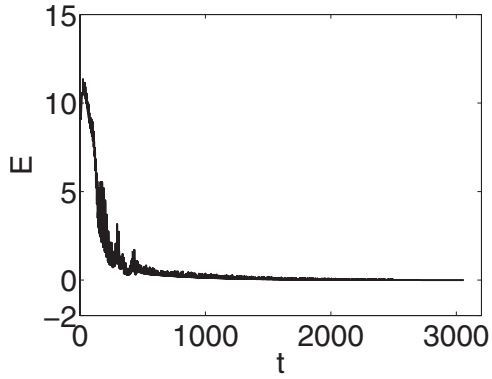

FIG. 1. The average error E as a function of time t. The parameters are $N=1000$, $M=5$, $\tau=1$, $\varepsilon=0.001$, and $n_0=1200$.

During the transition to synchronization, the ratio $\mathrm{Re}(\lambda_N)/\mathrm{Re}(\lambda_2)$ in network (7) with $G^0=G$ decreases towards the optimal synchronizability $R_{\mathrm{opt}}\approx 3.8$ (Fig. 2). The value R_{opt} is decided by the eigenratio of the Laplacian matrix of $G'(0)$, where $G'(\alpha)=(G'_{ij}(\alpha))$ with $G'_{ij}(\alpha)=(k_ik_j)^\alpha/\Sigma_{j\in K_i}(k_ik_j)^\alpha$ and $G'_{ii}(\alpha)=-1$.[11] From Eqs. (2) and (5), the incoming link to be adjusted for each oscillator is always chosen to be the pair of oscillators with the maximal synchronization difference in the previous time interval, which greatly decrease the ratio $\mathrm{Re}(\lambda_N)/\mathrm{Re}(\lambda_2)$. However, there still exists the discrepancy between the ultimate value of $\mathrm{Re}(\lambda_N)/\mathrm{Re}(\lambda_2)$ and R_{opt}. Now we explain the reason for the discrepancy. Due to the "winner-take-all" strategy inherent in the DO mechanism, the coupling strengths W_{ij} for oscillator i are almost uniform statistically as the time step n approaches infinity; namely, $W_{ij}\sim k_i^{-1}$. Unfortunately, the exact uniform coupling strength $W_{ij}=k_i^{-1}$ cannot be realized by dynamical mechanisms. In order to show it, we define the average standard deviation $E_{\mathrm{sd}}(k)=(1/l_k)\Sigma E_l^0$ between G^0

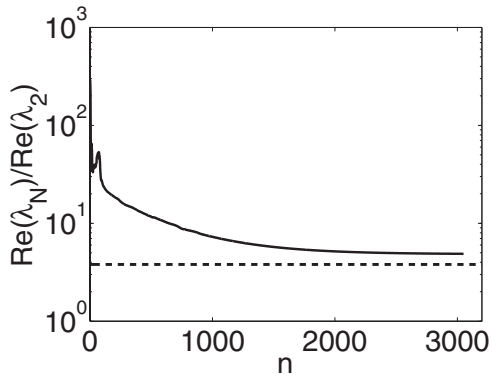

FIG. 2. The ratio $\mathrm{Re}(\lambda_N)/\mathrm{Re}(\lambda_2)$ as a function of the adjustment step n. Solid line: the ratio by the modified DO mechanism; dashed line: R_{opt}. The parameters are the same as those in Fig. 1.

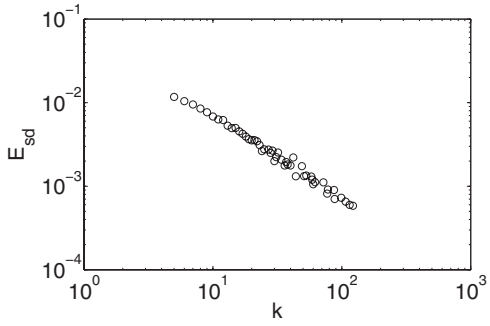

FIG. 3. Standard deviation $E_{sd}(k)$ as a function of degree k. The parameters are the same as those in Fig. 1.

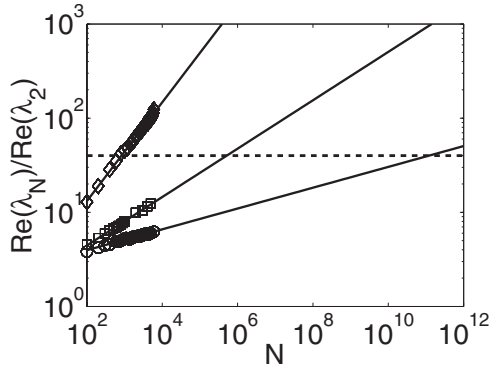

FIG. 5. The ratio $\mathrm{Re}(\lambda_N)/\mathrm{Re}(\lambda_2)$ for different size of network (7). Diamond: unweighted networks; square: networks with adaptive coupling (see Ref. 18); circle: the ratio by the modified DO mechanism; solid line: fitting; dashed line: $R_\rho=\delta_2/\delta_1\approx 40$. The parameters M, τ, ε, n_0 are the same as those in Fig. 1. All the estimates are averaged over 20 realizations of networks.

given by the following Eq. (8) and $G'(0)$, where l_k is the number of oscillators with degree k and $E_l^0=(1/k)\sqrt{\Sigma_{j\neq i}(G_{ij}^0-1/k)^2}$ (Fig. 3). From this figure, the exact uniform coupling strength $W_{ij}=k_i^{-1}$ cannot be realized by dynamical mechanisms. This may be the reason for the discrepancy between the ultimate value of $\mathrm{Re}(\lambda_N)/\mathrm{Re}(\lambda_2)$ and R_{opt}.

We assign the coupling matrix G^0 in network (7) by

$$G^0=G_{\mathrm{norm}}=G_{\mathrm{end}}/\bar{S}, \tag{8}$$

where G_{end} is the coupling matrix of network (1) after the adaptation. Since all the oscillators have uniform intensities, the Laplacian matrices of G_{norm} and G_{end} have equal ratios $\mathrm{Re}(\lambda_N)/\mathrm{Re}(\lambda_2)$. When $\sigma=1.5$, all the nonzero eigenvalues of the Laplacian matrix of σG_{norm} are located in a very narrow region around the real axes in the region $\mathcal{R}$, and the absolute values of imaginary parts are sufficiently small [Figs. 4(b) and 4(c)].

The ratio $\mathrm{Re}(\lambda_N)/\mathrm{Re}(\lambda_2)$ in network (7) with $G^0=G_{\mathrm{norm}}$ increases slightly with increasing the network size N, and this can be well fitted by a power-law dependence, which means the synchronizability decreases slightly (Fig. 5). From the fitting and the value R_ρ, we find that the network (7) is still synchronizable until $N\approx 10$.[11] The size of the network (7) that can be synchronizable exceeds by several orders of magnitude the size of unweighted networks ($\approx 10^3$) and networks with adaptive coupling ($\approx 8\times 10^5$).[18] Obviously, this is a great enhancement of the synchronizability in networks, compared with unweighted networks and networks with adaptive coupling.[18] It should be pointed out that for different size of networks, $\max|\mathrm{Im}(\lambda_l)|$ is sufficiently small (the maximal value is less than 0.1).

For the coupling matrix $G^0=G_{\mathrm{norm}}$, all the eigenvalues are fully contained within the unit circle centered at 1.[24] Thus, $0\leqslant \mathrm{Re}(\lambda_l)\leqslant 2$, $|\mathrm{Im}(\lambda_l)|\leqslant 1$, and the largest $\mathrm{Re}(\lambda_N)$ never diverges, independently of the network size N.[10] During the transition to synchronization in network (1), $S_{\max}/S_{\min}$ is always equals to 1. But in Refs. 14 and 18, the synchronizability decreases with the increasing of $S_{\max}/S_{\min}$, and $S_{\max}/S_{\min}$ increases with the increasing of the size N. Hence, the synchronizability here is better than Ref. 18, whose main aim is to reduce the heterogeneity of the intensities adaptively.

For the fixed n_0 and N, we discuss the effect of parameters τ and ε on the synchronizability in network (7) with $G^0=G_{\mathrm{norm}}$ [Figs. 6(a) and 6(b)]. The value ε can be chosen in a wide range, and the length τ can be arbitrary large. In our simulations, the value ε belongs to $[0.0001, 0.005]$ From Figs. 6(a) and 6(b), the ratio $\mathrm{Re}(\lambda_N)/\mathrm{Re}(\lambda_2)$ is almost independent of the values of τ and ε.

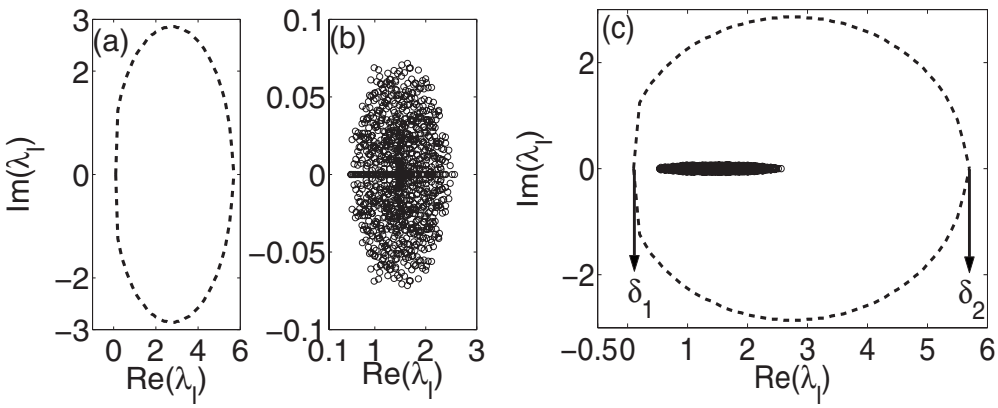

FIG. 4. (a) The stability region $\mathcal{R}$ bounded by the dashed line. (b) Distribution of nonzero eigenvalues λ_l of the Laplacian matrix of σG_{norm}. (c) The location of nonzero eigenvalues λ_l in the region $\mathcal{R}$. Circles: nonzero eigenvalues by the modified DO mechanism; $\delta_1\approx 0.144$ and $\delta_2\approx 5.76$ are the minimum and maximum of real parts in the region $\mathcal{R}$, respectively. The parameters N, M, τ, ε are the same as those in Fig. 1, and $\sigma=1.5$.

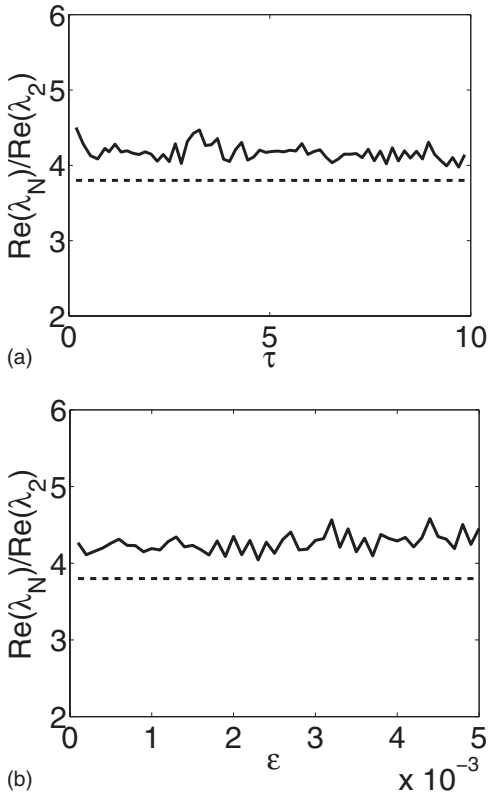

FIG. 6. The ratio $\mathrm{Re}(\lambda_N)/\mathrm{Re}(\lambda_2)$ for different τ (a) and ε (b). Solid line: the ratio by the modified DO mechanism. Dashed line: R_{opt}. The parameters N, M, n_0 are the same as those in Fig. 1. All the estimates are averaged over 20 realizations of networks.

IV. CONCLUSION

In this paper, we introduce a modified dynamical optimization coupling scheme to enhance the synchronizability in the scale-free networks as well as to keep uniform and converging intensities during the transition to synchronization. Moreover, the size of networks that can be synchronizable exceeds by several orders of magnitude the size of unweighted networks.

ACKNOWLEDGMENTS

M.C. was supported by NSFC project (No. 60804046), Special Doctoral Fund in the University by Ministry of Education (No. 20070003129), and the Alexander von Humboldt Foundation. Y.S. thanks the partial support by NSFC Project Nos. 60736011 and 60603002, and 863 Project No. 2007AA01Z325. J.K. was supported by SFB 555 (DFG) and BRACCIA (EU).

[1]S. H. Strogatz, Nature (London) **410**, 268 (2001).
[2]R. Albert and A. L. Barabási, Rev. Mod. Phys. **74**, 47 (2002).
[3]D. J. Watts and S. H. Strogatz, Nature (London) **393**, 440 (1998).
[4]A. L. Barabási and R. Albert, Science **286**, 509 (1999).
[5]M. Barahona and L. M. Pecora, Phys. Rev. Lett. **89**, 054101 (2002).
[6]T. Nishikawa, A. E. Motter, Y. C. Lai, and F. C. Hoppenstead, Phys. Rev. Lett. **91**, 014101 (2003).
[7]G. A. Polis, Nature (London) **395**, 744 (1998).
[8]V. Latora and M. Marchioric, Phys. Rev. Lett. **87**, 198701 (2001).
[9]M. Chavez, D. Huang, A. Amann, H. G. E. Hentschel, and S. Boccaletti, Phys. Rev. Lett. **94**, 218701 (2005).
[10]M. Chavez, D. Huang, A. Amann, and S. Boccaletti, Chaos **16**, 015106 (2006).
[11]A. E. Motter, C. Zhou, and J. Kurths, Phys. Rev. E **71**, 016116 (2005).
[12]D. Huang, M. Chavez, A. Amann, and S. Boccaletti, Phys. Rev. Lett. **94**, 138701 (2005).
[13]X. Wang, Y. Lai, and C. Lai, Phys. Rev. E **75**, 056205 (2007).
[14]C. Zhou, A. E. Motter, and J. Kurths, Phys. Rev. Lett. **96**, 034101 (2006).
[15]T. Nishikawa and A. E. Motter, Phys. Rev. E **73**, 065106 (2006).
[16]L. Donetti, P. I. Hurtado, and M. A. Munoz, Phys. Rev. Lett. **95**, 188701 (2005).
[17]B. Wang, H. Tang, T. Zhou, and Z. Xiu, "Optimizing synchronizability of networks," arXiv:cond-mat/0512079, v2, 23 March 2007.
[18]C. Zhou and J. Kurths, Phys. Rev. Lett. **96**, 164102 (2006).
[19]Q. Ren and J. Zhao, Phys. Rev. E **76**, 016207 (2007).
[20]Y. Wu, Y. Shang, M. Chen, C. Zhou, and J. Kurths, Chaos **18**, 037111 (2008).
[21]M. Chen, Y. Shang, Y. Zou, and J. Kurths, Phys. Rev. E **77**, 027101 (2008).
[22]L. M. Pecora and T. L. Carroll, Phys. Rev. Lett. **80**, 2109 (1998).
[23]The adjustment time n is counted when the number of zero eigenvalues of matrix G is 1.
[24]R. S. Varga, *Gersgorin and His Circles* (Springer, Heidelberg, 2004).

Matrix-measure criterion for synchronization in coupled-map networks

Ping Li,[1,2] Maoyin Chen,[3] Ye Wu,[2] and Jürgen Kurths[4,5]
[1]*University of Electronic Science and Technology of China, Chengdu 610054, People's Republic of China*
[2]*Institute of Physics, University of Potsdam, Am Neuen Palais 10, D-14469 Potsdam, Germany*
[3]*Department of Automation, TNlist, Tsinghua University, Beijing 100084, People's Republic of China*
[4]*Potsdam Institute for Climate Impact Research (PIK), Telegraphenberg A 31, 14473 Potsdam, Germany*
[5]*Institute of Physics, Humboldt University, 10099 Berlin, Germany*
(Received 31 March 2009; published 8 June 2009)

We present conditions for the local and global synchronizations in coupled-map networks using the matrix measure approach. In contrast to many existing synchronization conditions, the proposed synchronization criteria do not depend on the solution of the synchronous state and give less limitation on the network connections. Numerical simulations of the coupled quadratic maps demonstrate the potentials of our main results.

DOI: 10.1103/PhysRevE.79.067102 PACS number(s): 89.75.−k, 82.40.Bj

Synchronization, as one of the most remarkable phenomena that arise in many fields of sciences, ranging from natural to social systems, has attracted a lot of attention in a few coupled subsystems but recently also in networks with complex topology [1–13]. It has been shown that the topological properties of coupled dynamical systems affect crucially the synchronizability of subsystems in a network [3,6,12]. These topological properties include the small-world [14] property and scale-free [15] nature of the connectivity distribution, typical for many real world networks. Random small-world and scale-free networks are generally better synchronizable than regular networks [3]. Moreover, systems with a homogenous connectivity are better synchronizable than heterogeneous ones. Until now, many criteria for network synchronization have been derived (e.g., [16–19]).

Pecora and Carroll [3] proposed the *master-stability-function* (MSF) method to study complete synchronization of coupled dynamical systems with complex network connections. Its main idea is to transform the stability of the synchronous manifold into the stability of the corresponding master-stability equation. It is valid for small perturbations around the synchronous state. Another choice to derive synchronization conditions is the Lyapunov direct method by which one can construct a Lyapunov function and then analyze the local or global synchronization [12,20–22]. Recently, the *connection-graph stability* was proposed in [13] to provide global synchronization conditions by combining graph properties.

The previous results obtained by these methods, to some extent, have their limitations. The MSF method requires that the Laplacian matrices are diagonal or block diagonal. Some of the existing local stability criteria (such as [22]) are based on the prerequirement of a synchronous state. Here we develop local and global synchronization conditions for much wider applications, especially without assuming that the coupling matrix is non-negative and diagonal. By means of the *matrix measure approach* [8,9], we achieve synchronization criteria independent of the uncoupled solution of the synchronous state.

We study the following coupled-map networks:

$$x_i(t+1) = f[x_i(t)] + \varepsilon \sum_{j=1}^{N} W_{ij}\{f[x_j(t)] - f[x_i(t)]\} \qquad (1)$$

for $1 \le i \le N$, where $f[x_i(t)]$ is a continuously differential function governing the dynamics of the individual nodes, often chosen to be a chaotic map. $W=(W_{ij})_{N\times N} \in \mathbb{R}^{N\times N}$ describes the coupling configuration: if there is a connection between node i and node j, then $W_{ij} \neq 0$; otherwise $W_{ij}=0$. Here W is not restricted to be completely symmetric and non-negative. The network becomes synchronized if $\lim_{t\to\infty}|x_i(t)-x_j(t)|=0$ for all $1 \le i,j \le N, i \neq j$. In this case, each node evolves in the same manner, i.e., $s(t+1)=f[s(t)]$ and $x_1(t)=x_2(t)=\cdots=x_N(t)=s(t)$. Denote $\mathbf{S}=\{x=(x_1,x_2,\ldots,x_N)^T, x_i \in R, x_i=x_j, i,j=1,2,\ldots,N\}$ be the synchronization manifold. Without loss of generality, let $x_1(t)$ be the reference synchronized direction. Then we define the stability of the synchronization manifold as follows: (i) system (1) is said to be *locally synchronized* if there exists a constant $\delta>0$ such that if $\|x_i(t_0)-x_1(t_0)\|<\delta$ for $1 \le i \le N$, then for arbitrary $\epsilon>0$, there exists a constant $T>t_0$ such that $\|x_i(t)-x_1(t)\|<\epsilon$ for all $t \ge T$ and $1 \le i \le N$ and (ii) system (1) is said to be *globally synchronized* if for arbitrary $\epsilon>0$, there exists a constant $T>t_0$ such that $\|x_i(t)-x_1(t)\|<\epsilon$ for all $t \ge T$ and $x_i(t_0) \in R, 1 \le i \le N$.

Denote by $X_{1i}(t)=x_i(t)-x_1(t)$, then

$$X_{1i}(t+1) = f[x_i(t)] - f[x_1(t)] + \varepsilon \sum_{j=1}^{N} W_{ij}(f[x_j(t)] - f[x_i(t)]) - \varepsilon \sum_{j=1}^{N} W_{1j}(f[x_j(t)] - f[x_1(t)])$$

for $2 \le i \le N$. Define the matrix S_w,

$$S_w = \begin{bmatrix} -\left(W_{12} + \sum_{j\neq 2} W_{2j}\right) & W_{23} - W_{13} & \cdots & W_{2N} - W_{1N} \\ W_{32} - W_{12} & -\left(W_{13} + \sum_{j\neq 3} W_{3j}\right) & \cdots & W_{3N} - W_{1N} \\ \vdots & \vdots & \ddots & \vdots \\ W_{N2} - W_{12} & W_{N3} - W_{13} & \cdots & -\left(W_{1N} + \sum_{j\neq N} W_{Nj}\right) \end{bmatrix}.$$

Then, we get one compact form,

$$\bar{X}(t+1) = (I_{N-1} + \varepsilon S_w)\bar{f}[x(t)], \tag{2}$$

where $\bar{X}(t)=[X_{12}(t),X_{13}(t),\ldots,X_{1N}(t)]^T$ and $\bar{f}[x(t)]=\{\bar{f}_1[x_2(t)],\ldots,\bar{f}_{N-1}[x_N(t)]\}=\{f[x_2(t)]-f[x_1(t)],\ldots,f[x_N(t)]-f[x_1(t)]\}^T$.

We first introduce the concept of matrix measure. Let C denote the field of complex numbers; the matrix measure of a complex square matrix $B \in C^{n\times n}$ is defined by [23]

$$\mu(B) = \lim_{h\to 0^+} \frac{\|I_n + hB\| - 1}{h}, \tag{3}$$

in which $\|\cdot\|$ is a matrix norm and I_n is the identity matrix. For the matrix norms $\|B\|_1=\max_j \Sigma_{i=1}^N |b_{ij}|$, $\|B\|_2=\sqrt{\lambda_{\max}(B^TB)}$, and $\|B\|_\infty=\max_i \Sigma_{j=1}^n |b_{ij}|$, we obtain the matrix measure [23]: $\mu_1(B)=\max_j\{\mathrm{Re}(b_{jj})+\Sigma_{i=1,i\neq j}^n |b_{ij}|\}$, $\mu_2(B)=\frac{1}{2}\lambda_{\max}(B^H+B)$, and $\mu_\infty(B)=\max_i\{\mathrm{Re}(b_{ii})+\Sigma_{j=1,j\neq i}^n |b_{ij}|\}$, respectively, where $\lambda_{\max}(\cdot)$ denotes the maximum eigenvalue of a complex matrix and B^H is the complex-conjugate transpose of a complex matrix. Note that $B^H=B^T$ if B is a real square matrix.

To obtain the condition for local synchronization, we consider small perturbations $\eta_i(t)(1\leq i\leq N-1)$ near the reference direction of the synchronization manifold. Then $\bar{f}_i[x_{i+1}(t)]$ can be approximated by

$$\bar{f}_i[x_{i+1}(t)] = f'[x_1(t)]\eta_i(t), \tag{4}$$

where $f'[x_1(t)]$ is the derivative at the reference synchronized direction. Then Eq. (2) is rewritten as

$$\eta(t+1) = f'[x_1(t)](I_{N-1} + \varepsilon S_w)\eta(t), \tag{5}$$

where $\eta(t)=[\eta_1(t),\eta_2(t),\ldots,\eta_{N-1}(t)]^T$. Next we construct a non-negative function,

$$V(t) = \eta^T(t) P \eta(t), \tag{6}$$

where P is an arbitrary positive definite matrix. Clearly, $V(t)\geq 0$ and the equality holds only if all components of $\eta(t)$ are equal to zero. That is, the synchronization errors with respect to the reference direction will disappear as $V(t)$ converges to zero. Note that P can be decomposed into $P=M^TM$, where M is an $(N-1)\times(N-1)$ nonsingular square matrix. Then

$$V(t) = \eta^T(t)M^TM\eta(t) = f'[x_1(t-1)]^2\eta^T(t-1)M^T \times[M^{-T}(I_{N-1}+\varepsilon S_w)^TM^TM(I_{N-1}+\varepsilon S_w)M^{-1}]M\eta(t-1). \tag{7}$$

We introduce $U=M^{-T}(I+\varepsilon S_w)^TM^TM(I+\varepsilon S_w)M^{-1}$. Then

$$V(t) \leq f'[x_1(t-1)]^2\mu_\theta(U)V(t-1) = \prod_{k=0}^{t-1}\{f'[x_1(t)]^2\mu_\theta(U)\}V(0), \tag{8}$$

where $\mu_\theta(U)$ is the matrix measure of U [23] and $\theta \in \{1,2,\infty\}$. Thus if

$$\lim_{t\to\infty}\prod_{k=0}^{t-1}|f'[x_1(k)]|\sqrt{\mu_\theta(U)} = 0, \tag{9}$$

then

$$\lim_{t\to\infty} V(t) = \lim_{t\to\infty} \eta^T(t)M^TM\eta(t) = 0.$$

Accordingly, the synchronization error $\eta(t)$ can be asymptotically stable. Hence Eq. (9) holds if

$$\lim_{t\to\infty}\frac{1}{t}\log\prod_{k=0}^{t-1}|f'[x_1(k)]|\sqrt{\mu_\theta(U)} = 0, \tag{10}$$

that is,

$$\log\sqrt{\mu_\theta(U)} + \lim_{t\to\infty}\frac{1}{t}\sum_{k=0}^{t-1}\log|f'[x_1(k)]| = 0. \tag{11}$$

Then a sufficient condition for local synchronization is

$$\mu_\theta(U) \leq e^{-2\lambda^f}, \tag{12}$$

where $\lambda^f=\lim_{t\to\infty}\frac{1}{t}\Sigma_{k=0}^{t-1}\log|f'[x_1(k)]|$ is the Lyapunov exponent of the map f. For a chaotic map, the Lyapunov exponent can be calculated. Therefore, the upper bound of the matrix measure can be determined in Eq. (12). Further, the proposed condition can be used to evaluate the stability of the synchronization manifold of coupled-map networks.

In Ref. [22], the authors presented a local stability condition for synchronization in which the norm of the Jacobian is related to the synchronization trajectory (a solution of the uncoupled system). However, it is well known that the synchronization trajectory is unknown in advance, and the criterion is hard to be used in applications. As for the condition

given by Eq. (12), the upper bound of the matrix measure is only controlled by the Lyapunov exponent of the map f which can be calculated independently. In addition, the condition is less conservative than those in Refs. [17,18] where the coupling matrices are diagonal or block diagonal. Moreover, the coupling in this Brief Report can be cooperative or competitive, i.e., $W_{ij}>0$ or $W_{ij}<0$. Thus the condition derived from the matrix measure has a wider range of application.

The above analysis is based on the linear expansion around the synchronization manifold, which is valid only for small perturbations around the synchronization manifold. To derive a global criterion that guarantees synchronization of the coupled-map networks for arbitrary initial values, we assume a basic property for f,

$$|f(x)-f(y)| \le \sup|f'||x-y|. \tag{13}$$

A natural way is to choose a non-negative function for Eq. (2) as

$$V(t)=\bar{X}^T(t)P\bar{X}(t), \tag{14}$$

and we can derive a condition under which

$$V(t)\to 0 \quad \text{as} \quad t\to\infty. \tag{15}$$

We get then

$$\begin{aligned} V(t+1) &= \bar{X}^T(t+1)P\bar{X}(t+1) \\ &= \bar{f}^T[x(t)](I_{N-1}+\varepsilon S_w)^T P(I_{N-1}+\varepsilon S_w)\bar{f}[x(t)] \\ &\le \mu_\theta(U)\bar{f}^T[x(t)]M^T M\bar{f}[x(t)] \le \mu_\theta(U)\sup|f'|^2 V(t). \end{aligned} \tag{16}$$

Then

$$V(t)\le V(0)[\mu_\theta(U)\sup|f'|^2]^t. \tag{17}$$

Therefore, network (1) globally asymptotically synchronizes if

$$\mu_\theta(U)\le \frac{1}{\sup|f'|^2}. \tag{18}$$

Above criterion (18) allows us to consider any solution $x(t)$ of Eq. (1).

To verify our criteria, we took a quadratic map for the unit dynamics, that is, $f(x)=ax(1-x), x\in[0\ \ 1]$. The Lyapunov exponent for this map can be directly calculated for constant $a\in[3\ \ 4]$. As the simplest case, the globally coupled network with $N=100$ is considered. The coupling matrix has then the form

$$W=\begin{bmatrix} 0 & 1 & 1 & \cdots & 1 \\ 1 & 0 & 1 & \cdots & 1 \\ \vdots & \ddots & \ddots & \ddots & \vdots \\ 1 & 1 & \cdots & 0 & 1 \\ 1 & 1 & \cdots & 1 & 0 \end{bmatrix},$$

which yields

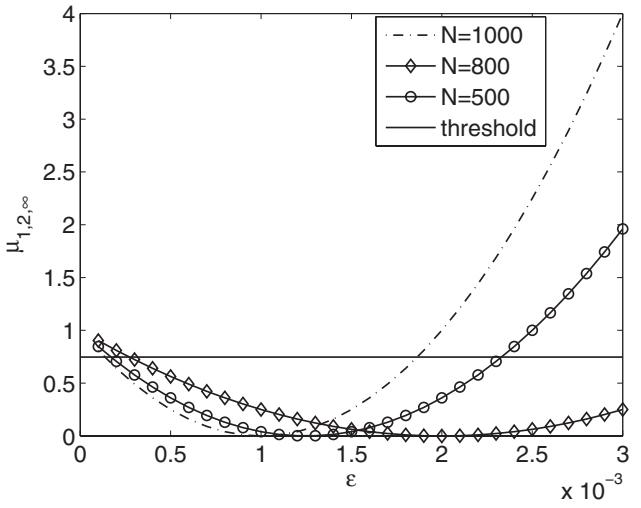

FIG. 1. The matrix measure vs coupling strength in the global coupled networks for different scales. In this case, $a=3.59$.

$$S=\begin{bmatrix} -N & 0 & \cdots & 0 \\ 0 & -N & \cdots & 0 \\ \vdots & \ddots & \ddots & \vdots \\ 0 & 0 & \cdots & -N \end{bmatrix}.$$

We take M as the identity matrix (i.e., $M=I_N$) and get $U=I+\varepsilon(S_w^T+S_w)+\varepsilon^2 S_w^T S_w$. From the definition of the matrix measure [23], we have

$$\mu_{\{1,2,\infty\}}[I+\varepsilon(S_w^T+S_w)+\varepsilon^2 S_w^T S_w]=(\varepsilon N-1)^2. \tag{19}$$

So we choose an $\varepsilon\sim\frac{1}{N}$ such that $\mu[I+\varepsilon(S_w^T+S_w)+\varepsilon^2 S_w^T S_w]<e^{-2\lambda^F}$. For different scales, the critical points for local synchronization can be found as shown in Fig. 1. Then the condition for local synchronization is obtained. For the case of global synchronization, we have $\sup|f'|^2=a^2$. Applying the condition in Eq. (18) we find that the system will globally synchronize if $(\varepsilon N-1)^2<\frac{1}{a^2}$. Further more, we also validate

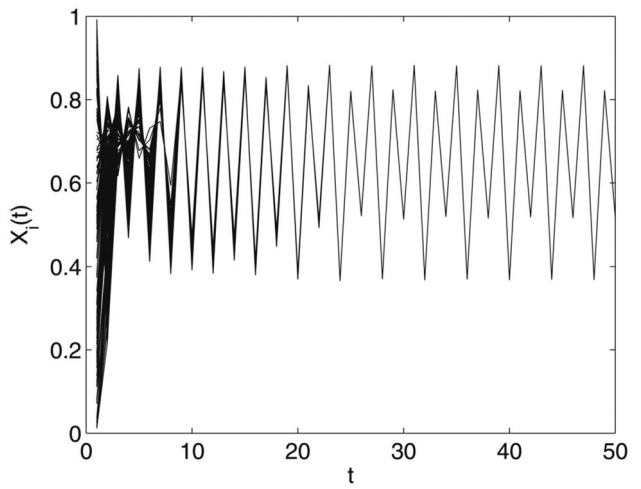

FIG. 2. The dynamic behaviors of each node in the weighted network. Here network parameters are $N=100$, $m=5$, and $\langle k\rangle=10$

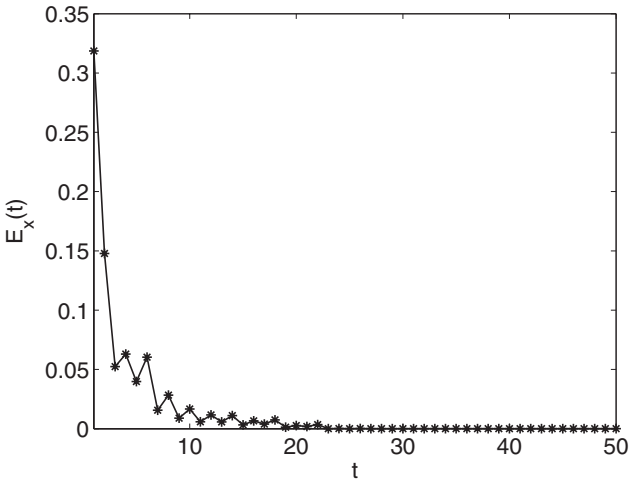

FIG. 3. Synchronization absolute errors varying with time in weighted network with $N=100$, $m=5$, and $\langle k\rangle=10$.

our results for directed weighted networks by numerical simulations. In contrast with the case of globally coupled networks, there is no general expression of the matrix measure with respect to the coupling strength. For directed weighted networks, we consider scale-free networks which are generated by using the Barabasi-Albert (BA) model [15] with $N=100$, $m=5$, and $\langle k\rangle=10$. The weight on each connection in the scale-free networks is given by $W_{ij}=1/k_i$ for all i,j.

Letting $a=3.53$ in the map, we take the coupling strength $\varepsilon=0.4$ which satisfies our criteria. From the time series of each unit in coupled system, it can be seen that all units very fast evolve in the same oscillating manner, as shown in Fig. 2. This synchronization process can also be detected by considering the average synchronization absolute error $E_X(t)=\frac{1}{N-1}\Sigma_{j=2}^{N}|X_{1j}(t)|$ with respect to x_1. It is shown in Fig. 3 that this system rapidly synchronizes to the reference direction.

To conclude, we study synchronization of coupled-map networks. Conditions for the local and global synchronizations are derived using matrix measure approach. Comparing with many existing synchronization conditions, the proposed criteria do not depend on the solution of the synchronous state and give less limitations on the network connections.

P.L. and Y.W. are indebted to the financial support by China Scholarship Council. M.C. thanks NSFC project (Grant No. 60804046) and Special Doctoral Fund at University by Ministry of Education (Grant No. 20070003129). J.K. thanks the supports by SFB 555 (DFG) and BIO SIM (EU).

[1] R. Albert and A. L. Barabási, Rev. Mod. Phys. **74**, 47 (2002); S. Boccaletti, V. Latora, Y. Moreno, M. Chavez, and D.-U. Hwang, Phys. Rep. **424**, 175 (2006).
[2] A. Pikovsky, M. Rosemblum, and J. Kurths, *Synchronization: A Universal Concept in Nonlinear Sciences* (Cambridge University Press, Cambridge, 2001).
[3] L. M. Pecora and T. L. Carroll, Phys. Rev. Lett. **80**, 2109 (1998); M. Barahona and L. M. Pecora, *ibid.* **89**, 054101 (2002).
[4] C. S. Zhou, A. E. Motter, and J. Kurths, Phys. Rev. Lett. **96**, 034101 (2006).
[5] Chai Wah Wu and L. O. Chua, IEEE Trans. Circuits Syst., I: Fundam. Theory Appl. **42**, 775 (1995).
[6] A. E. Motter, C. S. Zhou, and J. Kurths, Europhys. Lett. **69**, 334 (2005); C. S. Zhou and J. Kurths, Chaos **16**, 015104 (2006).
[7] S. Boccaletti, D.-U. Hwang, M. Chavez, A. Amann, J. Kurths, and L. M. Pecora, Phys. Rev. E **74**, 016102 (2006).
[8] M. Chen, Phys. Rev. E **76**, 016104 (2007).
[9] M. Chen, IEEE Trans. Circuits Syst., II: Express Briefs **53**, 1185 (2006).
[10] Chai Wah Wu, Proceedings of the 1998 IEEE International Symposium on Circuits and Systems, 1998 (unpublished), Vol. 3, p. 302.
[11] M. Chen, IEEE Trans. Circuits Syst., I: Regul. Pap. **55**, 1335 (2008).
[12] X. F. Wang and G. Chen, IEEE Trans. Circuits Syst., I: Fundam. Theory Appl. **49**, 54 (2002); X. Li and G. Chen, *ibid.* **50**, 1381 (2003).
[13] V. N. Belykh, I. V. Belykh, and M. Hasler, Physica D **195**, 159 (2004).
[14] D. J. Watts and S. H. Strogatz, Nature (London) **393**, 440 (1998).
[15] A.-L. Barabási and R. Albert, Science **286**, 509 (1999).
[16] A. Arenas, A. Díaz-Guilera, J. Kurths, Y. Moreno, and C. S. Zhou, Phys. Rep. **469**, 93 (2008).
[17] J. Jost and M. P. Joy, Phys. Rev. E **65**, 016201 (2001).
[18] K. Li, M. Small, and X. Fu, Phys. Rev. E **76**, 056213 (2007).
[19] F. M. Atay, T. Bıyıkoğlu, and J. Jost, Physica D **224**, 35 (2006).
[20] R. E. Amritkar, S. Jalan, and C.-K. Hu, Phys. Rev. E **72**, 016212 (2005).
[21] R. He and P. G. Vaidya, Phys. Rev. E **57**, 1532 (1998).
[22] W. L. Lu and T. P. Chen, Physica D **198**, 148 (2004).
[23] R. A. Horn and C. R. Johnson, *Matrix Analysis* (Cambridge University Press, Cambridge, 1985).

Synchronization in small-world networks

Ye Wu,[1] Yun Shang,[2] Maoyin Chen,[3,a)] Changsong Zhou,[4] and Jürgen Kurths[1]
[1]*Center for Dynamics of Complex Systems, Potsdam Universität, Am Neuen Palais 10, D-14469 Potsdam, Germany*
[2]*Institute of Mathematics, AMSS, Academia Sinica, Beijing 100080, China*
[3]*Tsinghua National Laboratory for Information Science and Technology, Beijing 100084, China and Department of Automation, Tsinghua University, Beijing 100084, China*
[4]*Department of Physics, Hong Kong Baptist University, Kowloon Tong, Hong Kong*

(Received 8 February 2008; accepted 15 May 2008; published online 22 September 2008)

In this paper we consider complete synchronization in small-world networks of identical Rössler oscillators. By applying a simple but effective dynamical optimization coupling scheme, we realize complete synchronization in networks with undelayed or delayed couplings, as well as ensuring that all oscillators have uniform intensities during the transition to synchronization. Further, we obtain the coupling matrix with much better synchronizability in a certain range of the probability p for adding long-range connections. Direct numerical simulations fully verify the efficiency of our mechanism. © *2008 American Institute of Physics*. [DOI: 10.1063/1.2939136]

In the past decade, synchronization in complex networks, especially the question of synchronizability, attracts a lot of interest. The works on synchronizability in networks with a given topology can be divided into two classes according to the coupling matrix in networks. One is the static mechanism, where the coupling matrix remains fixed during the transition to synchronization. From the degree and load based weighted networks, the synchronizability becomes optimal when the intensities of all oscillators become uniform. The other one is the dynamical mechanism, where the coupling matrix evolves in time by introducing adaptive strengths between connected oscillators. The adaption process can enhance synchronization by modifying the coupling matrix in networks, but the synchronizability is still far from being optimal. This is because the resulting networks have nonuniform intensities even for networks with homogeneous degrees. In this paper we consider complete synchronization in small-world networks of identical Rössler oscillators by applying a simple but effective dynamical optimization coupling scheme. We realize complete synchronization in networks with undelayed or delayed couplings, as well as ensure that all oscillators have uniform intensities during the transition to synchronization. Moreover, we obtain the coupling matrix with much better synchronizability in a certain range of the probability p for adding long-range connections.

I. INTRODUCTION

In the past decade, the dynamics of complex networks has been extensively investigated, with special emphasis on the interplay between the complexity in the overall topology and the local dynamical properties of the coupled oscillators.[1–28] As a typical kind of dynamics on complex networks, synchronization, especially the ability of networks to become synchronized (synchronizability), has attracted a lot of interest in multidisciplinary fields.[8–28] The works on synchronizability in networks with a given topology can be divided into two classes according to the coupling matrix. One is the static mechanism, where the coupling matrix remains fixed during the transition to synchronization. The character is that the coupling matrix unidirectionally affects synchronization.[9,10,13–20] It has been recently shown that for randomly enough unweighted and weighted networks,[20] the synchronizability is controlled by $S_{\max}/S_{\min}$, where $S_{\max}$ and $S_{\min}$ are the maximum and minimum of the intensities S_i, defined by the sum of the couplings for oscillator i. For unweighted scale-free networks (SFNs) generated by the Barabási–Albert model,[2] $S_{\max}/S_{\min}=k_{\max}/k_{\min}\sim N^{1/2}$, where N is the network size, $k_{\max}$ and $k_{\min}$ are the maximal and minimal degrees, respectively. From the degree[15,16] and load[13,14] based weighted networks, the synchronizability becomes optimal when the intensities of all oscillators become uniform.

The other is the dynamical mechanism, where the coupling matrix evolves in time by introducing adaptive strengths between connected oscillators. The adaptation process can enhance synchronization by modifying the coupling matrix. However, during the transition to synchronization, the dynamical mechanism[21,22] cannot ensure uniform intensities even for small-world networks (SWNs), which is not consistent with the necessary condition for the optimal synchronizability in the static mechanism.[13–16,19] Zhou and Kurths proposed a dynamical mechanism using local information among each oscillator and its neighbors.[21] In the corresponding networks the connections between different oscillators are strengthened. The adaptive process drives the network into the direction of a more homogeneous topology, ongoing with an enhanced ability for synchronization. Thereby it is possible to synchronize networks that exceed by several orders of magnitude the size of the largest com-

a)Author to whom correspondence should be addressed. Electronic mail: mychen@mail.tsinghua.edu.cn.

parable random graph that is still synchronizable.[29] For simplicity, we call this mechanism the Zhou–Kurths method. It shows that the Zhou–Kurths method is very effective to realize synchronization in SFNs, and can enhance the synchronizability in SFNs substantially. After the adaptation of the couplings, the weights of incoming links V_i scale with the degree k of the corresponding oscillator $\mathbf{x}_i$ as $V(k)\sim k^{-\theta}$, and the synchronizability is characterized by $S_{\max}/S_{\min}\sim N^{\beta/2}$ with $\beta=1-\theta$ and $\theta=0.54\pm0.01$ for SFNs of Rössler oscillators, and the average intensity $S(k)$ over oscillators with degree k increases as $S(k)\sim k^{\beta}$ (Ref. 21).

In this paper we consider complete synchronization in SWNs, especially the Newman–Watts (NW) model,[28] by introducing a simple but effective dynamical mechanism. Our aims are to (i) realize complete synchronization in SWNs with undelayed or delayed couplings, whose oscillators all have uniform intensities during the transition to synchronization, and (ii) to assign the coupling matrix with enhanced synchronizability in certain cases.

By applying the *dynamical optimization* (DO) mechanism,[24] we will achieve the above aims. The DO mechanism adjusts the coupling strengths based on the "winner-take-all" strategy. It realizes complete synchronization in SFNs with undelayed couplings, as well as enhances the synchronizability greatly.[24] In this paper, we extend the DO mechanism to NW networks with undelayed or delayed couplings. We show that the DO mechanism is more effective in realizing synchronization in NW networks than the Zhou–Kurths method. Since the DO mechanism can ensure the uniform intensities of all oscillators, it can also effectively realize synchronization in NW networks with delayed couplings. But the Zhou–Kurths method cannot realize synchronization in networks with delayed couplings. Moreover, in a certain range of the probability p for adding long-range connections, we design a coupling matrix for NW networks, which has much better synchronizability than unweighted networks, degree based weighted networks and the Zhou–Kurths method.

This paper is organized as follows: In the next section, by applying the DO mechanism, we can realize complete synchronization in NW networks of identical Rössler oscillators, as well as ensure the uniform intensities of all oscillators during the transition to synchronization. In Sec. III, we enhance the synchronizability in NW networks by designing the coupling matrix. We draw up our conclusions in the last section.

II. SYNCHRONIZATION IN SMALL-WORLD NETWORKS

Our general model for networks consisting of N coupled identical Rössler oscillators with a time-varying coupling matrix is given by

$$\dot{\mathbf{x}}_i=\mathbf{F}(\mathbf{x}_i)+\sum_{j=1}^{N}G_{ij}\mathbf{H}(\mathbf{x}_j,\mathbf{x}_i), \tag{1}$$

where $\mathbf{x}_i$ is the state, $\mathbf{F}(\mathbf{x}_i)$ is the dynamics of the individual oscillator $\mathbf{x}_i$, $\mathbf{H}(\mathbf{x}_j,\mathbf{x}_i)$ is the inner coupling function, $G=(G_{ij})$ is the outer coupling matrix. $G_{ij}=A_{ij}W_{ij}$, where $A=(A_{ij})$ is the binary adjacency matrix, W_{ij} is the coupling strength of the incoming link $(\mathbf{x}_i,\mathbf{x}_j)$ pointing from oscillator $\mathbf{x}_j$ to oscillator $\mathbf{x}_i$ if they are connected, $G_{ii}=-\Sigma_{j\in K_i}A_{ij}W_{ij}$, K_i is the neighbor set of oscillator $\mathbf{x}_i$.

In this paper we consider complete synchronization in network (1) in two cases. (i) One case is the network (1) with undelayed couplings, where the function $\mathbf{H}(\mathbf{x}_j,\mathbf{x}_i)=\mathbf{H}_0(\mathbf{x}_j)-\mathbf{H}_0(\mathbf{x}_i)$, and $\mathbf{H}_0$ is the output function for each oscillator. (ii) The other case is the network (1) with delayed couplings, in which the function $\mathbf{H}(\mathbf{x}_j,\mathbf{x}_i)=\mathbf{H}_0[\mathbf{x}_j(t-\tau)]-\mathbf{H}_0[\mathbf{x}_i(t)]$ with a time delay $\tau>0$.

Our aim is to realize complete synchronization in network (1), as well as ensure that all oscillators in network (1) have uniform intensities during the transition to synchronization. Recently, we have already obtained some results on this problem. For different variants of the Kuramoto model, we have proposed a *dynamical gradient network* (DGN) approach to realize phase synchronization.[23] It shows that all the oscillators have uniform intensities during the transition to synchronization. However, the DGN approach is very special in two aspects. One is that it should assign a scale potential to each oscillator within any time interval, which depends on the extent of the local synchronization among itself and its neighbor oscillators. The other is that the incoming link to be adjusted by the DGN approach is often not mostly effective. Inspired by the idea of the DGN approach,[23] we have further introduced a DO mechanism for SFNs.[24] It reflects the "winner-take-all" strategy, where the incoming link to be adjusted is always chosen as a pair of oscillators with the weakest synchronization. This means that the DO mechanism is more effective than the DGN approach. We also show that the DO mechanism has much better synchronizability in SFNs than the Zhou–Kurths method.[24]

In this paper, we apply the DO mechanism to SWNs with undelayed or delayed couplings. Here we first introduce the idea of the DO mechanism. The DO mechanism is to increase the strength of only one incoming link of each oscillator by a small amount ε, at every time step $t_n=t_0+nT$ for $n\geqslant 1$, where t_0 is the transient time, and $T>0$ is the length of time intervals. For oscillator $\mathbf{x}_i$ and its neighbor oscillator $\mathbf{x}_j$, the total synchronization difference,

$$E_n(i,j)=\int_{t_{n-1}}^{t_n}\phi(\mathbf{x}_i,\mathbf{x}_j)dt \tag{2}$$

within the interval $[t_{n-1},t_n)$ is evaluated, where ϕ is a synchronization error function. For complete synchronization in SWNs, the function ϕ is a non-negative error function if oscillators i,j are not synchronized, and satisfies $\phi(\mathbf{x}_i,\mathbf{x}_i)=0$ if oscillators i,j are synchronized. To check complete synchronization in network (1), the function ϕ is chosen as $\phi(\mathbf{x}_i,\mathbf{x}_j)=|x_i-x_j|+|y_i-y_j|+|z_i-z_j|$.

The total synchronization difference $E_n(i,j)$ reflects the competition ability of the incoming link $(\mathbf{x}_i,\mathbf{x}_j)$ within the time interval $[t_{n-1},t_n)$. For oscillator $\mathbf{x}_i$, the incoming link with the weakest synchronization, i.e., $(\mathbf{x}_i,\mathbf{x}_{j^n_{\max}})$, is the winner within the interval $[t_{n-1},t_n)$, where the index $j^n_{\max}$ is decided by the following dynamical optimization problem:

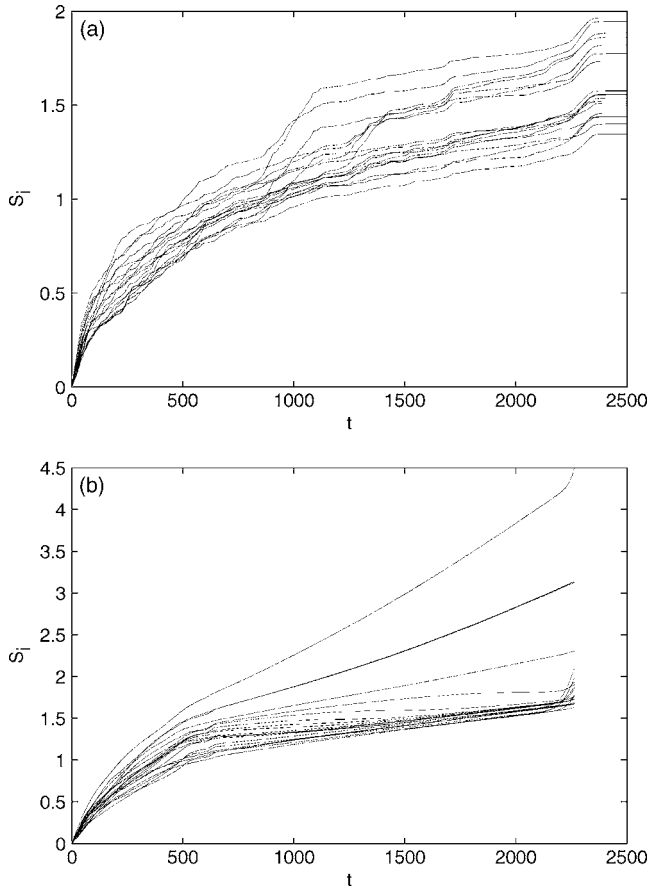

FIG. 1. The intensities S_i as a function of time t for arbitrarily 20 oscillators in networks with undelayed couplings (a), or delayed couplings (b), by the Zhou–Kurths method. The parameters are $N=500$, $K=4$, $p=0.003$, $\gamma=0.002$, $\tau=0.01$ s.

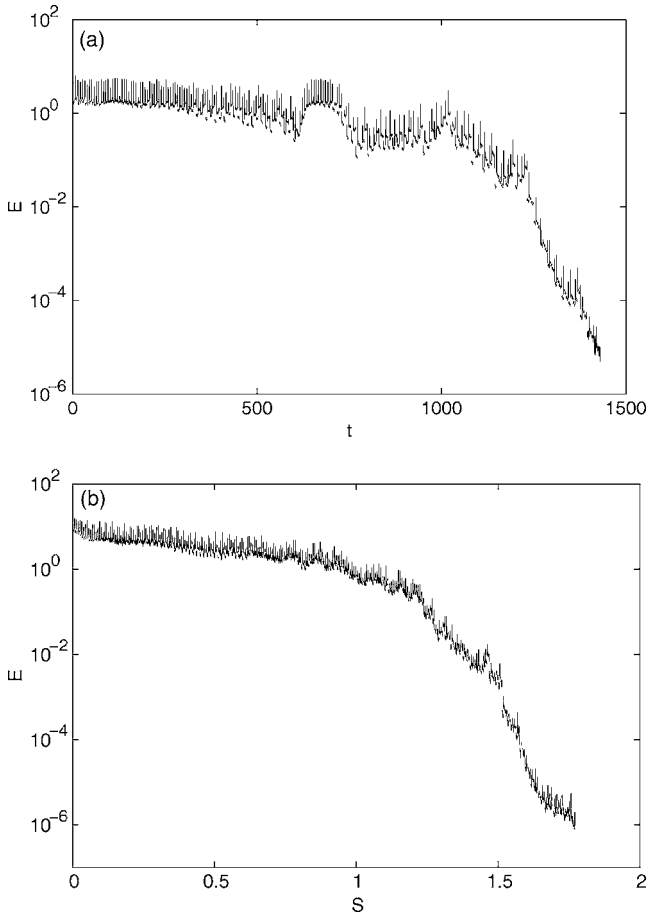

FIG. 2. The average synchronization error E in networks with undelayed couplings as a function of (a) time t, and (b) the intensity S, by the DO mechanism. The parameters are $N=500$, $K=4$, $p=0.003$, $T=1$ s, $\varepsilon=0.001$.

$$j_{\max}^n = \arg\max_{j\in K_i} E_n(i,j). \tag{3}$$

The solutions of the optimization (3) within different intervals are also different, which depends on the dynamics of oscillators. The connection strength is then adjusted dynamically by

$$W_{ij_{\max}^n}^{n+1} = W_{ij_{\max}^n}^n + \varepsilon, \quad W_{ij}^{n+1} = W_{ij}^n, \quad j \neq j_{\max}^n, \tag{4}$$

where $\varepsilon>0$ is a small value, and W_{ij}^n is the coupling strength in the interval $[t_{n-1},t_n)$.

From Eqs. (3) and (4), we strengthen the incoming link with the weakest synchronization, namely, the link with the maximal competition ability. For complete synchronization in SWNs with undelayed couplings, the additional term $\varepsilon(\mathbf{x}_{j_{\max}^n}-\mathbf{x}_i)$ can be regarded as the negative feedback term for the unidirectional synchronization from oscillator $\mathbf{x}_{j_{\max}^n}$ to oscillator $\mathbf{x}_i$. This could make the synchronization difference between oscillator $\mathbf{x}_i$ and its neighbor $\mathbf{x}_{j_{\max}^n}$ be smaller, which implies the synchronization in SWNs be realized.

Note that the intensities of all oscillators in network (1) are uniform, since at each step the intensity of each oscillator increases by the same amount ε. This is consistent with the necessary condition for optimal synchronizabiliy in the static mechanism.[13–16,19]

In order to show the effectiveness of the DO mechanism, our analysis and simulations are based on SWNs generated by the NW model.[28] The initial network is a K nearest-neighbor coupled network consisting of N oscillators arranged in a ring, with each oscillator $\mathbf{x}_i$ being adjacent to its neighbor oscillators $\mathbf{x}_{i\pm1},\cdots,\mathbf{x}_{i\pm K/2}$, and with K being even. Then one adds with probability p a connection between a pair of oscillators. In the following, network (1) is a network of Rössler oscillators, $\mathbf{x}_i=(x_i,y_i,z_i)$, $\mathbf{F}(\mathbf{x}_i)=[-0.97y_i-z_i,0.97x_i+0.15y_i,z_i(x_i-8.5)+0.4]$, the function $\mathbf{H}_0(\mathbf{x}_i)=(x_i,0,0)$. In order to show complete synchronization, we define the average synchronization error as $E=\frac{1}{N}\Sigma_{i=1}^N\|\mathbf{x}_i-\bar{\mathbf{x}}\|$, where $\bar{\mathbf{x}}=(\bar{x},\bar{y},\bar{z})$ is the mean-field of all $\mathbf{x}_i$. In our simulations, the initial coupling strengths for all incoming links are zero, the transient time is $t_0=100$ s, the length of time intervals is $T=1$ s, and the small value is $\varepsilon=0.001$. Further, initial conditions for all oscillators are randomly chosen from the chaotic attractor. The solution of network (1) is solved by using the Euler method with the time step $h=0.01$ s, and our ending condition for the DO mechanism is $E<10^{-5}$.

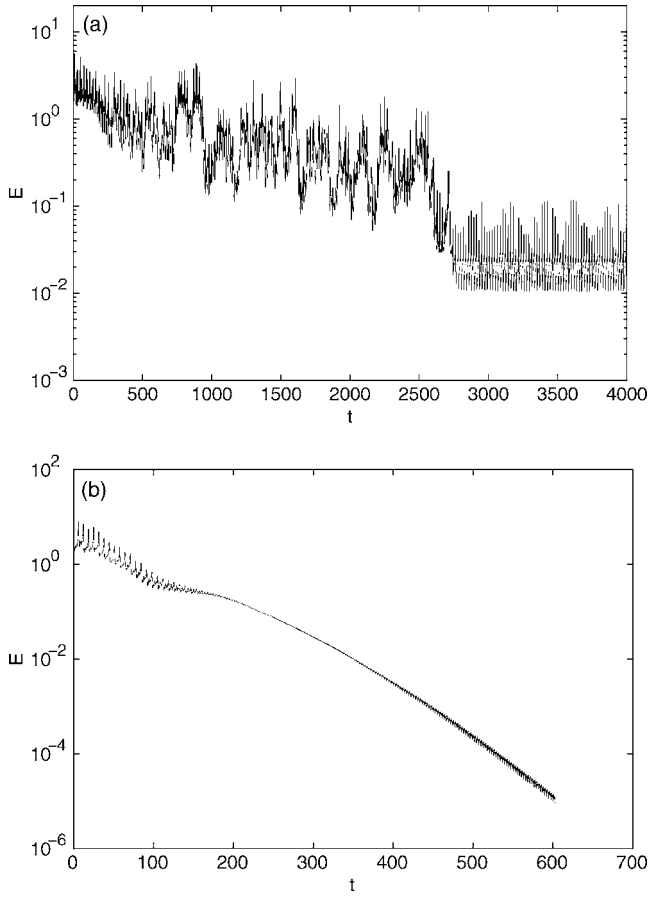

FIG. 3. The average synchronization error E in networks with delayed couplings as a function of time t. (a) The Zhou–Kurths method ($\tau=0.01$ s). (b) The DO mechanism ($\tau=2$ s). The parameters $N=500$, $p=0.003$, $\gamma=0.002$, $T=1$ s, $\varepsilon=0.001$.

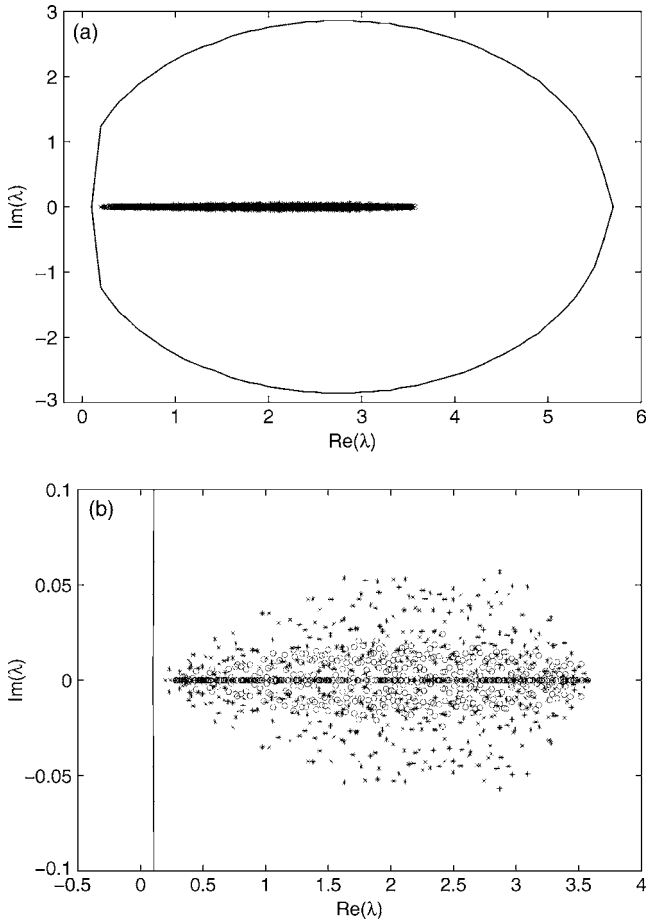

FIG. 4. [(a) and (b)] Distribution of eigenvalues of the Laplacian matrix of σG_{norm} in network (1) with undelayed couplings (○) and delayed couplings (∗). Solid line: The stability region $\mathcal{R}$. The parameters are $N=500$, $K=4$, $p=0.003$, $T=1$ s, $\varepsilon=0.001$, $\sigma=2$, $\tau=1$ s.

In this paper we consider complete synchronization in NW networks in two cases. (i) One case is the network (1) with undelayed couplings, where the function $\mathbf{H}(\mathbf{x}_j,\mathbf{x}_i)=\mathbf{H}_0(\mathbf{x}_j)-\mathbf{H}_0(\mathbf{x}_i)$. From recent works,[21,22] the dynamical mechanism can realize complete synchronization both in SFNs with undelayed couplings and in SWNs with undelayed couplings. However, even for NW networks with homogeneous degrees, the dynamical mechanisms cannot ensure uniform intensities if all oscillators have different initial conditions. We plot the intensities S_i, defined by the sum of the coupling strengths of neighbor oscillators of oscillator i (i.e., $S_i=\Sigma_{j\in K_i}G_{ij}$), for 20 arbitrarily chosen oscillators in NW networks according to the Zhou–Kurths method [Fig. 1(a)]. When the adaptation parameter is chosen as $\gamma=0.002$ in the Zhou–Kurths method, we find that the Zhou–Kurths method cannot ensure uniform intensities during or after the adaptation. Based on the DO mechanism, complete synchronization in NW networks are realized effectively [Fig. 2(a)], and the intensities are always uniform during the transition to synchronization. From Fig. 2(b), the intensity $S=S_i$ is also a good indicator for synchronization in networks. As S increases to a critical value, a network becomes synchronous.

(ii) The other case is the network (1) with delayed couplings, in which the function $\mathbf{H}(\mathbf{x}_j,\mathbf{x}_i)=\mathbf{H}_0[\mathbf{x}_j(t-\tau)]-\mathbf{H}_0[\mathbf{x}_i(t)]$ with a time delay $\tau>0$. Even for a small time delay τ (such as $\tau=0.01$ s), the Zhou–Kurths method cannot realize synchronization in NW networks [Fig. 3(a)]. The synchronization error between two connected oscillators is about $10^{-2}\times 500=5$ for networks with $N=500$. Due to the DO mechanism, complete synchronization can be realized effectively when the time delay $\tau=2$ s [Fig. 3(b)]. The synchronization error is about $10^{-5}\times 500=0.005$. Hence the DO mechanism is more effective than the Zhou–Kurths method. The main reason is that the DO mechanism ensures that the intensities are always uniform during the transition to synchronization. But the Zhou–Kurths method cannot ensure uniform intensities even for the small time delay [Fig. 1(b)]. Though the difference of intensities between oscillators is small initially, it becomes large as time increases. The uniformity of intensities is the necessary condition for the existence of a synchronous manifold in NW networks with delayed couplings. After the adaptation, the synchronous manifold is given by $\mathbf{x}_i(t)=\mathbf{x}_0(t)$, $i=1,\ldots,N$, where $\mathbf{x}_0(t)$ is the solution of the isolated dynamics $\dot{\mathbf{x}}_0(t)=\mathbf{F}[\mathbf{x}_0(t)]+S_0\{\mathbf{H}_0[\mathbf{x}_0(t-\tau)]-\mathbf{H}_0[\mathbf{x}_0(t)]\}$, $S_0=\varepsilon n_0$ is the ultimate intensity, and n_0 is the ending adjustment step.

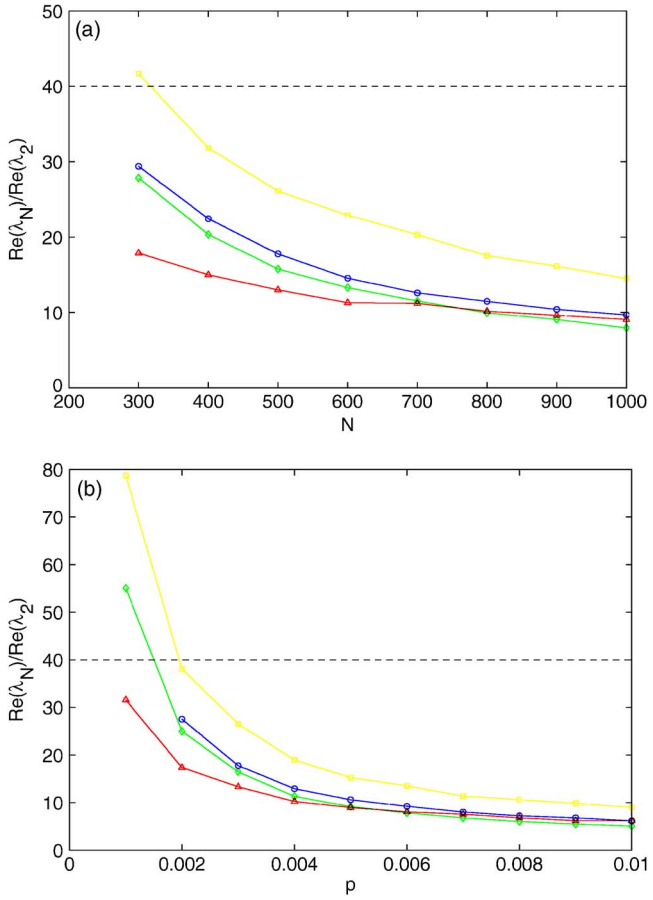

FIG. 5. (Color online) The ratio $\mathrm{Re}(\lambda_N)/\mathrm{Re}(\lambda_2)$ as a function of network size N for a fixed probability $p=0.003$ (a), and the probability p for a fixed size $N=500$ (b). Yellow line (□): type I networks; green line (◇): type II networks; blue line (○): type III networks; red line (△): type IV networks; black dashed line: the maximal ratio $\mathrm{Re}(\lambda_N)/\mathrm{Re}(\lambda_2)$ in the region $\mathcal{R}$. The parameters are $K=4$, $\gamma=0.002$, $T=1$ s, $\varepsilon=0.001$. All the estimates are averaged over 20 realizations of networks.

III. SYNCHRONIZABILITY IN SMALL-WORLD NETWORKS

In this section we discuss the synchronizability of NW networks. We first briefly review the stability of networks,

$$\dot{\mathbf{x}}_i = \mathbf{F}(\mathbf{x}_i) + \sigma \sum_{j=1}^{N} G_{ij}^0 [\mathbf{H}_0(\mathbf{x}_j) - \mathbf{H}_0(\mathbf{x}_i)], \tag{5}$$

where $\mathbf{H}_0$ is the output function, and σ is the overall coupling strength in networks. Without loss of generality, we assume that the coupling matrix $G^0=(G_{ij}^0)$ is asymmetric. The coupling matrix $G^0=(A_{ij}W_{ij}^0)$ is similarly defined as the matrix G in network (1). The variational equation for the synchronous state $\{\mathbf{x}_i=\mathbf{s}, \forall i\}$ is given by $\dot{\xi}_i=[D\mathbf{F}(\mathbf{s}) - \sigma\lambda_l D\mathbf{H}_0(\mathbf{s})]\xi_i$, where $\dot{\mathbf{s}}=\mathbf{F}(\mathbf{s})$ is the dynamics of the isolated oscillator, D is the Jacobian operator, and λ_l is a complex eigenvalue of the Laplacian matrix L $(=-G^0)$, satisfying $\mathrm{Re}(\lambda_1)\leqslant\mathrm{Re}(\lambda_2)\leqslant\cdots\leqslant\mathrm{Re}(\lambda_N)$. The largest Lyapunov exponent (LLE), $\Lambda(\alpha,\beta)$, of the master stability equation $\dot{\eta} =[D\mathbf{F}_0(\mathbf{s})-(\alpha+i\beta)D\mathbf{H}_0(\mathbf{s})]\eta$ is a function of the parameters α and β, which is known as the master stability function (MSF).[25,26] Let $\mathcal{R}$ be the region in the complex plane where the MSF provides a negative LLE [Figs. 4(a) and 4(b): The region $\mathcal{R}$ bounded by the solid line]. The condition for complete synchronization in network (5) is that the set $\{\sigma\lambda_l, \lambda_l \neq 0\}$ is entirely contained in $\mathcal{R}$.[25,26] Here we only consider the case where the region $\mathcal{R}$ is bounded. For the networks of Rössler oscillators in this paper, the stability region $\mathcal{R}$ is shown by the solid line in Fig. 4(a). In order to judge whether the set $\{\sigma\lambda_l, \lambda_l \neq 0\}$ is in the stability region in the case of the complex eigenvalues of the Laplacian matrix L, one should minimize the ratio $\mathrm{Re}(\lambda_N)/\mathrm{Re}(\lambda_2)$ for a fixed value of $\max|\mathrm{Im}(\lambda_l)|$, and one should minimize $\max|\mathrm{Im}(\lambda_l)|$ for a fixed value of the ratio $\mathrm{Re}(\lambda_N)/\mathrm{Re}(\lambda_2)$. Summing up the above minimization, a good condition is that $\mathrm{Re}(\lambda_N)/\mathrm{Re}(\lambda_2)$ and $\max|\mathrm{Im}(\lambda_l)|$ are simultaneously minimized.[14,17]

In this section we analyze the synchronizability in NW networks by applying the DO mechanism. From our recent work[24] the DO mechanism can ensure uniform intensities of all oscillators in networks, regardless of the initial conditions of the oscillators in networks with undelayed or delayed couplings. Here we design the coupling matrix G^0 in network (5) through the adaptation of the coupling strengths in network (1). After the adaptation by the DO mechanism, the coupling matrix G^0 in network (5) is assigned by the following matrix:

$$G^0 = G_{\mathrm{norm}} = G_{\mathrm{end}}/S_0, \tag{6}$$

where G_{end} is the coupling matrix of network (1) after the adaptation. For the coupling matrix $G^0=G_{\mathrm{norm}}$, all eigenvalues are fully contained within the unit circle centered at 1.[14,17] So $0\leqslant\mathrm{Re}(\lambda_l)\leqslant 2$, $|\mathrm{Im}(\lambda_l)|\leqslant 1$, and the largest $\mathrm{Re}(\lambda_N)$ will never diverge. During the transition to synchronization in network (1), $S_{\max}/S_{\min}$ always equals 1 in the DO mechanism.

It should be pointed out that $\max|\mathrm{Im}(\lambda_i)|$ is sufficiently small due to the DO mechanism (the maximal value is less than 0.1). Even for a large coupling strength $\sigma=2$, all the nonzero eigenvalues of the Laplacian matrix of σG_{norm} are located in a narrow region around the real axes in the stabil-

TABLE I. The ratio $\mathrm{Re}(\lambda_N)/\mathrm{Re}(\lambda_2)$ as a function of network size N for a fixed probability $p=0.003$.

	N							
Type	300	400	500	600	700	800	900	1000
I	41.66	31.83	26.10	22.91	20.34	17.55	16.17	14.51
II	27.84	20.36	15.77	13.29	11.53	9.96	9.08	7.97
III	29.38	22.44	17.61	14.56	12.60	11.49	10.42	9.68
IV	17.88	15.00	12.99	11.31	11.22	10.17	9.63	9.08

TABLE II. The ratio $\mathrm{Re}(\lambda_N)/\mathrm{Re}(\lambda_2)$ as a function of the probability p for a fixed size $N=500$.

	p								
Type	0.002	0.003	0.004	0.005	0.006	0.007	0.008	0.009	0.01
I	38.04	26.53	18.98	15.25	13.52	11.38	10.63	9.88	9.01
II	24.98	16.45	11.32	9.16	7.85	6.78	6.03	5.50	5.07
III	27.52	17.77	12.92	10.61	9.22	8.02	7.23	6.80	6.18
IV	17.37	13.33	10.26	8.96	8.06	7.55	6.79	6.22	6.19

ity region $\mathcal{R}$ [Fig. 4(a)]. Hence the ratio $\mathrm{Re}(\lambda_N)/\mathrm{Re}(\lambda_2)$ indicates the synchronizability in networks. In order to show the enhanced synchronizability in NW networks, we compare the synchronizability in the unweighted network (5) (type I network: $W_{ij}^0=1$), the degree based weighted network (5) (type II network: $W_{ij}^0=1/k_i$), network (5) with adaptive couplings by the Zhou–Kurths method (type III network), and network (5) with the coupling matrix being designed by network (1) with undelayed couplings (type IV networks).

We find that for a fixed small probability p (such as $p=0.003$) for adding long-range connections, the synchronizability in type III networks is better than that in type I networks, but it is worse than that in type II networks, no matter how large the size N of the networks is [Fig. 5(a), Table I]. However, we find that type IV networks have a better synchronizability than both type II networks and type III networks when the size is not too large. Of course, the smaller the probability p, the larger the size of type IV networks with better synchronizability than both type II networks and type III networks. For the fixed size $N=500$, we observe similar results in a certain range of the probability p [Fig. 5(b), Table II]. From Fig. 5 and Tables I and II, we see that the synchronizability in type IV networks is better than those in type II networks and type III networks in some cases. It is reasonable that type IV networks have better synchronizability than type III networks. This is because the DO mechanism ensures uniform intensities of all oscillators in type IV networks. Now we further analyze the reason why type IV networks have better synchronizability than type II networks in a certain range of the probability p.

In order to do so, we slightly modify NW networks. The initial network is a K-nearest-neighbor coupled network consisting of N oscillators arranged in a ring, with each oscillator $\mathbf{x}_i$ being adjacent to its K neighbor oscillators $\mathbf{x}_{i\pm1},\ldots,\mathbf{x}_{i\pm K/2}$, and with K being even. Then one adds with probability p a long-range connection between a pair of os-

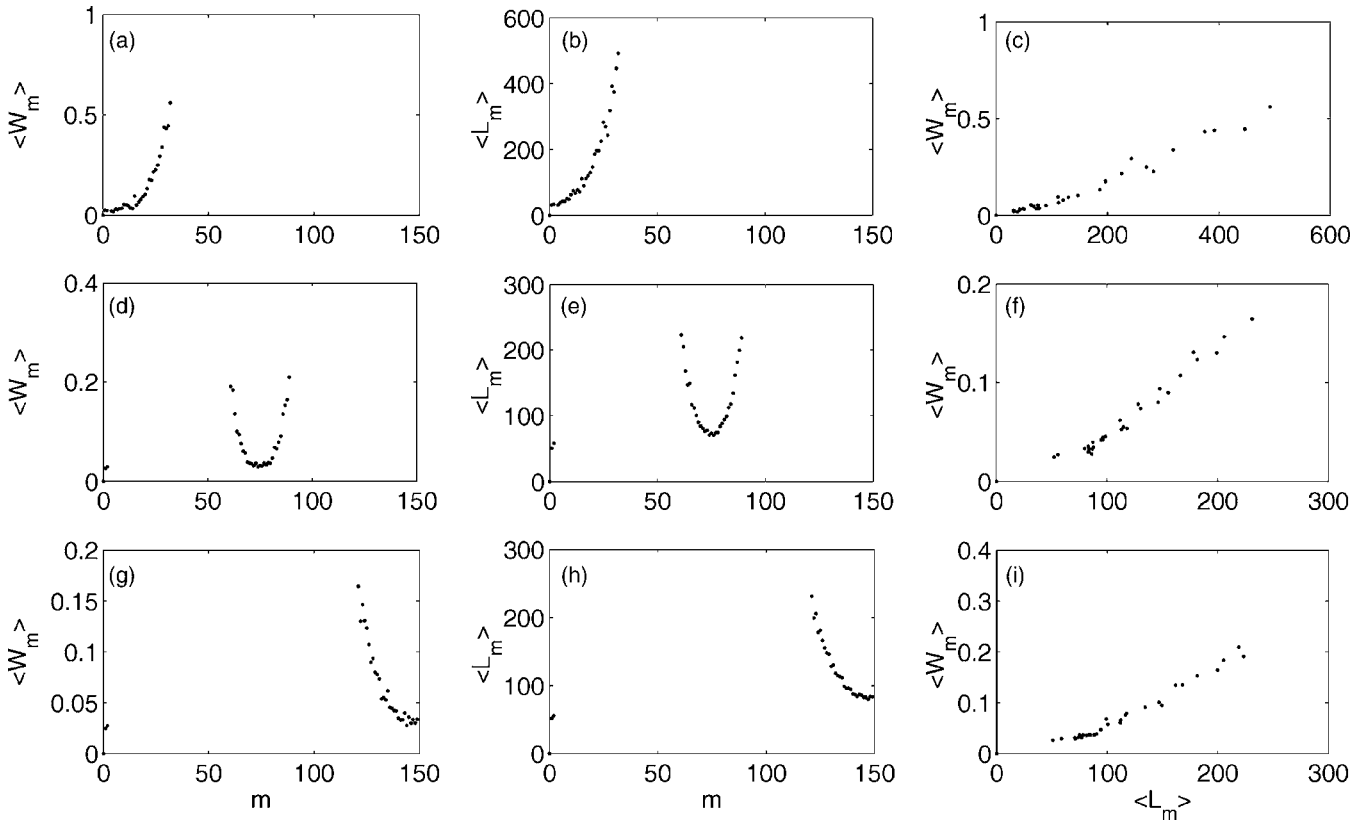

FIG. 6. The dependence of $\langle W_m\rangle$ on m in (a), (d), and (g) of $\langle L_m\rangle$ on m in (b), (e), and (h), and the relationship between $\langle W_m\rangle$ and $\langle L_m\rangle$ in (c), (f), and (i), respectively. $n_1=0$, $n_2=30$ [(a), (b), and (c)]; $n_1=60$, $n_2=90$ [(d), (e), and (f)]; $n_1=120$, $n_2=150$ [(g), (h), and (i)]. The parameters in type V networks are $N=300$, $K=4$, $p=0.2$, $T=1$ s, $\varepsilon=0.001$.

cillators with indices satisfying $n_1 \leqslant \min\{|i-j|, N-|i-j|\} \leqslant n_2$, where $0 \leqslant n_1$, $n_2 \leqslant N/2$ are two positive integers. This kind of network is called type V networks. Based on type V networks, we adjust the coupling strengths by the DO mechanism. After the adaptation, we define the average coupling strength $\langle W_m \rangle$ over the k_W links having the same $m = \min\{|i-j|, N-|i-j|\}$,

$$\langle W_m \rangle = \frac{1}{k_W} \sum G_{ij}. \tag{7}$$

Further, for the unweighted type V networks, the average load $\langle L_m \rangle$ over the k_L links having the same m is given by

$$\langle L_m \rangle = \frac{1}{k_L} \sum L_{ij}, \tag{8}$$

where the load L_{ij} of the link connecting oscillators $\mathbf{x}_i$ and $\mathbf{x}_j$ quantifies the traffic of the shortest paths passing that link. Here the size of type V networks is $N=300$ and the probability $p=0.2$. For different n_1 and n_2, we plot the relationship between $\langle W_m \rangle$ and m [Figs. 6(a), 6(d), and 6(g)], and the relationship between $\langle L_m \rangle$ and m [Figs. 6(b), 6(e), and 6(h)], respectively. From these subfigures, we conclude that $\langle W_m \rangle$ has a similar dependence on m as $\langle L_m \rangle$, which is further verified by the relationship $\langle W_m \rangle \sim \langle L_m \rangle$ [Figs. 6(c), 6(f), and 6(i)]. This implies that the adaptation due to the DO mechanism may lead to a similar synchronizability as the load based weighted networks. This may in part explain why type IV networks have a better synchronizability than type II networks in a certain range of the probability p for adding long-range connections.

IV. CONCLUSION

This paper considers complete synchronization in small-world networks of identical Rössler oscillators. Differing from the exiting dynamical mechanism, we apply a simple but effective DO mechanism to networks with undelayed or delayed couplings. We realize complete synchronization in networks, as well as ensure that all oscillators have uniform intensities during the transition to synchronization. The uniformity of the intensities is consistent with the necessary condition for the optimal synchronizability in the static mechanism. Further, we design a coupling matrix with much better synchronizability in a certain range of the probability p for adding long-range connections.

The DO mechanism can also be applied to the phase synchronization in SWNs with nonidentical oscillators. For example, we consider the phase synchronization in the Kuramoto model.[22,23,30,31] In this case, $\mathbf{x}_i = \theta_i$, $\mathbf{F}(\mathbf{x}_i) = w_i$, w_i are frequencies uniformly distributed in the interval $[-\triangle, \triangle]$ with $\triangle > 0$, $\mathbf{H}(\mathbf{x}_j, \mathbf{x}_i) = \sin(\theta_j - \theta_i)$ for the undelayed couplings and $\mathbf{H}(\mathbf{x}_j, \mathbf{x}_i) = \sin[\theta_j(t-\tau) - \theta_i]$ for the delayed couplings, the error function $\phi(\mathbf{x}_i, \mathbf{x}_j) = 1 - r_n(i,j)$ with $r_n(i,j)e^{\zeta \Psi_n(i,j)} = (e^{\zeta\theta_j} + e^{\zeta\theta_i})/2$ and $\zeta^2 = -1$, where $0 \leqslant r_n(i,j) \leqslant 1$ measures the extent of the synchronization of oscillators i,j, and $\Psi_n(i,j)$ stands for an average phase. Hence $\phi(\mathbf{x}_i, \mathbf{x}_j)$ are non-negative oscillators $\mathbf{x}_i, \mathbf{x}_j$ are not synchronized, and $\phi(\mathbf{x}_i, \mathbf{x}_j) = 0$ if oscillators $\mathbf{x}_i, \mathbf{x}_j$ are synchronized. Of course, our mechanism can be applicable to the synchronization in networks with nonidentical chaotic oscillators (such as Rössler oscillator) provided that the term of "phase" in networks is well-defined.[8]

ACKNOWLEDGMENTS

Y.S. was supported by NSFC under Grant No. 60603002. M.C. was supported by the Alexander von Humboldt Foundation and Special Doctoral Fund at the University by the Ministry of Education under Grant No. 20070003129. J.K. was supported by SFB 555 (DFG) and BRACCIA (EU).

[1] D. J. Watts and S. H. Strogatz, Nature (London) **393**, 440 (1998).
[2] A. L. Barabási and R. Albert, Science **286**, 509 (1999).
[3] S. H. Strogatz, Nature (London) **410**, 268 (2001).
[4] I. Z. Kiss, Y. Zhai, and J. L. Hudson, Science **296**, 1676 (2002).
[5] R. Albert and A. L. Barabási, Rev. Mod. Phys. **74**, 47 (2002).
[6] S. Strogatz, *Sync: The Emerging Science of Spontaneous Order* (Hyperion, New York, 2003).
[7] L. F. Lago-Fernández, R. Huerta, F. Corbacho, and J. A. Siguenza, Phys. Rev. Lett. **84**, 2758 (2000).
[8] G. Osipov, J. Kurths, and C. Zhou, *Synchronization in Oscillatory Networks* (Springer-Verlag, Berlin, 2007).
[9] M. Barahona and L. M. Pecora, Phys. Rev. Lett. **89**, 054101 (2002).
[10] T. Nishikawa, A. E. Motter, Y. Lai, and F. C. Hoppensteadt, Phys. Rev. Lett. **91**, 014101 (2003).
[11] G. A. Polis, Nature (London) **395**, 744 (1998).
[12] V. Latora and M. Marchioric, Phys. Rev. Lett. **87**, 198701 (2001).
[13] M. Chavez, D. Huang, A. Amann, H. G. E. Hentschel, and S. Boccaletti, Phys. Rev. Lett. **94**, 218701 (2005).
[14] M. Chavez, D. Huang, A. Amann, and S. Boccaletti, Chaos **16**, 015106 (2006).
[15] A. E. Motter, C. Zhou, and J. Kurths, Phys. Rev. E **71**, 016116 (2005).
[16] A. E. Motter, C. Zhou, and J. Kurths, Europhys. Lett. **69**, 334 (2005).
[17] D. Huang, M. Chavez, A. Amann, and S. Boccaletti, Phys. Rev. Lett. **94**, 138701 (2005).
[18] L. Donetti, P. I. Hurtado, and M. A. Munoz, Phys. Rev. Lett. **95**, 188701 (2005).
[19] X. Wang, Y. Lai, and C. Lai, Phys. Rev. E **75**, 056205 (2007).
[20] C. Zhou, A. E. Motter, and J. Kurths, Phys. Rev. Lett. **96**, 034101 (2006).
[21] C. Zhou and J. Kurths, Phys. Rev. Lett. **96**, 164102 (2006).
[22] Q. Ren and J. Zhao, Phys. Rev. E **76**, 016207 (2007).
[23] M. Chen, Y. Shang, Y. Zou, and J. Kurths, Phys. Rev. E **77**, 027101 (2008).
[24] M. Chen, Y. Shang, C. Zhou, Y. Wu, and J. Kurths, "Dynamical optimization and enhanced synchronizability in complex networks," Phys. Rev. E (submitted).
[25] J. F. Heagy, T. L. Carroll, and L. M. Pecora, Phys. Rev. Lett. **74**, 4185 (1995).
[26] L. M. Pecora and T. L. Carroll, Phys. Rev. Lett. **80**, 2109 (1998).
[27] M. Chen, Phys. Rev. E **76**, 016104 (2007).
[28] M. E. J. Newman and D. J. Watts, Phys. Lett. A **263**, 341 (1999).
[29] T. Gross and B. Blasius, "Adaptive coevolutionary networks—a review," arXiv:0709.1858v1 [physics. soc-ph] 12 September 2007.
[30] Y. Kuramoto, *Chemical Oscillations, Waves, and Turbulence* (Springer, Berlin, 1984).
[31] J. Acebron, L. L. Bonilla, C. J. P. Vicente, F. Ritort, and R. Spigler, Rev. Mod. Phys. **77**, 137 (2005).

Physica A 388 (2009) 2987–2994

Contents lists available at ScienceDirect

Physica A

journal homepage: www.elsevier.com/locate/physa

Response of scale-free networks with community structure to external stimuli

Ye Wu [a,b,*], Ping Li [a,c], Maoyin Chen [f], Jinghua Xiao [b], Jürgen Kurths [d,e]

[a] Interdisciplinary Center for Dynamics of Complex Systems, University Potsdam, Am Neuen Palais 10, D-14469, Germany

[b] School of Science, Beijing University of Posts and Telecommunications, Beijing 100876, PR China

[c] Computational Intelligence Laboratory, School of Computer Science and Engineering, University of Electronic Science and Technology of China, Chengdu, 610054, PR China

[d] Potsdam Institute for Climate Impact Research (PIK) Telegraphenberg A31, 14473 Potsdam, Germany

[e] Institute of Physics, Humboldt University, 10099 Berlin, Germany

[f] Tsinghua National Laboratory for Information Science and Technology, Department of Automation, Tsinghua University, Beijing 100084, PR China

ARTICLE INFO

Article history:
Received 1 December 2008
Received in revised form 18 March 2009
Available online 29 March 2009

Keywords:
Complex network
Community
Response
Robustness

ABSTRACT

The response of scale-free networks with community structure to external stimuli is studied. By disturbing some nodes with different strategies, it is shown that the robustness of this kind of network can be enhanced due to the existence of communities in the networks. Some of the response patterns are found to coincide with topological communities. We show that such phenomena also occur in the cat brain network which is an example of a scale-free like network with community structure. Our results provide insights into the relationship between network topology and the functional organization in complex networks from another viewpoint.

1. Introduction

Many natural systems are found, on one hand, to be able to react to small selected stimuli with large alterations, whereas, on the other hand, they can withstand large environmental variations (sometimes even unpredictable ones) with minimal changes or loss of functionality. This implies two complementary attributes of dynamical systems: sensitivity and robustness. Sensitivity implies the possibility of a large response to small stimuli and robustness implies the possibility of a small response to large stimuli. Not only biological systems but also several man-made complex systems, such as power grids or communication systems require this combination of traits to optimize the system's performance. Recently, the focus on understanding the interplay between dynamical behavior and their topologies has attracted a lot of interest [1–7]. Recent research [8] shows that the observed network topologies which are often scale-free or scale-free like [9] are not necessarily optimal in their connectivity and connectivity-related attributes. Moreover, it is manifest [10] that scale-free networks are fragile to intentional attack but resilient to random failures, in the face of node removal. We ask why so many networks found in nature have a scale-free (like) architecture with a lack of optimal network connectivity? In this paper, we study the properties which determine the efficiency of networks by analyzing the response of such systems to external perturbations.

To describe a complex system, one can take the units of response as nodes and the interactions between them as edges and then generate a network model. It is well known that many complex networks exhibit not only short average distances, but also a high clustering coefficient, the 'small-world' property [11]. Moreover, several of them can be approximated well

* Corresponding author at: Interdisciplinary Center for Dynamics of Complex Systems, University Potsdam, Am Neuen Palais 10, D-14469, Germany.
E-mail address: wuyept@gmail.com (Y. Wu).

0378-4371/$ – see front matter © 2009 Elsevier B.V. All rights reserved.
doi:10.1016/j.physa.2009.03.037

by a power-law degree distribution, $P(k) \sim k^{-\gamma}$, the 'scale-free' property [9]. Many real-world networks exhibit not only the 'small-world' and 'scale-free' property, but also have a community structure which is defined as collections of nodes within which the connections are dense, but between the communities the connections are sparse. Community structures are supposed to play an important role in many real networks. For example, communities in a citation network might represent related papers on a single topic [12]; communities on the web might represent pages on related topics [13]; communities in a biochemical network or neuronal system might correspond to special functional units [14,15]. Therefore, it is important to study the response of a scale-free network with community structure.

In this paper, we use the dynamical model presented by Bar-Yam and Epstein [16] to study the response of scale-free networks with community structure to external stimuli. Our investigation reveals that the community characteristic of the networks is crucial to enhance its robustness. Some of the response patterns are found to coincide with the topology communities. As an example of scale-free like networks with community structure, such phenomena also occur in mammal brain networks.

This paper is organized as follows: In Section 2, the model of the network is introduced. The dynamical attractor network model is presented in Section 3. Numerical simulations and a detailed analysis are presented in Section 4. In Section 5, we study the response of the cat brain network to stimuli as an example. Finally, our conclusions are given in Section 6.

2. The model of the network

In order to create a scale-free network with community structure, we use a modified procedure of the algorithm proposed in [17]. We assume that there are $M(M \geq 2)$ communities in the network. This model is defined by the following scheme:

Step 1: Initialization: Start from a small number $m_0(m_0 > 1)$ of fully connected nodes in each community. There are n random links between every two communities.

Step 2: Growth: At each time step, a new node is added to the network. We assume that the probability $P(I)$ of which community I the new node is added to depends on the number of nodes in the communities n_I, i.e.:

$$P(I) = \frac{n_I}{\sum_I n_I}. \tag{1}$$

The new node will be connected to m ($m_0 \geq m \geq 1$) nodes inside the same community I through m intra-community links (defined as the links that connect nodes in the same community), and with probability α connected to n ($m \geq n \geq 1$) nodes (none with probability $1 - \alpha$) to the other $M - 1$ communities through inter-community links (defined as the links that connect nodes among different communities). We assume that the probability $P(i, I)$ that a new node will be connected to node i in community I which is selected before depends on the inner-degree s_{iI} (define as the number of intra-links connected to node i) of that node, i.e.:

$$P(i, I) = \frac{s_{iI}}{\sum_k s_{kI}}. \tag{2}$$

We also assume that the probability $P(j, K)$ that a new node will be connected to node i in community $K(K \neq I)$ depends on the inter-degree l_{jK} (defined as the number of inter-links connected to the node), i.e.:

$$P(j, K) = \frac{l_{jK}}{\sum_{m,N,N\neq K} l_{mN}}. \tag{3}$$

We call this network a community-scale-free (CSF) network (compare with scale-free network (SF)). It is shown in Fig. 1 that such a CSF network has also a power-law degree distribution $P(k) \sim k^{-\gamma}$.

3. The dynamic model

To investigate the response of CSF networks, we choose a conventional multi-attractor network model; which describes a dynamical system. The node states $s_i = \pm 1, i \in 1, 2, \ldots, N$ are binary. The states of the network system are then composed by the set of the node states s_i. The dynamical attractor system evolves as follows:

$$s_i(t + 1) = \text{sign}\left(\sum_{j=1}^{N} A_{ij} s_j(t)\right) \tag{4}$$

where $A = (A_{ij})_{N\times N}$ is the connection matrix whose elements A_{ij} are positive if there is a link going from node i to node j with $i \neq j$ and zero otherwise ($A_{ii} = 0$) (A is symmetric if the network has no weights and no directions). This model can also be interpreted as social opinion models of binary states, such as yes ($+1$) or no (-1). It is known [18] that there are multiple attractors generated by this model. Any attractor with a non-empty attracting basin is stable to perturbation and thus can represent a functional state of the system.

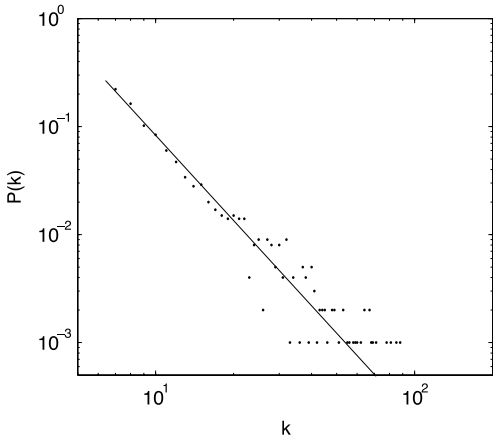

Fig. 1. The degree distribution of CSF. $N = 1000$, $M = 5$, $n = 6$, $m = 1$, $\alpha = 1$, $\gamma = 3$.

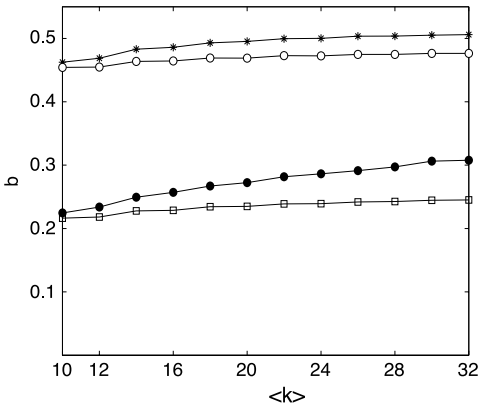

Fig. 2. Size of the basin of attraction (fraction of total nodes, b) as a function of the average degree $\langle k\rangle$, * CSF network and random stimulus, ○ SF network and random stimulus, ● CSF network and directed stimulus, □ SF network and directed stimulus, $\langle k\rangle = m$ in SF, $\langle k\rangle = m + \alpha n$ in CSF, $N = 1000$, $M = 4$.

External stimuli are modeled by flipping the signs of a specified set of nodes. When the states of some nodes are changed, the system either evolves back to its initial state or switches to other attractors. The response of the network system is described as a process of switching between the attractors. The size of the basin of attraction, i.e., the number of nodes whose states can be changed before the dynamics of the network fails to bring the systems back to its original states, indicates the degree of stability of the system. The system is said to be sensitive to a certain disturbance if it changes its current state to another one, and vice versa. We calculate the size of the basin of attraction in different cases of stimuli to reveal the sensitivity and robustness of the network [19,20].

4. Numerical simulations and analysis

We study the CSF networks mentioned in Section 2 and the Barabási–Albert model of SF networks. Without loss of generality, we can randomly choose two states to represent the functional states of the system. To ensure that these states are stable, we adopt the Hebbing imprinting rule $J_{ij} = \sum_\alpha s_i^\alpha s_j^\alpha$ to construct the desired attractors. For sufficiently many links and for a broad range of network topologies, this form of non-zero links will make the pre-selecting functional states into stable attractors of the network dynamics [18]. For the sake of convenience, we consider two attractors $S1$ and $S2$ ($S1 = (+1, +1, \ldots, +1)$, $S2 = (-1, -1, \ldots, -1)$) as the stable states between which the system can switch. Initially, all the nodes are set to be in the state $+1$, that is, $s_i = +1$, $i = 1, 2, \ldots, N$. We suppose, at some time t, such environment changes or new information arises, which induce the states of some nodes being selected to flip to the opposite state $s_{k_i} = -1$, $i = 1, 2, \ldots, r_s$, where r_s is the number of the nodes whose states are flipped. Then after a period of transient time, the system evolves into a stable state which is either its original state or another attractor. To explore the changes of the system state, 100 simulations are performed for each different average degrees.

We find (Fig. 2) that for the two basic types of stimuli: direct stimuli (changes are made to the most highly connected nodes, the hubs) and random stimuli (changes are made to randomly chosen nodes), CSF networks are more robust than SF networks. Therefore, the community structure enhances the robustness of the networks. In order to see how the community

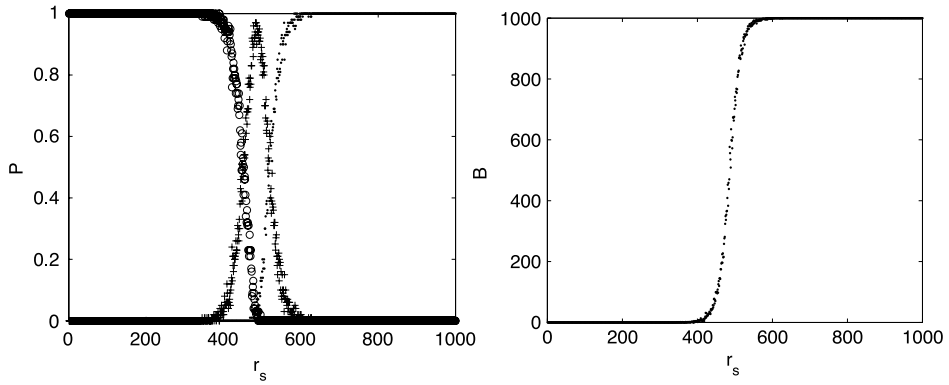

Fig. 3. CSF networks: $N = 1000$, $M = 4$. (a) The probability P that the system evolves into S1, S2 or other steady states under different disturbances r_s: o all the nodes were in status $+1$, i.e. the system evolves back to its initial state. $+$ some of the nodes were in status $+1$, others were in status -1, $\cdot$ all the nodes were in status -1, i.e. all the nodes were influenced. (b) The average number of influenced nodes B in the long-time behavior for different r_s.

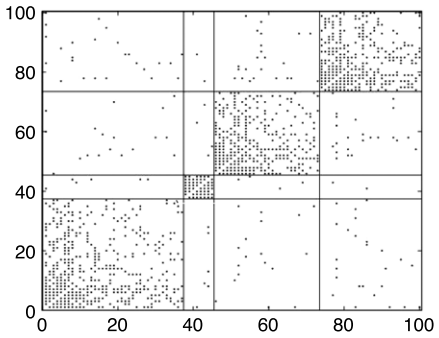

Fig. 4. Connection matrix A of the CSF network, $\cdot$ $A_{ij} = 1$, blank: $A_{ij} = 0$. The parameters of the CSF network $N = 100$, $M = 4$, $m = 6$, $n = 1$.

structure influences the robustness of the network, we randomly chose a CSF network to investigate the probability P that the system evolves into S1, S2 or other steady states under different random disturbances.

It is shown in Fig. 3 that the CSF network maintains the original states under a small perturbation, which illustrates its robustness to some extent, until the strength of perturbation (numbers of flips r_s) exceeds a critical value. For intermediate stimuli, the system converges to mixed steady states in which some node states are $+1$ but the others are -1. By increasing the stimuli continuously, all of the nodes are influenced and the system evolves into an all -1 state (S2), which is an extreme response. It should be noted that there are two phase transition points in the process of response. The first one corresponds to the transition of the system from a normal state to partial destruction. The second one corresponds to the transition from partial destruction to complete destruction.

It is interesting to ask: why is the response of a CSF network different from a SF network without modular structure, though the degree distribution of the CSF is also scale-free? In the following, we explore the response patterns for r_s in the intermediate region i.e. in the region between both phase transitions. We randomly choose some nodes to be flipped and identify whose states are changed in the network as the system evolves into a steady state, which illustrates the response to stimuli. To describe the response patterns, a new variable is defined as follows:

$$R_{ij} = \begin{cases} -1, & \text{if } A_{ij} > 0 \text{ and } s_i = -1, s_j = -1 \\ +1, & \text{if } A_{ij} > 0 \text{ and } s_i, s_j \text{ are not in status-1 at the same time} \\ 0, & \text{if } A_{ij} = 0. \end{cases} \tag{5}$$

R indicates which part of the network was influenced. In order to see the patterns clearly, we use a small size network here as an example.The connection matrix is shown in the Fig. 4. We have also found similar results in much larger CSF networks and smaller networks. It is shown in Fig. 5 that for a certain r_s in the intermediate region, some patterns of R appear with large probability, which almost correspond to the topological communities. Clearly, the community structure plays a crucial role in response to the stimuli. When some segments of the network are destroyed, the community structure can prevent the damage from spreading to other segments. A similar impact of clustering has been also found in Ref. [21]. This phenomenon can be explained by the underlying structure of communities which has a high density of connections inside the communities and sparse connections with the outside nodes. Therefore, those nodes which connect two communities can hardly be affected by the negative nodes with respect to our majority opinion-like model. In this sense, the network

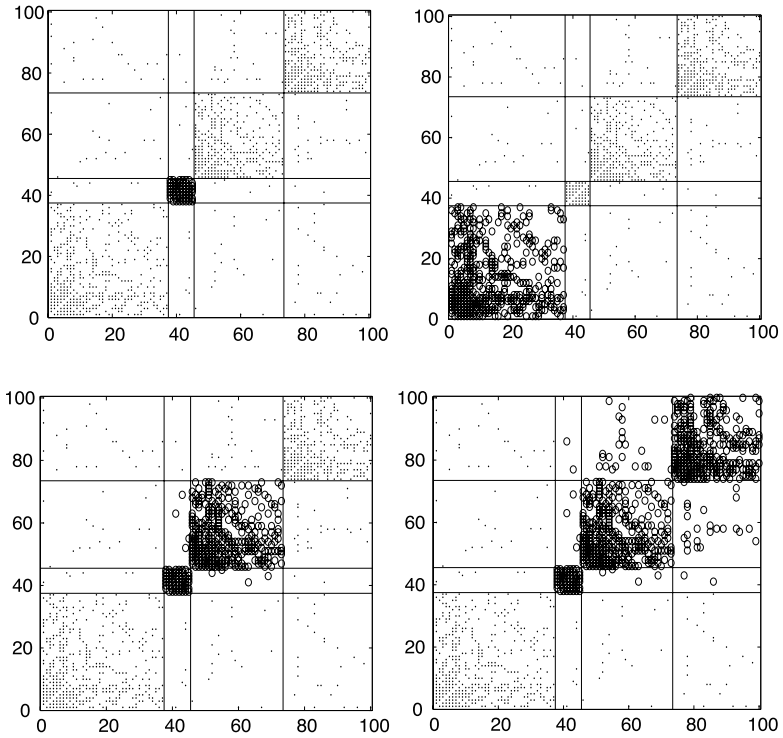

Fig. 5. The pattern of R with different initial conditions: o $R_{ij} = -1$, · $R_{ij} = 1$, blank: $R_{ij} = 0$. The parameters of the CSF network $N = 100$, $M = 4$, $m = 6$, $n = 1$, $\alpha = 1$. $r_s = 48$.

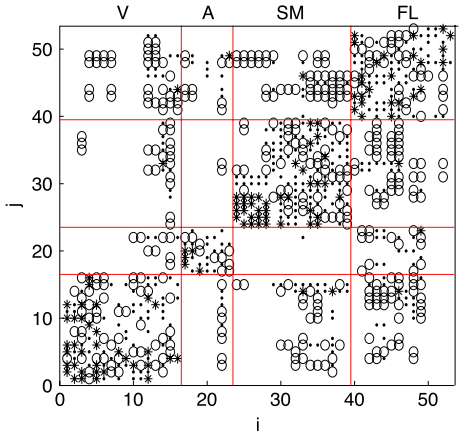

Fig. 6. Connection matrix A of the cortical network of cat brain. The different symbols represent different connection weights: 1 (o sparse), 2 (. intermediate), 3 (* dense).

structure coincides well with the dynamical pattern. By detecting some special patterns appearing with high probability, our results are expected to provide a new approach for community detection.

5. Response of cat brain networks to stimuli

As an example, the response of cat brain networks to stimuli is analyzed here. The cerebral cortex of a cat can be parcellated into 53 areas, linked by about 830 fibres of different densities into a weighted complex network as shown in Fig. 6 [22]. This network displays a heterogeneous structure, where some nodes have only 2 links while others have up to 35 connections. It is clear that the size of the network is too small to claim that the degree distribution is scale-free. Nevertheless, the distribution is very close to that of networks of the same size and density generated by scale-free models. Moreover, the cortical network of cats exhibits a hierarchically clustered organization. There exists a small number of topological clusters that broadly agree with four functional cortical sub-divisions: visual cortex (V,16 areas), auditory (A, 7 areas), somato-motor

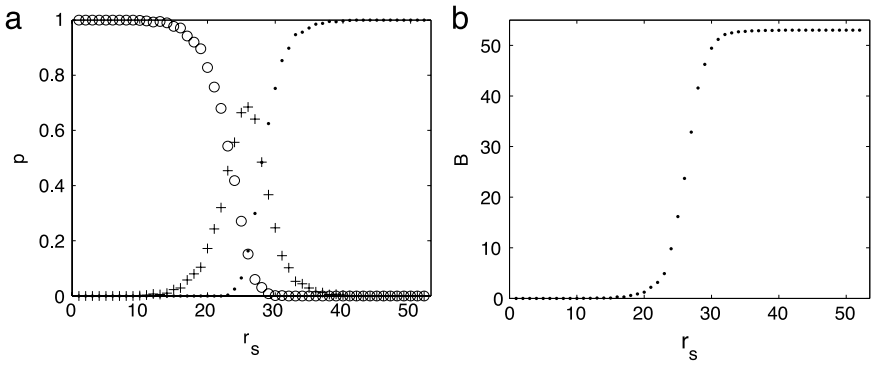

Fig. 7. Cat brain network (a) Probability P that the system evolves into S1, S2 or other steady states under different disturbances r_s: o all the nodes were in status $+1$, i.e. the system evolves back to its initial states. $+$ some of the nodes were in status $+1$, others were in status -1, · all the nodes were in status -1, i.e. all the nodes were influence. (b) The average number of influenced nodes B in the long-time behavior for different r_s.

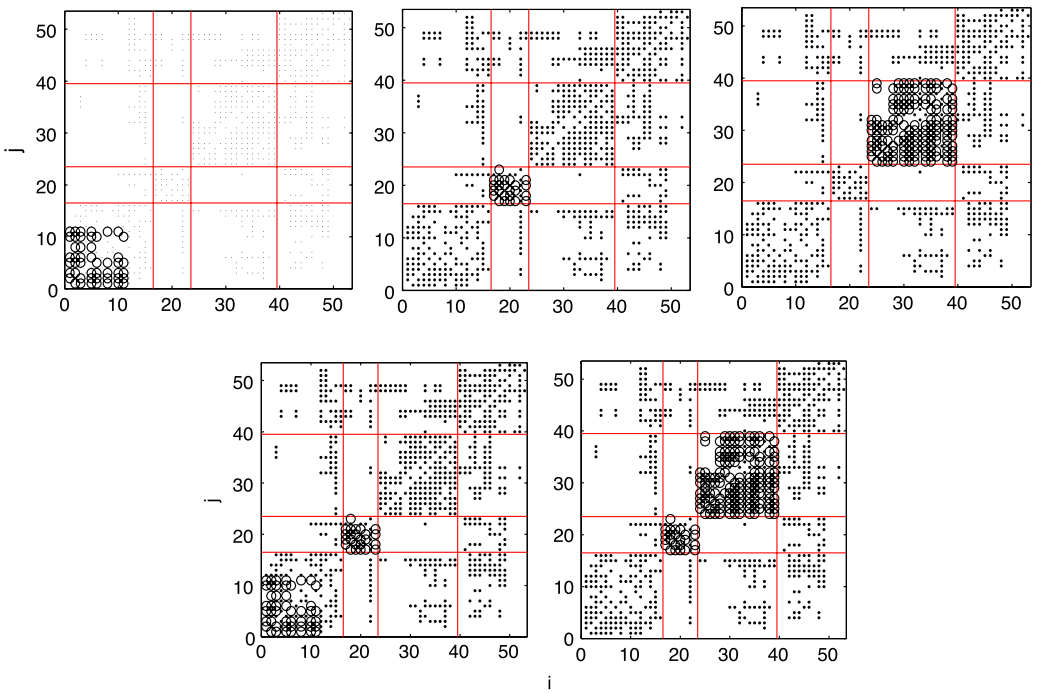

Fig. 8. Cat brain network. The pattern of R with different initial conditions: o $R_{ij} = -1$, · $R_{ij} = 1$, blank: $R_{ij} = 0$. $r_s = 25$.

(SM,16 areas) and fronto-limbic (FL,14 areas). In addition, this network also displays typical small-world properties, i.e. short average path length and high clustering coefficient [23–26].

We perform simulations on this network by applying the same dynamics as in our CSF model (Section 3). The responsivity under different external perturbations can be found in Figs. 7 and 8, which is similar to the case of our network model. It can provide insights into the relationship between network topology and functional organization of the cat brain networks from another viewpoint [27]. Furthermore, we make the stimuli acting on large-intensity nodes or on small-intensity nodes (directed stimuli) other than random stimuli and then see the response pattern of the network. We define the intensity c_i of node i as follows:

$$c_i = \sum_{j=1, j\neq i}^{N} A_{ij}. \tag{6}$$

In particular, for unweighted networks, the intensity of a node is the degree of this node. It is known that scale-free networks are more robust to random attacks, while more sensitive to directed disturbance to the large-degree nodes. As shown in Fig. 8, the brain network can be partially disturbed when $30 > r_s > 16$ directed stimuli are acting on small-degree nodes (shown in Fig. 9(b)). On the other hand, the system can be entirely disturbed when $r_s > 24$ for large-node perturbation (shown in Fig. 9(a)). It is manifest that the robustness for directed stimuli acting on large-degree nodes is stronger than the

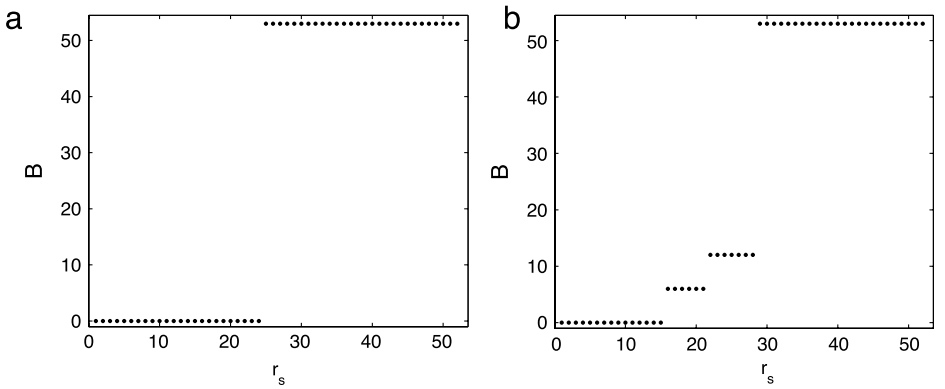

Fig. 9. The number of nodes (B) whose states are changed in long-time behavior for different stimuli. (a) The responses for directed stimuli acting on large-degree nodes. (b) The responses for directed stimuli acting on small-degree nodes.

case for directed stimuli on small-degree nodes. This enhanced robustness is also better than the case for random stimuli, which is different from the result in Refs. [16,28] for scale-free networks.

Compared with the robustness of the classical scale-free network model, a complex brain network is likely to be more robust for direct stimuli. It should be noted that the brain network displays not only heterogeneity on the degree distribution but also hierarchical clustering characteristic. These special properties may play an important role in the response to stimuli. However, more evidence should be presented in future studies.

6. Conclusion

In this letter, we investigate the relationship between dynamics of complex networks and their topology properties by studying the response of the whole system. An adaptive system should be robust for large stimuli, which makes the system stable. Additionally, it also should be sensitive for small stimuli, which makes the system react rapidly on the new external changes. According to the analysis of the response of scale-free networks with community structure, we find that the hierarchical characteristic of the networks enhances their robustness to external stimuli. Switching patterns are found to coincide with the topology communities. We verify our results in a real-world -cat brain network which has similar topological properties as our model. We show that the robustness for directed stimuli acting on large-degree nodes is better than in the case of directed stimuli on small-degree nodes, which is different from the response in the scale-free networks. Our results provide new insights into the relationship between network topology and the functional organization of the cat brain networks from another viewpoint.

Acknowledgements

The authors thank Changsong Zhou for valuable discussion. Y. Wu and P. Li thanks the financial support by China Scholarship Council. M. Chen. was supported by NSFC project (No. 60804046), Special Doctoral Fund in the University by Ministry of Education (No. 20070003129), and the Alexander von Humboldt Foundation. J. Kurths thanks the supported by SFB 555 (DFG) and BIO SIM (EU).

References

[1] S. Boccaletti, V. Latora, Y. Moreno, M. Chavez, D.-U. Hwang, Phys. Rep. 424 (2006) 175–308.
[2] T.C. Jarrett, D.J. Ashton, M. Fricker, N.F. Johnson, Phys. Rev. E 74 (2006) 026116.
[3] J.A. Acebrn, S. Lozano, A. Arenas, Phys. Rev. Lett. 99 (2007) 128701.
[4] E.A. Variano, J.H. Mccoy, H. Lipson, Phys. Rev. Lett. 92 (2004) 188701.
[5] C. Piccardi, R. Casagrandi, Phys. Rev. E 77 (2008) 026113.
[6] A. Arenas, A. Díaz-Guilera, J. Kurths, Y. Moreno, C. Zhou, Phys. Rep. 469 (2008) 93–153.
[7] S.N. Dorogovtsev, A.V. Goltsev, J.F.F. Mendes, Rev. Modern Phys. 80 (2008) 1275.
[8] B. Shargel, H. Sayama, I.R. Epstein, Y. Bar-Yam, Phys. Rev. Lett. 90 (2003) 068701-1-4.
[9] A.-L. Barabási, R. Albert, Science 286 (1999) 509–512.
[10] Béla Riordan Bollobás, Oliver localización: Robustness and vulnerability of scale-free random graphs, Internet Math. 1 (1) (2003) 1–35.
[11] D.J. Watts, S.H. Strogatz, Nature 393 (1998) 440–442.
[12] S. Redner, Eur. Phys. J. B 4 (1998) 131.
[13] G.W. Flake, S.R. Lawrence, C.L. Giles, F.M. Coetzee, IEEE Comput. 35 (2002) 66.
[14] P. Holme, M. Huss, H. Jeong, Bioinformatics 19 (2003) 532.
[15] O. Sporns, D.R. Chialvo, M. Kaiser, C.C. Hilgetag, Trends Cogn. Sci. 8 (2004) 418.
[16] Y. Bar-Yam, I.R. Epstein, Proc. Natl. Acad. Sci. USA 101 (2004) 4341.
[17] C.G. Li, P.K. Maini, J. Phys. A 38 (2005) 9741.
[18] J.J. Hopfield, Proc. Natl. Acad. Sci. 79 (1982) 2554.
[19] L.K. Gallos, P. Argyrakis, Phys. Rev. E 72 (2005) 017101.

[20] G. Bianconi, M. Marsili, Phys. Rev. E 73 (2006) 066121.
[21] M. Kaiser, M. Görner, C.C. Hilgetag, New. J. Phys. 9 (2007) 110.
[22] C.S. Zhou, L. Zemanova, G. Zamora-Lopez, C.C. Hilgetag, J. Kurths, Phys. Rev. Lett 97 (2006) 238103.
[23] O. Sporns, J.D. Zwi, Neuroinformatics 2 (2004) 145.
[24] C.C. Hilgetag, G. Burns, M.A. O'Neill, J.W. Scannell, M.P. Young, Philos. Trans. Soc. Lond. B 355 (2000) 91.
[25] C.C. Hilgetag, M. Kaiser, Neuroinformatics 2 (2004) 353.
[26] Ed Bullmore, Olaf Sporns, Nature Reviews, Neuroscience 10 (2009) 186.
[27] L. Zemanova, C.S. Zhou, J. Kurths, Physica D 224 (2006) 202.
[28] S.J. Wang, A.C. Wu, Z.X. Wu, X.J. Xu, Y.H. Wang, Phys. Rev. E 75 (2007) 046113.